UNIVERSIDAD NACIONAL AUTÓNOMA DE MÉXICO
POSGRADO EN CIENCIAS FÍSICAS

Modeling the cosmic acceleration through the equation of state: Dark energy and Modified gravity confronted with observations

T E S I S

QUE PARA OPTAR POR EL GRADO DE:

DOCTOR EN CIENCIAS (FÍSICA)

PRESENTA

MARIANA JABER BRAVO

TUTOR

DR. AXEL RICARDO DE LA MACORRA PETTERSSON
MORIEL (IF)

MIEMBROS DEL COMITÉ TUTOR

DR. JOSÉ OCTAVIO VALENZUELA TIJERINO (IA)
DR. MIGUEL ALCUBIERRE MOYA (ICN)

CIUDAD DE MÉXICO, ENERO 2019

Resumen

El descubrimiento, a finales de los años noventa, de la expansión acelerada del Universo, cambió de manera radical nuestro paradigma cosmológico. Las mediciones, llevadas a cabo de manera independiente por dos grupos de astrónomos (Riess et al. (1998) y Perlmutter et al. (1999)) son consistentes con un Universo que se expande de forma acelerada.

El conjunto de observaciones recabadas desde entonces concuerda con un Universo constituido en un 95% por componentes de naturaleza desconocida y cuya existencia implica física más allá del Modelo Estándar de Partículas o modifaciones a las leyes de gravitación como las dicta la Teoría de Relatividad General.

De acuerdo a las diferentes observaciones, tanto de candelas estándar (como lo son las Supernovas de tipo Ia: Suzuki et al. (2012), Betoule et al. (2014)), reglas estándar inferidas a partir de censos de galaxias (Eisenstein et al. (2005), Tegmark et al. (2004), Alam et al. (2016), Kazin et al. (2014), Beutler et al. (2011),Sanchez et al. (2016)), o las anisotropías en el Fondo Cósmico de Radiación de Microondas (Bennett et al. (2013), Ade et al. (2016a)), entre otras, tenemos sólo un 4% de materia ordinaria, mientras que el resto se compone de dos componentes exóticos llamados Materia Oscura y Energía Oscura, constando de aproximadamente 26% y 70% del total del contenido energético del Universo, respectivamente.

El modelo que logra, adecuadamente, explicar la evidencia observacional antes mencionada se conoce como ΛCDM, por sus siglas en inglés. En éste se invoca un término constante conocido como *Constante Cosmológica* y denotado por Λ para explicar la reciente aceleración en la expansión del Universo, mientras que la formación de estructura a gran escala es explciada mediante un tipo de materia oscura fría que domina a la componente bariónica (visible) y que interactúa con ella solo a través de la gravedad.

Dada la falta de una comprensión de primeros principios para la naturaleza de dicha Constante Cosmológica, numerosas explicaciones han surgido en la literatura. De entre dichos modelos alternativos, los más populares han sido los llamados Modelos de Quintaescencia (Wang and Steinhardt (1998), Cooray and Huterer (1999), de la Macorra and Piccinelli (2000), de la Macorra and Stephan-Otto (2001), de la Macorra and Stephan-Otto (2002), De la Macorra (2003), Caldwell and Linder (2005), Linder (2006a), Huterer and Peiris (2007), Linder (2008)).

Alternativamente, modelos que modifican la Teoría de Relatividad General a gran escala han sido propuestos. Sin embargo, la enorme complejidad que requieren los análisis de datos observacionales que se llevan a cabo actualmente o que se están plane-

ando para las décadas por venir, demandan un enfoque simplificado mediante el cual se puedan poner a prueba modelos teóricos diversos. Los enfoques paramétricos o también llamados fenomenológicos proveen este puente entre modelos teóricos provenientes de física de partículas o de teorías de gravedad modificada y las observaciones cosmológicas.

En esta tesis se exploraron dos parametrizaciones para la ecuación de estado de la Energía oscura (el cociente entre el término asociado a la presión de este componente y su densidad).

En los capítulos 1-3 se introduce las nociones mínimas necesarias para seguir los contenidos de esta tesis: en el Capítulo 1 se introduce el problema de la expansión acelerada, el paradigma cosmológico actual y se inclueyen los dos artículos publicados en los que se basan la presente tesis. En el Capítulo 2, las ecuaciones básicas de la Cosmología, tanto a nivel de fondo como en el régimen perturbativo, son explícitamente derivadas con la finalidad de poder utilizarlas en los capítulos posteriores. Igualmente se explica en detalle la física detrás de la señal generada por las Oscilaciones Acústicas de Bariones, la cual se puede extraer estadísticamente de censos de galaxias como los llevados a cabo experimentos como eBOSS (Blanton et al., 2017), DESI (Levi et al., 2013) o EUCLID (Laureijs et al., 2011).

En el Capítulo 3 se introducen las bases teóricas para modelos alternativos a la Constante Cosmológica. En un primer apartado se tratan las generalidades de los modelos de campo escalar mínimamente acoplado, llamados Quintaescencia. Igualmente se elabora en la filosofía detrás del enfoque conocido como Gravedad Modificada para explicar la aceleración cósmica en épocas recientes del Universo. Se hace particular énfasis en el tipo de modificaciones la gravedad llamados modelos $f(R)$, los requistos que deben cubrir para ser cosmológicamente viables y los candidatos teóricos que cumplen dichos requisitos. En la parte final de dicho capítulo se introduce el enfoque fenomenológico para tratar a la entidad responsable de la expansión acelerada como un fluido que puede carcterizarse por su ecuación de estado y se revisan algunos candidatos en la literatura para modelar dicho término.

El primer modelo tratado fue una parametrización inspirada en los modelos de Quintaescencia, el cual fue constreñido a nivel de fondo usando observaciones actuales. El modelo, su comportamiento y las cotas a sus parámetros libres fue objeto del Capítulo 4. Los datos implementados en la búsqueda de parámetros mediante técnicas de Montecarlo se explica en la primera mitad de dicho capítulo, así como el análisis estadístico de las tensiones que surgen al combinar diferentes tipos de observaciones. La segunda parte de dicho capítulo trata del estudio de las perturbaciones en el régimen lineal de dicho modelo. Su implementación en un código numérico para resolver la parte no lineal del crecimiento de sobredensidades de materia, se indica al final del Capítulo 4.

El segundo modelo tratado en esta tesis se inspira en modelos de graveda modificada, en particular, aquellos denominados $f(R)$. Estos modelos proveen una explicación natural a la forma de la ecuación de estado para la energía oscura que fue reconstruida en (Zhao et al., 2017) y la cual no puede obtenerse del estudio de campos escalares mínimamente acoplados como en el caso de modelos de Quintaescencia.

La parametrización presentada en el Capítulo 5 es introducida por primera vez, siendo la única ecuación paramétrica inspirada en teorías tipo $f(R)$ y la cual alcanza una precisión bastante deseable para los experimentos futuros. En dicho capítulo se aborda tanto la base teórica para este modelo, así como su comparación con soluciones numéricas de los modelos particulares de $f(R)$ bajo consideración. Igualmente se aborda su comportamiento al ser contrastado con observaciones y se plantea el trabajo que puede realizarse a partir de esta nueva ecuación de estado.

El Capítulo 6 recoge las conclusiones de esta tesis y el trabajo que a futuro se espera realizar teniendo como base lo aquí presentado.

Abstract

In the current paradigm of cosmology the largest portion of the energy budget constituted by unknown ingredients. Roughly 70% of the Universe is in the form of an exotic component responsible for the cosmic acceleration at present times. The biggest question of current cosmology is the unknown nature and dynamics of this constituent, called Dark Energy. The amount of observational evidence supporting the cosmic acceleration at present times comes from a variety of scales, yet the understanding of Dark Energy properties is less robust. Many theoretical models have been proposed to explain the nature of Dark Energy and big observational efforts are being designed or under way to determine with better precision its dynamics. Nevertheless the incorporation of models beyond the minimal picture into these experiments is a challenging task and parametric descriptions can offer an efficient way to overcome this challenge.

In Chapter *"Dark energy models"* I describe the theory behind parametrizations of the Dark Energy as a time-varying fluid or scalar field. The most popular parametrizations inspired in these kind of models are described in the first part of the Chapter *"Dark energy models"*. On the second part of this chapter I describe a different kind of models for cosmic acceleration. These come from particular modifications to General Relativity and are known as $f(R)$ theories.

In this thesis two parametric models for the behaviour of Dark Energy at late times are presented and tested against observational data. The foundation of the first model comes from dynamics of scalar fields such as in quintessence. The resulting parametric form of the equation of state allows for a richer behaviour compared to other popular proposals. In Chapter *" Steep equation of state"*, I describe the model and its corresponding background behaviour. The free parameters were sampled with Montecarlo techniques using data from the late time Universe. The different sets of observations used for the numerical implementation of the Montecarlo sampler are described. To compare the predictions of the model against data from Large Scale Structure I detail the solutions up to second order for the growth of matter overdensities in the Lagrangian framework. The second part of chapter *" Steep equation of state"* contains the resulting analysis of the perturbative regime: the linear growth functions and the study of the non-linearities using an N-body code. The contents of this part of the analysis are work on progress.

Finally, in Chapter "$f(R)$ *for surveys*" I describe the second model presented in this thesis. The foundation for this parametrization comes from Modified gravity theories, in particular, $f(R)$ modifications of gravity. This parametric form of the geometric equation of state is presented for the first time and it incorporates in a single equation

the three competitive $f(R)$ theories for gravity with sub-percent accuracy. I describe the theoretical support of the parametrization and its background evolution. The implementation of numerical exploration of its free parameters and the resulting constraints are in the first part of "$f(R)$ *for surveys*" chapter. The tension among different datasets and its statistical analysis is also detailed in this chapter.

Contents

List of Figures

List of Tables

Every beginning after all, is nothing but a sequel, and the book of events is always open in the middle. **–Wisława Szymborska.**

There is no need to build a labyrinth when the entire Universe is one. **–Jorge Luis Borges**

Dark energy is not only terribly important for astronomy, it's the central problem for physics. It's been the bone in our throat for a long time. **–Steven Weinberg.**

1 Introduction

Cosmology is the study of our Universe, its origin and evolution and is currently entering an era of high precision measurements, which will undoubtedly shape our understanding of our Universe and the physics that describes it.

As a discipline we can trace the origin of cosmology back to the beginning of 20th century with the theory of General Relativity proposed by A. Einstein and the discovery of the expansion of the Universe made by Edwin Hubble. These fundamental pieces along with the Cosmological Principle set the basis for the first cosmological models.With the increase of observations, the Cold Dark Matter paradigm of structure formation settled in CfA survey measurements led to the CDM model (Blumenthal et al., 1984; Davis et al., 1985). And with the increase in available observations from large scale structure , the paradigm of hierarchical structure formation .

However it was the discovery of the accelerated expansion of the Universe, made by two independent teams at the end of last century Riess et al. (1998); Perlmutter et al. (1999), the piece that led to the current cosmological paradigm called ΛCDM and which has become the standard model to describe the set of observations currently available. Although the cause of this acceleration is unknown, it is described as the consequence of a Cosmological Constant, Λ, with density ρ_Λ constant in space and time, term that is added to the Einstein-Hilbert action in order to produce late time acceleration even when there is no physical grounds to justify it.

Despite its simplicity, there is no fundamental understanding of its origin and this framework has serious theoretical issues namely the coincidence and fine-tunning problems (Weinberg, 1989; Sahni, 2002).

For these reasons alternative models that either modify gravity at large scales as prescribed by General Relativity or introduce a dynamical Dark Energy (DE) component have arisen.

Dynamical dark energy models are often characterized by the DE equation of state (EoS), $w \equiv P/\rho$, which is the ratio of the DE pressure to its density. Several models to parametrize its EoS as a function of time, $w(z)$, have arisen in the literature (Doran and Robbers, 2006; Rubin et al., 2009; Mortonson et al., 2010; Hannestad and Mortsell, 2004; Jassal et al., 2005; Ma and Zhang, 2011; Huterer and Turner, 2001; Weller

and Albrecht, 2002; Huang et al., 2011; de la Macorra, 2015). One of the most popular among them is the CPL parametrization (Chevallier and Polarski (2001),Linder (2003)), widely used in cosmological observational analysis.

The present value of DE EoS is restricted by observations to be close to -1 ($w = -1.019^{+0.075}_{-0.080}$ according to the 95% limits imposed by *Planck* data combined with other astrophysical measurements Ade et al. (2016a)). Nevertheless, the DE behavior and its properties at different cosmic epochs are much poorly constrained by current cosmological observations.

According to astrophysical observations our Universe is flat and dominated at present time by the DE component (Ade et al., 2016a), so data coming from late-time, low-redshift measurements such as Baryon Acoustic Oscillations (BAO) from Large Scale Structure surveys are those best suited for its analysis.

In my thesis I explored the observational signatures of alternative models for Dark Energy.

I was mainly focused on testing alternative models to a cosmological constant and constraining them with the current observational data.

Structure of the thesis

The structure of my thesis is the following. The required theoretical framework is covered in Chapter 2, where the observables of cosmic acceleration are introduced, as well as the derivation of basic equations for cosmology at background level and in a perturbative treatment.

In 3 I review the basic theoretical approaches for alternative models for cosmic acceleration. I consider the particular case of quintessence and $f(R)$-gravity models, in preparation for the two main results of this thesis.

Chapter 4 presents a model inspired in quintessence dynamics and which was published in Jaber and de la Macorra (2018), where the free parameters were tested against observations coming from late time dynamics, in concrete, Baryon acoustic oscillations from galaxy surveys and Lymann-α forest measurements, combined with the latest determination of the Hubble constant and the comprised CMB likelihood from Ade et al. (2016a). The second part of this chapter will deal with the linear and non-linear analysis of the perturbations for the model. The linear treatment was made in the Eulerian framework and considering two scenarios: clustering and smooth dark energy. The theoretical treatment of perturbations in Lagrangian scheme is discussed in the last part of Chapter 4, as well as their role in N-body simulations.

For the second part of this thesis I present an alternative model inspired in Modified Gravity models, in particular, $f(R)$ theories of gravity. The results of this are published in Jaime et al. (2018).

The abstracts of these papers are given at the end of this introduction.

Probing a Steep EoS for Dark Energy with latest observations

We present a parametrization for the Dark Energy Equation of State “EoS" which has a rich structure, performing a transition at pivotal redshift z_T between the present day value w_0 to an early time $w_i = w_a + w_0 \equiv w(z \gg 0)$ with a steepness given in terms of q parameter. The proposed parametrization is $w = w_0 + w_a(z/z_T)^q/(1 + (z/z_T))^q$, with w_0, w_i, q and z_T constant parameters. It reduces to the widely used EoS $w = w_0 + w_a(1 - a)$ for $z_T = q = 1$. This transition is motivated by scalar field dynamics such as for example quintessence models. We study if a late time transition is favored by BAO measurements combined with local determination of H_0 and information from the CMB. We find that our dynamical DE model allows to simultaneously fit H_0 from local determinations and Planck CMB measurements, alleviating the tension obtained in a ΛCDM model. We obtain a smaller χ^2 in our DE model than in ΛCDM showing that a dynamical DE is preferred with a reduction of 4.8%, 20.2% and 42.8% using BAO + H_0, BAO + CMB and BAO + CMB + H_0 datasets, respectively. However due to the increased number of free parameters in the EoS information criteria favors ΛCDM over our DE model at this stage. Nevertheless it is crucial to obtain the dynamics of DE from the observational data to show the path for theoretical DE models based on fundamental physics.

New parameterized equation of state for dark energy surveys

We present a new parameterization for the equation of state (EoS) $\omega_X = P_X/\rho_X$, which can reproduce a $f(R)$-like evolution with a precision between $[0.5\% - 0.8\%]$ over the numerical solutions. Also, our proposal can render a variety of popular $f(R)$ models that are considered as viable candidates for the cosmic late time acceleration. By using observational data from baryonic acoustic oscillations, supernovae and cosmic chronometers we investigate the constraints on the new EoS parameters. This proposal set a EoS formulation which can be used in an efficient way and makes a good candidate to be implemented in a variety of surveys in order to test the $f(R)$ generic behaviour.

2 Theoretical Background

This chapter revisits the Standard Cosmological Model, the evidence supporting the accelerated expansion of the Unive rse and the theoretical background required to follow the contents of Chapters 4-5. The derivations and notations here presented can be found in several textbooks and reviews. I have followed Dodelson (2003) and Amendola and Tsujikawa (2015) for the ideas on the standard cosmological model and its extensions and Peebles (1980), Bouchet et al. (1995b), Ma and Bertschinger (1995), and Bernardeau et al. (2002) for the perturbed regime.

2.1 Cosmological Model

In order to extract information on the nature of Dark Energy from observations we require a theoretical framework.

In 1917 Einstein (Einstein, 1917) introduced a cosmological model for a spatially homogeneous and isotropic Universe, filled with matter and positive curvature. He also assumed, incorrectly, that the Universe should be static and to this end he introduced an additional term known as a *Cosmological constant*, Λ. Edwin Hubble's direct discovery of the expansion of the Universe in 1929 proved the cosmological constant term to be unnecessary and the detection and interpretation of the Cosmic Microwave Background radiation (CMB) by Penzias and Wilson in 1965 ((Penzias and Wilson, 1965), (Dicke et al., 1965)) provided the evidence to support an Universe originated by a hot Big Bang. The discoveries made by Hubble led to the picture of an Universe which is homogeneous and isotropic (above certain scale of roughly 100Mpc) and whose dynamic follows the Einstein equations.

The Einstein Field Equations are

$$G_{\mu\nu} = 8\pi G T_{\mu\nu}, \tag{2.1}$$

where the Einstein tensor, $G_{\mu\nu}$, describes the properties of the geometry of space-time and is given by

$$G_{\mu\nu} = R_{\mu\nu} - \frac{1}{2} g_{\mu\nu} R \tag{2.2}$$

where $g_{\mu\nu}$ represents the metric tensor whereas the Ricci tensor, $R_{\mu\nu}$, and the Ricci scalar, R, are defined in terms of the metric through the relations:

$$R_{\mu\nu} \equiv g^{\lambda\kappa} R_{\lambda\mu\kappa\nu} \tag{2.3}$$

$$R \equiv g^{\lambda\kappa} g^{\mu\nu} R_{\lambda\mu\kappa\nu} = g^{\mu\nu} R_{\mu\nu}. \tag{2.4}$$

The homogeneous Universe

The Friedmann-Lemaître-Robertson-Walker (FLRW) metric describes an expanding Universe with an homogeneous and isotropic distribution of matter and energy. The line element in spheric comoving coordinates for this metric is:

$$ds^2 = g^{(0)}_{\mu\nu} dx^\mu dx^\nu = -dt^2 + a^2(t) \left[\frac{dr^2}{1 - Kr^2} + r^2 (d\theta^2 + sin^2\theta d\phi^2) \right], \tag{2.5}$$

where $c = 1$ (in natural units), $a(t)$ is the scale factor, and K, the spatial curvature parameter. For $K = 1$, the line element reduces to a three-dimensional sphere with fixed radius $a(t)r$, called *closed* Universe. In the case $K = 0$ we obtain a spatially *flat* Euclidean space, and finally $K = -1$ describes a pseudo-sphere called *open* Universe.

We can rewrite the FLRW metric in terms of the comoving radial coordinate χ, like

$$ds^2 = -dt^2 + a^2(t) \left[d\chi^2 + \Sigma^2(\chi)(d\theta^2 + sin^2\theta d\phi^2) \right] \tag{2.6}$$

where χ is defined as

$$d\chi = \frac{dr}{1 - Kr^2} \tag{2.7}$$

and

$$\Sigma(\chi) = \begin{cases} \sin\chi, & \text{if } K = +1, \\ \chi, & \text{if } K = 0, \\ \sinh\chi, & \text{if } K = -1. \end{cases} \tag{2.8}$$

From Equation (2.6) we note that $\chi = r$ if $K = 0$ and thus the normalization of $a(t)$ is arbitrary. Therefore, in flat space, we can set $a(t_0) = a_0 = 1$ at present time t_0.

The scale factor, $a(t)$, is a function of time and its evolution is described through the Einstein field equations (2.1).

The Universe, like many macroscopic physic systems, can be modeled like a perfect fluid. The isotropy and homogeneity conditions imply for the components of the stress tensor

$$\begin{aligned} T^{00} &= \rho(t) \\ T^{0i} &= 0 \\ T^{ij} &= \tilde{g}^{ij}(\vec{x}) a^{-2}(t) p(t) \end{aligned} \tag{2.9}$$

which can be put as

$$T^{\mu}_{\nu} = pg^{\mu}_{\nu} + (p+\rho)u^{\mu}u_{\nu}, \tag{2.10}$$

where u^{μ} is the four-velocity of the fluid (i.e. the local value of $\frac{dx^{\nu}}{d\tau}$ for a comoving element of the fluid), p the pressure and ρ the energy-density. Equation (2.5) and components (0-0) and (i-i) of Einstein equations give the Friedmann equations:

$$\left(\frac{\dot{a}}{a}\right)^2 = \frac{8\pi G\rho}{3} - \frac{K}{a^2} \tag{2.11}$$

$$\frac{d}{dt}\left(\frac{\dot{a}}{a}\right) + 4\pi G(\rho + p) = 0. \tag{2.12}$$

Equation (2.12) can be written alternatively as

$$\frac{1}{a}\frac{d^2a}{dt^2} = -\frac{4\pi G}{3}(\rho + 3p), \tag{2.13}$$

which states the conditions for the accelerated expansion of the Universe. From this equation we know that $\frac{d^2a}{dt^2} > 0$ only when $(\rho + 3p) < 0$.

Combining equations (2.11) and (2.12) we get the continuity equation,

$$\frac{d\rho}{dt} + 3\frac{\dot{a}}{a}(\rho + p) = 0, \tag{2.14}$$

which can be expressed like

$$d(\rho a^3) = -pd(a^3) \tag{2.15}$$

From (2.15) and the relation among pressure and density, $p = w\rho$, we get

$$\frac{dln\rho}{da} = -\frac{3(1+w)}{a} \tag{2.16}$$

which can be solved for every fluid following the continuity equation. We can integrate Equation (2.15) to obtain the evolution of the energy density for a fluid, as function of $a(t)$:

$$\rho a^{3(w+1)} = \rho_0, \tag{2.17}$$

where $\rho_0 \equiv \rho(a_0)$ is the present density and w the dimensionless constant parameter describing the fluid. In the case of a fluid with a varying equation of state, $w = w(a)$, we have

$$\rho(a) = \rho_0 \exp\left(3\int d\ln a(1 + w(a))\right) \equiv \rho_0 F(a) \tag{2.18}$$

In the standard cosmological scenario we have an Universe constituted by matter, also known as *dust*, radiation, and dark energy, which, in the case of a Cosmological constant, would appear as the term $\rho_\Lambda = \Lambda/(8\pi G)$ in equation (2.11).

In this work we identify the contributions to the *total* energy density as $\rho_{tot} = \rho_m + \rho_r + \rho_{DE}$, with ρ_m the matter energy density and ρ_r the radiation content. The energy density of neutrinos, ρ_ν, is neglected although in some texts it is absorbed in the radiation term. As for the the matter contribution, it contains both the baryonic matter (or ordinary matter), ρ_b, and the dark matter, ρ_c. The term ρ_{DE} represents the Dark Energy component and will be subject of Chapter 3.

The matter is modelled as a pressureless fluid, which is described by an equation of state, $w_m = 0$, while for the radiation we have $w_r = 1/3$ and $w_\Lambda = -1$ for the cosmological constant term, Λ.

We now may arrange Equation (2.11) as

$$\rho_{tot} = \frac{3H^2}{8\pi G} + \frac{3K}{8\pi G a^2} \tag{2.19}$$

Thus, by defining the *critical energy density*

$$\rho_{crit}(t) = \frac{3H^2}{8\pi G}, \tag{2.20}$$

we can constrain the curvature term depending on the total energy density as

$$\begin{aligned} \rho_{tot} > \rho_{crit} \quad &\rightarrow \quad K = +1, \\ \rho_{tot} = \rho_{crit} \quad &\rightarrow \quad K = 0, \\ \rho_{tot} < \rho_{crit} \quad &\rightarrow \quad K = -1. \end{aligned} \tag{2.21}$$

It is convenient to write the energy density of any fluid, i, in terms of the critical energy density, as $\Omega_i \equiv \rho_i/\rho_{crit}$, and to define a corresponding curvature energy density as $\Omega_K \equiv -K/(H^2 a^2)$ in such a way that we can rewrite the Friedmann equation like

$$H^2(a) = H_0^2 \left[\Omega_{r,0}(a_0/a)^4 + \Omega_{m,0}(a_0/a)^3 + \Omega_{K,0}(a_0/a)^2 + \Omega_{DE,0}F(a)\right] \equiv H_0^2 E(a) \tag{2.22}$$

where $F(a) = 1$ for a Cosmological Constant and the integral defined in Equation (2.18) in the most general case. We also defined the normalized Hubble function, $E(a) \equiv H^2(a)/H_0^2$, for convenience.

Given that the measurements of the CMB radiation (Bennett et al., 2013) indicate that the geometry of the Universe is very close to flat, $\Omega_k \approx 0$, the curvature term will be neglected in the rest of this work.

Cosmic time and distance measures

To match theory and observations we need analytical expressions for the different cosmological distances in an expanding Universe. To this end we need to define the key

observable quantity know as *cosmological redshift* (simply *redshift* for brevity) as function of scale factor:

$$z \equiv \frac{\lambda_o - \lambda_e}{\lambda_e} = \frac{a(t_o)}{a(t_e)} - 1 \tag{2.23}$$

between the time of emission t_e and observation t_o.

Recalling our definition Equation (2.25), we can take the case of a light beam then the line element is null, *i. e.* $ds^2 = 0$, and re-write the comoving distance as follows:

$$\frac{dt}{a(t)} = \frac{dr}{\sqrt{1 - Kr^2}} \longrightarrow \int_{t_1}^{t_0} \frac{dt}{a(t)} = \int_{r_1}^{r} \frac{dr}{\sqrt{1 - Kr^2}} \tag{2.24}$$

and therefore

$$\chi = -\int_{t_0}^{t_1} \frac{dt}{a(t)} \tag{2.25}$$

$$= \frac{1}{a_0 H_0} \int_0^z \frac{dz'}{\tilde{E}(z')} = \frac{1}{H_0} \int_1^a \frac{da'}{a'^2 E(a')} \tag{2.26}$$

where $\tilde{E}(z) \equiv \frac{H(z)}{H_0}$ and we have set the normalization $a_0 = 1$.

Using $z_0 = 0$ we can find an expression for the *age of the Universe*:

$$t_0 = \int_0^{t_0} = H_0^{-1} \int_0^{a_0} \frac{da}{aE(a)} = H_0^{-1} \int_{z_0}^{\infty} \frac{dz}{(1+z)\tilde{E}(z)}. \tag{2.27}$$

Physical distances relate to the comoving one, χ, by the scale factor:

$$d_A(z) = a(t)\chi = \frac{\chi}{1+z} = \frac{1}{1+z} \frac{1}{H_0} \int_0^z \frac{dz'}{E(z')}, \tag{2.28}$$

and the luminous distance, d_L, useful in experiments measuring the luminous flux coming from supernovae, is given in terms of (2.25) by

$$d_L \equiv \frac{\chi}{a}. \tag{2.29}$$

These expressions have a direct relation to the parameters included in the Hubble function, (2.22), and so, they depend on the cosmological model assumed.

2.2 Cosmic acceleration

By the late 1990's, two independent astronomy research groups (Riess et al. (1998); Perlmutter et al. (1999)) made one of the biggest discoveries of our times when they measured the luminous flux of type IA supernovae and determined that the Universe is accelerating in it expansion, against the predictions from General Relativity. Supernovae are standard candles, as their intrinsic luminosity is related to the decay rate and

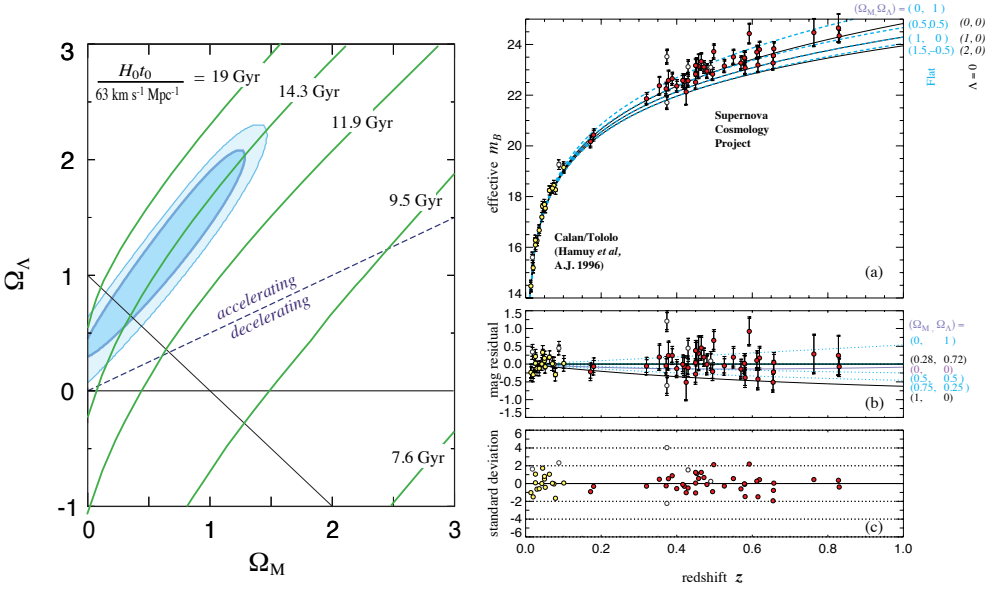

(a) Best-fit 68% and 90% confidence regions in the $\Omega_M - \Omega_\Lambda$ parameter space showing the statistical preference for a Cosmological constant term to account for the observed acceleration in the expansion rate of the Universe.

(b) Apparent magnitude m_B of the observed supernovae as function of redshift z. Solid and dashed lines correspond to different theoretical predictions for various combinations of Ω_M and Ω_Λ. In the bottom panels the residuals of the fits are shown.

Figure 2.1: Accelerated expansion of the Universe from SNeIa. Original f igures from (Perlmutter et al., 1999)

can therefore be robustly determined. Within these analysis the apparent magnitude of a SNIa is plotted against the redshift, and it was found that the observed supernovae at a given redshift appeared fainter than a decelerating universe would predict, shown in Figure 2.1 The plot shows that a dominating Ω_Λ is favoured by the statistical analysis of the data.

Ever since then, the community has tried to come up with an explanation for this acceleration. Even the less exotic among the different proposals postulates the existence of a new component of the Universe which could explain the repulsive force that seems to dominate over the gravity at large scales. This hypothesis and the Friedmann equations imply together the existence of an energetic component with negative pressure which corresponds to about two thirds of the total energetic budget of the Universe. Alternatively, the modification of General Relativity at large scales could be invoked as an explanation (Caldwell and Kamionkowski (2009), Woodard (2007)). More about this possibility would be the subject of Chapter 5

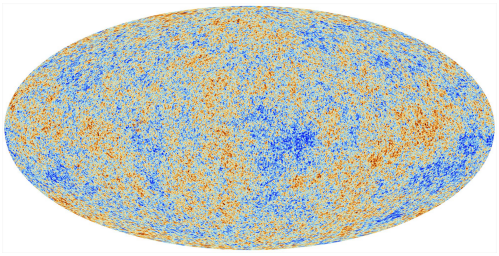

(a) The anisotropies of the Cosmic microwave background (CMB) as observed by Planck. The colour code represents the temperature fluctuations, hotter regions are shown in red, colder in blue

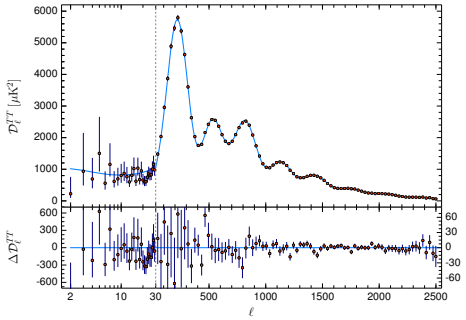

(b) Multipole expansion of the temperature anisotropies in spherical harmonics $\Delta T/T(\varphi, \vartheta)$

Figure 2.2: Most recent CMB temperature map taken with the Planck satellite (Planck Collaboration, 2018)

2.3 Cosmic Microwave Background and Baryonic Acoustic Oscillations

The cosmic microwave background (CMB) radiation is the best evidence supporting the Big Bang model and the most precise piece of observation in modern Cosmology (see Figure 2.2). It was formed when the Universe became transparent, at the *decoupling era*, and it originated fluctuations in the temperature of photons free-streaming that have been measured to be of the order of $\sim 10^{-5}$.

In the early Universe baryons and photons formed a hot plasma interacting through Thomson scattering. The radiation pressure of the photons prevented the structure formation while baryons and photons were tightly coupled. The competition between gravity and this pressure formed oscillations in the primordial plasma. Every single perturbation propagated outwards as an spheric acoustic wave with velocity c_s. In the primordial baryon-photon plasma we have

$$p = p_\gamma + p_b, \tag{2.30}$$

$$\rho = \rho_\gamma + \rho_b, \tag{2.31}$$

where ρ_γ is the photons energy density and ρ_b the baryonic component, and so c_s can be written in terms of the quantity known as baryon-to-photon ratio, $R \equiv \frac{3\rho_b}{4\rho_\gamma}$:

$$c_s = \frac{c}{\sqrt{3(1+R)}}. \tag{2.32}$$

Radiation and matter were in thermal equilibrium while there were enough free electrons but as the temperature cooled down nucleus were able to capture free electrons

forming atoms and so the free electron density dropped. The free mean path of photons increased up to the horizon distance and the Universe became transparent. At this point the interaction between photons and baryonic matter could not keep them in thermal equilibrium and so they decoupled. Since the radiation pressure could not prevent baryonic structures from collapsing, the era of growth of structure began while photons free-streamed to form the CMB.

When the pressure supported by the photons disappeared, the acoustic oscillations in the baryon-photon plasma got imprinted both in the CMB angular power spectrum and also in the spatial distribution of matter. Since baryons are only a small fraction of the matter content of the Universe and matter power spectrum has evolved significantly ever since the last scattering, the amplitude of these baryon acoustic oscillations is smaller than the corresponding acoustic peaks in the CMB.

The gravitational interaction drew the dark matter to cluster preferentially in the characteristic radius fixed in the baryons distribution when the acoustic oscillation stalled.

Characteristic for these oscillations is the *sound horizon* in comoving coordinates:

$$s = \int_0^{t_{dec}} \frac{c_s dt}{a} \sim 100 h^{-1} Mpc, \tag{2.33}$$

which is imprinted in the CMB and also in the perturbations of the matter density.

In this thesis we use these acoustic peaks to constrain the content of matter altogether with some alternative dark energy models.

The fluctuations imprinted in the matter distribution are called *Baryon acoustic oscillations* (BAO) and were first detected by (Colless et al., 2003), and (Eisenstein et al., 2005). Their measurement in galaxy surveys provides a *standard ruler* for length in the same way that supernovae provided a *standard candle* for astronomical observations.

The BAO feature has become the best way to probe the late time dynamics of the Universe and in consequence that of Dark Energy (DE). It is the cosmological tool explored by several experiments like the SDSS-IV (Dawson et al., 2016) and the Dark Energy Survey (DES) (Abbott et al., 2005) and the main probe that will be explored by future experiments like the Dark Energy Spectroscopic Instrument (DESI) (Levi et al., 2013) and Euclid (Laureijs et al., 2011).

The corresponding size, $r_{BAO}(z)$, is obtained by performing a geometric average of the distribution of galaxies both along and across the line of sight (Bassett and Hlozek, 2009):

$$r_{BAO}(z) \equiv \frac{s(z_d)}{D_V(z)}, \tag{2.34}$$

where the comoving sound horizon at the baryon drag epoch is represented by $s(z_d)$ and the dilation scale, $D_V(z)$, contains the information about the cosmology used in $H(z)$:

$$s(z_d) \equiv \frac{c}{H_0}\int_{z_d}^{\infty}\frac{dz}{H(z)\sqrt{3(R(z)+1)}}, \tag{2.35}$$

$$D_V(z) \equiv \left[\frac{z}{H(z)}\left(\int_0^z \frac{dz'}{H(z')}\right)^2\right]^{1/3} \tag{2.36}$$

The sound horizon $s(z_d) \equiv s_d$ depends upon the physics prior to the recombination era, given by $z_d \approx 1059$, and the baryon to photon ratio, $R(z) \equiv \frac{3\rho_b(z)}{4\rho_\gamma(z)}$. $D_V(z)$ (2.36), on the other hand, is sensitive to the physics of much lower redshifts, particularly to those surveyed by Large Scale Structure experiments. Such galaxy surveys often measure the distance ratio $\rho_b ao(z)$ as given by equation (2.51). However, it is also common to find reported the inverse ratio or measurements of the ratios $D_A(z)/s_d$ and $D_H(z)/s_d$ where $D_A(z)$ is the angular diameter distance (2.28) and $D_H(z) \equiv c/H(z)$.

Many experiments (Beutler et al. (2011), Kazin et al. (2014), Anderson et al. (2014), Ross et al. (2015), Font-Ribera et al. (2014), Delubac et al. (2015), and more recently Alam et al. (2016)) have measured this characteristic rule with increasing precision, providing a robust way to test the dynamics of DE through the study of Large Scale Structure of the Universe. Upcoming experiments like DESI (Dark Energy Spectroscopic Instrument Levi et al. (2013)) will probe the effects of DE on the expansion history using the BAO signature.

The size of sound horizon when baryons were released from the Compton drag of photons plays a key role in determining the acoustic peaks of baryons. This is called the *drag epoch* (Ade et al., 2016a) and it is defined by

$$\tau_d(\eta(z_{drag})) = 1 \tag{2.37}$$

where $\tau(\eta)$ is the optical depth given in terms of the electron mean number, n_e, and Thomson scattering cross section, σ_T:

$$\tau(\eta) \equiv \int_{\eta_0}^{\eta} \dot{\tau} d\eta' \tag{2.38}$$

and $\dot{\tau} = -an_e\sigma_T$. In this way the sound horizon can be written in terms of the speed

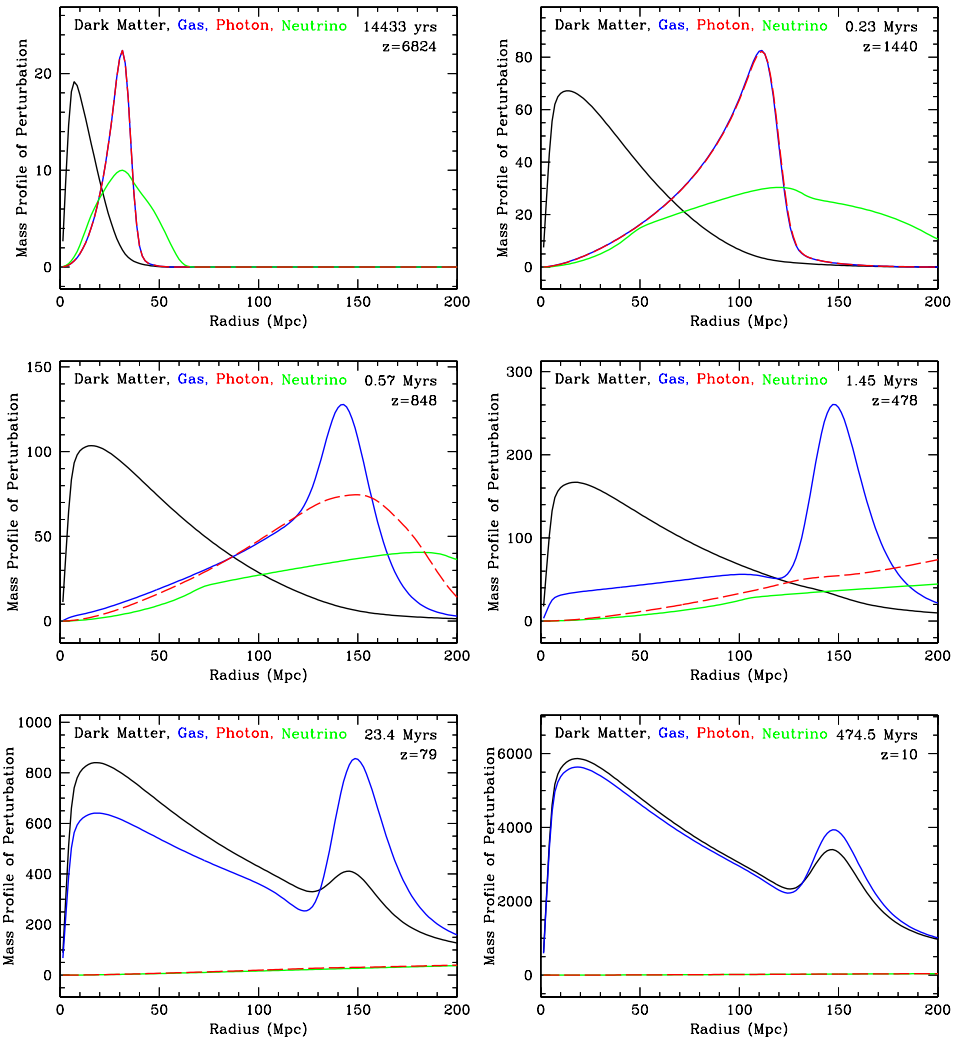

Figure 2.3: Snapshots of the evolution of a single spherical perturbation. The initial density perturbation propagates into the photons and baryons as a single pulse until the decoupling era. After decoupling, we can see the photons free-streaming to form the CMB. Since Dark Matter interacts only gravitationally it follows the baryonic potential forming a peak at a comoving radius of roughly 150Mpc where mass will eventually accrete during the structure formation process. Figure from (Bassett and Hlozek, 2009).

of sound in the fluid, c_s, and the Hubble function $H(z)$:

$$\begin{aligned} r_s(z_{drag}) &= \int_0^{\eta_{drag}} d\eta c_s(\eta) \\ &= \int_0^{\eta_{drag}} \frac{d\eta}{\sqrt{3(1+R)}} \\ &= \int_{z_{drag}}^{\infty} \frac{c_s dz}{H(z)} \end{aligned} \tag{2.39}$$

The acoustic oscillations set a preferred ruler for galaxies clustering which can be measured in their spatial distribution. As the Universe continues to expand so does this ruler. By measuring the size of this standard ruler in different epochs we can learn how the rate of expansion has changed in time.

Through observations we can measure the angular distribution and the redshift of galaxies:

$$\theta_s(z) = \frac{r_s(z_{drag})}{(1+z)d_A(z)} \tag{2.40}$$

$$\delta z_s = \frac{r_s(z_{drag})H(z)}{c} \tag{2.41}$$

Where $\theta_s(z)$ is obtained by observations perpendicular to the line of sight whereas δz_s comes from longitudinal observations. This means that the determination of the BAO signal both in tangential and radial directions provides us with measurements of the angular diameter distance (2.28) and the Hubble rate, respectively.

In figure 2.4 we can see the radial size along the line of sight given by $\frac{dz}{H(z)}$ and the transverse size is $d_A(z)\theta$. Since we do know the diameter, $r_s \equiv s$, we have:

$$s_\perp = d_A(z)\Delta\theta(1+z) \tag{2.42}$$

$$s_\parallel = \frac{cdz}{H(z)} \tag{2.43}$$

From (2.42) we have

$$\theta_s(z) = \frac{s_\perp(z_{drag})}{(1+z)d_A(z)} \tag{2.44}$$

while from (2.43) it follows

$$dz_s(z) = s_\parallel(z_{drag})H(z) \tag{2.45}$$

Furthermore, if $s_\perp = s_\parallel$ we obtain

$$d_A(z)\Delta\theta(1+z) = \frac{cdz}{H(z)} \Longrightarrow d_A(z)H(z) = \frac{cdz}{(1+z)\theta} \tag{2.46}$$

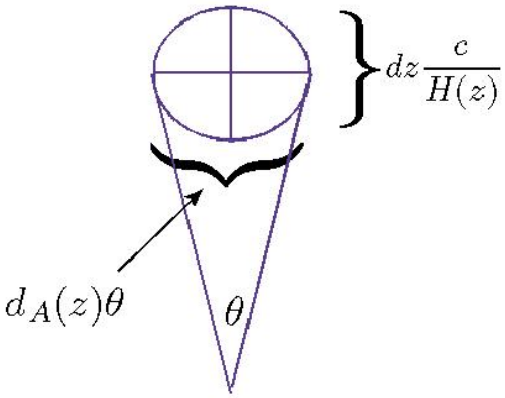

Figure 2.4: Schematic representation of the acoustic peak. The radial size of an object is given by $\frac{cdz}{H(z)}$ while the transverse is $d_A(z)\theta$. If it is spheric then we can constrain the product $d_A(z)H(z)$ by measuring $\frac{dz}{\theta}$. Figure from (Bassett and Hlozek, 2009)

from where we can constrain the product $d_A(z)H(z)$.

Since the value of $r_s \equiv s$ is known we actually can get $d_A(z)$ and $H(z)$ separately:

$$d_A(z) = \frac{s_\perp(z_{drag})}{(1+z)\theta_s} \tag{2.47}$$

$$H(z) = \frac{dz_s(z)}{cs_\parallel(z_{drag})} \tag{2.48}$$

A more robust measure (Seo and Eisenstein, 2003)is the geometric average of the parallel and transverse distances, which can be written in terms of the angular diameter distance, $d_A(z)$ and the Hubble function, $H(z)$:

$$\left[\theta_s^2(s)\delta z_s(z)\right]^{1/3} = \frac{r_s(z_{drag})}{[(1+z)^2 d_A^2(z) c H^{-1}(z)]^{1/3}} \tag{2.49}$$

From this we obtain what galaxy surveys refer to as dilation scale, $D_V(z)$,

$$D_V(z) \equiv \left[(1+z)^2 d_A^2(z)\frac{z}{H(z)}\right]^{1/3} \tag{2.50}$$

and from this, the so called *BAO distance* can be written as

$$r_{BAO} \equiv \frac{r_s(z_{drag})}{D_V(z)} \tag{2.51}$$

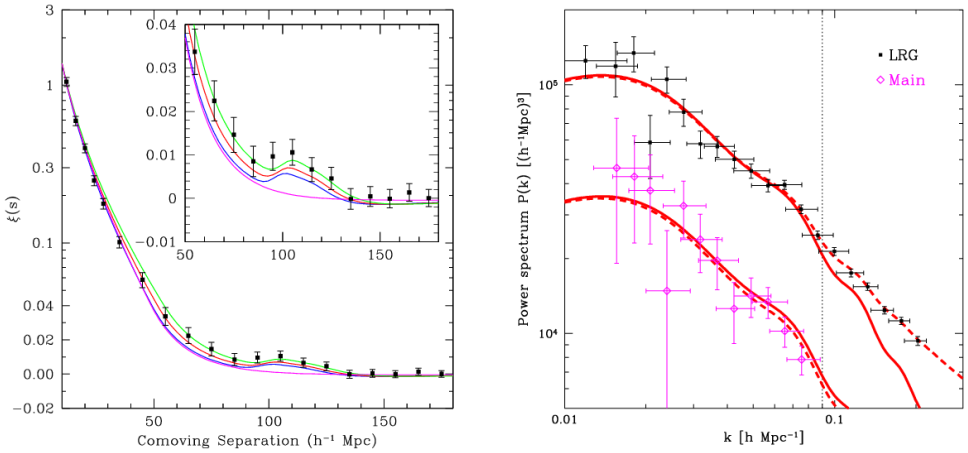

(a) BAO signature in the correlation function of SDSS red luminous galaxies sample. Detected originally by (Eisenstein et al., 2005). Curves are for different values of $\Omega_m h^2$ and $\Omega_b h^2$.

(b) Acoustic peaks imprinted in the matter power spectrum of SDSS galaxy sample both for Main sequence (magenta) and luminous red galaxies (red) samples. Figure taken from (Bassett and Hlozek, 2009).

Figure 2.5: First detection of the BAO signal both in configuration and Fourier space.

The BAO feature is a statistic standard ruler imprinted in the clustering of galaxies as a preferred scale which can be used to constrain the angular diameter distance and Hubble function when observed at different redshifts. The very first evidence of this signal detected both in the correlation function and also in the power spectrum can be seen in figure 2.5.

The two point correlation function, $\xi(r)$ and the power spectrum $P(k)$ are Fourier pairs. For instance for an one-dimensional spectra:

$$\xi(r) = \langle \delta(\vec{x})\delta(\vec{x}+r)\rangle \tag{2.52}$$

$$P(k) = \int_{-\infty}^{\infty} \xi(r) r^2 dr \tag{2.53}$$

Therefore any feature imprinted in the $\xi(r)$ will be observable as oscillations in the $P(k)$. This feature is what galaxy surveys use to study the history of expansion of the Universe.

In Chapters 4 and 5 we will use the measurements of this scale to study the dynamics of DE through its equation of state.

2.4 The perturbed Universe

Observations tell us that the Universe is highly inhomogeneous at scales smaller or around the order of 10Mpc. The origin of such inhomogeneities is understood via gravitational instabilities in the primordial fluid. In this paradigm, small density fluctuations became big enough to separate from the background expansion and collapsed gravitationally to form bounded systems (forming, eventually, the galaxies, clusters and voids observed in the Universe).

Here I briefly recap the derivation of the fluid equations in the Eulerian picture, and the assumptions that are made in perturbative treatments to solve the equations for a fluid in presence of gravity in an expanding Universe.

Perturbation theory in Cosmology (Bardeen, 1980a; Peebles, 1980; Mukhanov et al., 1992; Bernardeau et al., 2002), has been further worked out for higher orders (McDonald and Roy, 2009) and also a renormalized perturbation formalism up to certain scale have been developed (e.g. Crocce and Scoccimarro (2006)).

For completeness I also include the corresponding perturbative equations in a General Relativity framework (Malik) and point to the link between that regime and the Eulerian frame of the Newtonian regime.

Eulerian description for non-relativistic density perturbations

A first approximation to study the growth of primordial fluctuations is to consider the Universe like a Newtonian fluid and take into account the cosmic expansion. This approach will be valid only for scales well within the horizon so that curvature effects can be neglected and for the non-relativistic components.

The matter content of the Universe is modelled as a large collection of identical particles of mass m, interacting only through mutual gravitational attraction. In the case of low densities and sub-horizon scales, such forces are adequately described by Newtonian gravity in a uniformly expanding background, with the Newtonian potential sourced by inhomogeneities in the density field. The distribution function for such a set of particles obeys the Vlasov equation and its moments give the familiar fluid equations.

We are using the so called single-stream approximation, which assumes that all particles at a given point $\vec{x}$ move together with the same velocity $\vec{v}(\vec{x})$.

Perturbation analysis assume that the equations can be expanded in series:

$$\begin{aligned} \rho(\vec{r},t) &= \rho_0(t) + \delta\rho(\vec{r},t) \\ p(\vec{r},t) &= p_0(t) + \delta p(\vec{r},t) \\ \vec{v}(\vec{r},t) &= \vec{v_0}(t) + \delta\vec{v}(\vec{r},t) \\ \Phi(\vec{r},t) &= \Phi_0(t) + \delta\Phi(\vec{r},t) \end{aligned} \tag{2.54}$$

where we keep the background quantities as function of time only and add small perturbations which in general depend both of time and position. For instance, we assume $\delta\rho(\vec{r},t) << \rho_0(t)$, and so on for the other quantities (pressure, velocity and potential).

We can describe a fluid element with position and velocity

$$\vec{x} = a(t)\vec{r} \tag{2.55}$$

$$\vec{v} = \frac{d\vec{x}}{dt} \tag{2.56}$$

where $\vec{x}$ is the proper physical distance.

The temporal derivative along the direction of the trajectory in a fluid element gives

$$\frac{D}{Dt} = \frac{\partial}{\partial t} + \frac{d\vec{x}}{dt}\frac{\partial}{\partial \vec{x}} = \frac{\partial}{\partial t} + \vec{v}\cdot\vec{\nabla} \tag{2.57}$$

and writing down the acceleration of a fluid element gives the known *Euler equation*:

$$\frac{D\vec{v}}{Dt} = -\frac{1}{\rho}\vec{\nabla}p - \vec{\nabla}\Phi \longrightarrow \frac{\partial\vec{v}}{\partial t} + (\vec{v}\cdot\nabla)\vec{v} + \frac{1}{\rho}\vec{\nabla}p + \vec{\nabla}\Phi = 0. \tag{2.58}$$

The conservation of mass gives the *continuity equation*:

$$\frac{D\rho(\vec{r},t)}{Dt} = -\rho\vec{\nabla}\cdot\vec{v} \longrightarrow \frac{\partial\rho}{\partial t} + \nabla\cdot(\rho\vec{v}) = 0 \tag{2.59}$$

where Φ satisfies the *Poisson equation*:

$$\nabla^2\Phi = 4\pi G\rho. \tag{2.60}$$

To take into account the expansion of the Universe we make use of the chain rule in the derivatives

$$\vec{\nabla}_i \equiv \frac{\partial}{\partial x^i} = \frac{1}{a(t)}\frac{\partial}{\partial r^i} = \frac{1}{a(t)}\left(\vec{\nabla}_r\right)_i \tag{2.61}$$

$$\frac{d}{dt} \equiv \frac{\partial}{\partial t} + \vec{v_0}\cdot\vec{\nabla} = \frac{\partial}{\partial t}\mid_x + H(t)\frac{\partial}{\partial x}\mid_t \tag{2.62}$$

Inserting equations (2.54) in (2.58) - (2.59) and keeping terms up to first order in the perturbed quantities, we arrive to the following expressions

$$\delta\dot{\rho} + 3\frac{\dot{a}}{a}\delta\rho + \frac{\dot{a}}{a}(\vec{r}\cdot\vec{\nabla})\delta\rho + \rho_0\vec{\nabla}\cdot\delta\vec{v} = 0 \tag{2.63}$$

$$\delta\dot{\vec{v}} + \frac{\dot{a}}{a}\delta\vec{v} + \frac{\dot{a}}{a}(\vec{r}\cdot\vec{\nabla})\delta\vec{v} + \frac{c_s^2}{\rho_0}\vec{\nabla}\delta\rho + \vec{\nabla}\delta\Phi = 0 \tag{2.64}$$

$$\nabla^2\delta\Phi = 4\pi G\delta\rho. \tag{2.65}$$

were we used $\dot{()}$ to represent $\frac{\partial}{\partial t}$ and c_s^2 given by

$$c_s^2 = \left(\frac{\delta p}{\delta \rho}\right)_s, \tag{2.66}$$

where the subscript *s* denotes that the entropy does not change.

As long as the perturbations are small we can remain in the lineal regime. In this case the different modes evolve independently. To see this, we go to the Fourier space:

$$\Psi(\vec{r},t) = \frac{1}{(2\pi)^3}\int \Psi_k(t) exp\left[-\frac{i\vec{k}\cdot\vec{r}}{a(t)}\right] dr^3 \tag{2.67}$$

The density contrast can be defined like

$$\delta \equiv \frac{\delta\rho(\vec{r})}{\rho_0} \tag{2.68}$$

and the perturbation equations take the form

$$\begin{aligned} \dot{\delta_k} - \frac{i\vec{k}}{a}\cdot\vec{v_k} &= 0 \\ \frac{d(a\delta\vec{v_k})}{dt} - i\vec{k}c_s^2\delta_k - i\vec{k}\delta\Phi_k &= 0 \\ \delta\Phi_k = -\frac{4\pi G\rho_0}{k^2}a^2\delta_k & \end{aligned} \tag{2.69}$$

The decomposition of the perturbed velocity field in their perpendicular ($\vec{v_\perp}$) and parallel ($\vec{v_\parallel}$) parts

$$\delta\vec{v} = \vec{v_\perp} + \vec{v_\parallel}, \tag{2.70}$$

allows us to see that the rotational modes are not coupled to the density perturbations but they decay like $\frac{1}{a}$, i.e.

$$\frac{d[a\vec{v_\perp}(\vec{k})]}{dt} = 0 \Longrightarrow \vec{v_\perp} \propto \frac{1}{a(t)}. \tag{2.71}$$

We therefore have:

$$\vec{v_\parallel}(\vec{k}) = \frac{a}{i\vec{k}}\dot{\delta_k} \tag{2.72}$$

$$\ddot{\delta_k} + 2\frac{\dot{a}}{a}\dot{\delta_k} + \left(\frac{c_s^2k^2}{a^2} - 4\pi G\rho_0\right)\delta_k = 0 \tag{2.73}$$

From equation (2.73) we notice that the evolution of perturbations depends on the sign of the term in brackets, i.e., depends ons the difference between $\frac{c_s^2k^2}{a^2}$ and $4\pi G\rho_0$.

We can define the Jeans wavenumber like

$$K_J^2 \equiv 4\pi G\rho_0 \frac{a^2}{c_s^2} \tag{2.74}$$

and the corresponding Jeans wavelength

$$\lambda_J \equiv c_s \sqrt{\frac{\pi}{G\rho_0}} \tag{2.75}$$

This two quantities separate the gravitationally stable modes to those that are unstable and tell us that the modes with a wavelength $\lambda \ll \lambda_J$ are stabilized by pressure, or alternatively, modes with $k \gg K_J$ oscillate like a sound wave

$$\delta_k(t) \sim e^{\pm i\omega t} \tag{2.76}$$

with $\omega = \frac{c_s k}{a(t)(1-n)}$, assuming $a(t) \propto t^n$.[1]

On the other hand, for $\lambda > \lambda_J$ ($k \ll K_J$) we have growing modes or solutions that are gravitationally unstable.

In the particular case of a flat and matter dominated universe we can neglect the gradient of pressure term in c_s [2]

$$\begin{aligned} \frac{\dot{a}}{a} &= \frac{2}{3}t^{-1} \\ \rho_0 &= (6\pi G t^2)^{-1} \end{aligned} \tag{2.77}$$

and we end up with

$$\ddot{\delta_k} + \frac{4}{3t}\dot{\delta_k} - \frac{2}{3t^2}\delta_k = 0, \tag{2.78}$$

which has two independent solutions:

$$\begin{aligned} \delta_+(t) &= \delta_+(t_i)\left(\frac{t}{t_i}\right)^{2/3} \\ \delta_-(t) &= \delta_-(t_i)\left(\frac{t}{t_i}\right)^{-1} \end{aligned} \tag{2.79}$$

From this we can see that the growth of perturbations is a power law and it depends on the size of the particular mode (if it is bigger or smaller than the Jeans length) and the dominant fluid we have present.

[1] In general, the solution will be given in terms of a Bessel function and its exact form will depend on which fluid dominates the expansion of the universe and the evolution of c_s.

[2] Since $c_s^2 = 0$ for w=0, and the term in brackets in (2.73) becomes $4\pi G\rho_0 = \frac{8\pi G}{3}\rho_0 \frac{3}{2} = \frac{3}{2}H^2(t) = \frac{2}{3t^2}$.

The general solution will be a linear combination of $\delta_+(t)$ and $\delta_-(t)$: $\delta_m(\vec{r},t) = A(\vec{r})B(t) + C(\vec{r})D(t)$, but for late times we expect only the growing part to be important. In that case we see that in this regime, we can factorize the spatial and the time-depending parts.

The growing solution, $D(t)$ is usually normalized to the present time, this is, $D(z = 0) = 1$. With this, the evolution of δ at any position and time can be given in terms of the initial value, $\delta(\vec{r}, t_i)$ and the growth functions $D(t)$:

$$\delta(\vec{r},t) = \delta(\vec{r},t_i)\frac{D(t)}{D(t_i)} \tag{2.80}$$

Another useful quantity is the growh rate

$$f(a) = \frac{d\ln D(a)}{d\ln a} \tag{2.81}$$

and in (Wang and Steinhardt, 1998) it was shown that this can be fit by

$$f(a) = \Omega_m(a)^\gamma \tag{2.82}$$

with $\gamma \approx 6/11$ for ΛCDM.

For the radiation domination era we find that expansion occurs very rapidly and therefore it does not allow the perturbations to grow. In the epoch after matter-radiation equivalence (when radiation and matter energy densities are equal, i.e. $\rho_m(z_{eq}) = \rho_r(z_{eq})$; $z_{eq} \approx 3402$), the modes with $\lambda > \lambda_J$ grow like $\delta \propto a \propto t^{2/3}$, while those modes with $\lambda < \lambda_J$ oscillate like acoustic waves. The baryonic component of the matter perturbations do not grow until the decoupling era ($z_{dec} \approx 1091$) since they are tightly coupled to the photons prior the recombination. For a late time Universe we have a mixture of matter and dark energy and we know radiation to be subdominant. In that case we can rewrite Equation (2.65) as follows:

$$\begin{aligned}
\nabla_x^2\Phi &= 4\pi G(\rho_m + \rho_{DE}) \\
&= \frac{3H^2}{2\rho_{cr}}\left(\bar{\rho}_m(1+\delta_m) + \bar{\rho}_{DE}\right) \\
&= \frac{3H^2}{2}\left[\Omega_m(1+\delta_m) + \Omega_{DE}\right] \\
\nabla_r^2\Phi &= \frac{3a^2H^2}{2}\left[\Omega_m(1+\delta_m) + \Omega_{DE}(a)\right].
\end{aligned} \tag{2.83}$$

where we have assumed a flat Universe and smooth Dark Energy, which means $\delta_{DE} = 0$. For a multicomponent fluid we have:

$$\ddot{\delta} + 2\frac{\dot{a}}{a}\dot{\delta} + \left[\frac{c_s^2k^2}{a^2}\delta - 4\pi G\bar{\rho}\Sigma_j\epsilon_j\delta_j\right] = 0, \tag{2.84}$$

where $\epsilon_j \equiv \frac{\rho_j}{\bar{\rho}}$ is the term involving all the different fluids being considered (for instance $j = baryons, CDM, \Lambda, ...$).

In Chapter 4, the scenario of a late time Universe composed by matter and dark energy is analyzed and both the cases of clustering Dark Energy and Smooth Dark energy are discussed.

If we want to study the growth of perturbations from very early epochs, when the wavelength of any mode astrophysically relevant will be bigger than the horizon size, a relativistic treatment will be in order.

Relativistic regime

In perturbation theory the main goal is to find approximated solutions to Einstein field equations which can be considered as small deviations from a known exact solution, the background space-time solution. For perturbations evolving during the earlier stages of the Universe, the corresponding wavelength for astro-physically relevant modes will be bigger than horizon size and a fully relativistic treatment will be required.

The perturbation of any tensorial field $\mathbb{T}$ should then be given by the difference between its value in the physical space-time $\mathbb{T}$ and its value on the background space-time $\tilde{\mathbb{T}}$ In order to perform comparisons of such quantities one should consider them at the same point on a manifold. Since the manifolds representing the physical and background space-times are different the necessity for a prescription to identify events between them emerges. Such a prescription is what we understand as a gauge choice. In this case we will have to face the ambiguity of choosing the coordinate system, i.e., fixing the gauge ((Bardeen, 1980b), (Ma and Bertschinger, 1995)).

We need to modify both sides of the Einstein field equations, writing the energy-momentum and the metric tensors as:

$$\begin{aligned} g_{\mu\nu} &= \bar{g_{\mu\nu}} + \delta g_{\mu\nu} \\ T_{\mu\nu} &= \bar{T}_{\mu\nu} + \delta T_{\mu\nu}, \end{aligned} \tag{2.85}$$

where $\bar{g_{\mu\nu}}$ and $\bar{T_{\mu\nu}}$ stand for the background FLRW metric and $\delta g_{\mu\nu}$, $\delta T_{\mu\nu}$ represent the fluctuations around the background. If $\delta g_{\mu\nu}$ and $\delta T_{\mu\nu}$ are small, then a perturbative treatment is possible and we can obtain the linearized Einstein equations.

In the longitudinal gauge (also called the Newtonian gauge) in conformal time τ ($dt \equiv a d\tau$) we have the modified FLRW line element:

$$ds^2 = a^2(\tau)\left[-(1+2\Psi)d\tau^2 + (1+2\Phi)\delta_{ij}dx^i dx^j\right] \tag{2.86}$$

We can write the Einstein equations split into background and perturbed parts:

$$G^{\mu(0)}_{\nu} + \delta G^{\mu}_{\nu} = 8\pi G \left(T^{\mu(0)}_{\nu} + \delta T^{\mu}_{\nu} \right) \tag{2.87}$$

$$G^{\mu(0)}_{\nu} = 8\pi G T^{\mu(0)}_{\nu} \tag{2.88}$$

$$\delta G^{\mu}_{\nu} = 8\pi G \delta T^{\mu}_{\nu} \tag{2.89}$$

The background solutions that we have studied in the first part of this Chapter, are obtained from the zero-th order of equation (2.87).

The procedure to obtain the left hand side of (2.89) is widely covered in any textbook of Cosmology. It requires computing the non-vanishing components of the perturbed Christoffel symbols and use them to derive the perturbed Ricci tensor and Ricci scalar. With these, we know how the Einstein tensor is derived and, in this case, yields the following components:

$$\delta G^0_0 = 2a^{-2} \left[2\mathcal{H}(\mathcal{H}\Psi - \Phi') + \nabla^2 \Phi \right], \tag{2.90}$$

$$\delta G^0_i = 2a^{-2} \left(\Phi' - \mathcal{H}\Psi \right)_{|i} \tag{2.91}$$

$$\delta G^i_j = 2a^{-2} \left[(\mathcal{H}^2 + 2\mathcal{H}')\Psi + \mathcal{H}\Psi' - \Phi'' - 2\mathcal{H}\Psi' \right] \delta^i_j + a^{-2} \left[\nabla^2(\Psi + \Phi)\delta^i_j - (\Psi + \Phi)_{|^i_j} \right] \tag{2.92}$$

where we have used the notation from Amendola and Tsujikawa (2015), where the subscript "|" represents a covariant derivative with the spatial 3-metric and $\nabla^2 f \equiv f^{;\mu}_{;\mu}$.

Additionally, we need to work out the right hand side of Equation (2.89). For a single fluid, the EMT reads as

$$T_{\mu\nu} = (\rho + P) u_\mu u_\nu + P g\mu\nu, \tag{2.93}$$

where we have neglected the terms arising from the *heat flux vector* and also the *viscous shear tensor* since we are assuming a perfect fluid in which the internal energy is dominant over the total energy.

The corresponding perturbed EMT, δT^{μ}_{ν} for a perfect fluid is:

$$\delta T^{\mu}_{\nu} = \rho \left[\delta \left(1 + \frac{\delta P}{\delta \rho} \right) u_\nu u^\mu + (1 + w) \left(\delta u_\nu u^\mu + u_\nu \delta u^\mu + \frac{\delta P}{\delta \rho} \delta \delta^\mu_\nu \right) \right] \tag{2.94}$$

The components of the energy-momentum tensor (EMT) are:

$$\delta T^0_0 = -\delta\rho, \tag{2.95}$$

$$\delta T^0_i = -\delta T^0_i = (1 + w)\rho v^i, \tag{2.96}$$

$$\delta T^1_1 = \delta T^2_2 = \delta T^3_3 = \frac{\delta P}{\delta \rho} \delta\rho. \tag{2.97}$$

With components (2.90)-(2.92) and (2.95)-(2.97) we can get the perturbed Einstein equations (2.89):

$$3\mathcal{H}(\mathcal{H}\Psi - \Phi') + \nabla^2\Phi = -4\pi G a^2 \delta\rho, \tag{2.98}$$

$$\nabla^2(\Phi' - \mathcal{H}\Psi) = 4\pi G a^2 (1+w)\rho\theta, \tag{2.99}$$

$$\Phi'' + 2\mathcal{H}\Phi' - \mathcal{H}\Psi' - (\mathcal{H}^2 + 2\mathcal{H}')\Psi = -4\pi G a^2 \frac{\delta P}{\delta\rho}\delta\rho. \tag{2.100}$$

The conservation of the energy-momentum tensor, $T^{\mu}_{\nu;\mu} = 0$, translates in the first-order continuity equation:

$$\delta T^{\mu}_{\nu;\mu} = 0 \tag{2.101}$$

Recalling the operation of covariant divergence and the conservation equation, (2.101), in addition to the perturbed Christoffel symbols, we arrive to the *perturbed continuity equation* and the *perturbed Euler equation*:

$$\delta T^{\mu}_{0;\mu} = 0 \quad \longrightarrow \quad (\delta\rho)' + 3\mathcal{H}(\delta\rho + \delta P) = -(\rho + P)(\theta + 3\Phi') \tag{2.102}$$

$$\delta T^{\mu}_{i;\mu} = 0 \quad \longrightarrow \quad (\delta q)' + 3\mathcal{H}\delta q = -a\delta P - (\rho + P)a\Psi \tag{2.103}$$

where we have used $\delta q \equiv a(\rho + P)v$ and v represents the velocity potential.

Using the continuity equation at zeroth order, we can rewrite (2.102) as follows:

$$\delta' + 3\mathcal{H}(c_s^2 - w)\delta = -(1+w)(\theta + 3\Phi') \tag{2.104}$$

and taking the gradient of equation (2.103), we get the more familiar form of the perturbed Euler equation:

$$\theta' + \left[\mathcal{H}(1 - 3w) + \frac{w'}{1+w}\right]\theta = -\nabla^2\left(\frac{c_s^2}{1+w} + \Psi\right) \tag{2.105}$$

The important remark to be made from the equations here presented is on the connection between this formalism and the one developed in section 2.4.

To see it we take the case of a fluid which is pressureless ($w = 0$) in the absence of perturbations but for which $\delta P/\delta\rho \ll 1$, and see how its perturbations behave when we take the sub-horizon limit. This limit means that the scales of interest, $\lambda_p = \left(\frac{2\pi}{k}\right)^4$, are well inside the Hubble radius, this is $\lambda_p \ll \mathcal{H}^{-1}$ and in this case equation (2.99) reduces to:

$$\nabla^2(\Phi' - \mathcal{H}\Psi) = 4\pi G a^2(1+w)\rho\theta \quad \longrightarrow \quad k^2(\Phi' - \mathcal{H}\Psi) = 4\pi G a^2(1+w)\rho\theta$$

$$(\Phi' - \mathcal{H}\Psi) \approx 0 \tag{2.106}$$

and so, the Fourier transform of (2.98) reduces to:

$$\begin{aligned} k^2\Phi &= 4\pi G a^2 \rho\delta \\ &= \frac{3}{2}\mathcal{H}^2\delta \end{aligned} \tag{2.107}$$

which we use in (2.104) we get the conservation equation in the Newtonian limit:

$$\delta' = -\theta, \tag{2.108}$$

and the perturbed Euler equation, (2.103), in Fourier space, reduces to:

$$\theta' = \mathcal{H}\theta + \delta P/\delta\rho k^2\delta - k^2\Phi. \tag{2.109}$$

These two equations, combined yield the second order differential equation for the density contrast in the sub-horizon limit:

$$\delta'' + \mathcal{H}\delta' + \left(c_s^2 k^2 - \frac{3}{2}\mathcal{H}^2\right)\delta = 0 \tag{2.110}$$

This shows that equation (2.73) can be derived from a fully relativistic approach and effectively describes cosmological perturbations of dust growing due to gravitational instabilities when inside the horizon.

3
Dark Energy models

This chapter is a brief revision of the main theoretical approaches for modeling the accelerated expansion as an alternative to the Cosmological Constant term. mostly relying on discussions presented in reviews like (Copeland et al., 2006), or textbooks such as (Amendola and Tsujikawa, 2015).

As stated in Chapter 2, the standard ΛCDM paradigm is based on the assumptions of homogeneity and isotropy of the Universe at large scales, the validity of General Relativity and the cosmological constant term as cause of the accelerated cosmic expansion. Although it has been proven successful when tested against observations it faces some major theoretical issues such as the extreme fine-tuning problem known as the *cosmological constant problem* (Weinberg, 1989) which leads to the necessity of extending it.

For instance, we can estimate the contribution of a Cosmological Constant term at present time to be $\rho_\Lambda^{obs} \approx \frac{3H_0^2}{8\pi G} \sim 10^{-47} GeV^4$. The origin of such low value for ρ_Λ remains as one of deepest problems in theoretical physics.

Instead of dealing with this matter, alternative routes have been proposed in a variety of flavors. It is customary in the literature to divide the approaches for the construction of dark energy models in two, depending on the physical interpretation for the origin of the modification, although there is no fundamental meaning in this classification.

In the first class, the so called *Modified matter models*, it is assumed that some exotic form of matter is contained in the energy momentum tensor of the Einstein equations (2.1), $T_{\mu\nu}$, which is responsible for the late time acceleration of the Universe. More on this kind of models will be subject of section 3.1.

The second approach, known as *modified gravity models*, refers to modifications of the Einstein tensor, $G_{\mu\nu}$ ((2.2)) and postulates that General Relativity has to be modified on cosmological distances. A particular example of these modifications will be contained in section 3.2.

In the simplest scenario we can take a phenomenological approach and consider the Dark Energy contribution, ρ_{DE} to be a perfect fluid so dissipative terms will not be

present. In this situation we have a function of $a(t)$ which is equivalent to have

$$p_{DE}(\rho_{DE}) = w(a)\rho_{DE} \tag{3.1}$$

where $w(a)$ is the equation of state of this dark fluid and it can be parameterized to match observations. In the section 3.3 we will review some of the proposals for this kind of proposals in the literature.

3.1 Quintessence

Scalar fields naturally arise in Particle Physics and are one of the most studied candidates for Dark Energy. These provide the possibility of explaining Dark Energy from first principles with physics beyond the Standard Model. Particularly well motivated are those scalar fields with only gravitational interaction Ratra and Peebles (1988); Wetterich (1995); Steinhardt et al. (1999); de la Macorra and Piccinelli (2000).

The evolution of Dark Energy in this kind of models will generally depend on the scalar field ϕ, the shape of the potential $V(\phi)$ and its initial conditions. However, special interest has been devoted to tracker fields Steinhardt et al. (1999), since in this case the behaviour of the scalar field ϕ is weakly dependent on the initial conditions set at an early epoch, well before matter-radiation equality. In this class of models a fundamental question is why dark energy is relevant now, known as the *coincidence problem*, and this can be understood by the insensitivity of the late time dynamics on the initial conditions of ϕ.

Scalar field theories which have a canonical scalar field, ϕ, that interacts with the other components only gravitationally, are known as *quintessence* and can be represented by a minimally coupled lagrangian replacing the cosmological constant term in the Einstein-Hilbert action:

$$\begin{aligned} S &= \int d^4x\sqrt{-g}\left[\frac{1}{2\kappa^2}R + \mathcal{L}(\phi)\right], \\ \mathcal{L}(\phi) &= -\frac{1}{2}g^{\mu\nu}\partial_\mu\partial_\nu\phi + V(\phi) \end{aligned} \tag{3.2}$$

where $\kappa^2 = 8\pi G$ and $V(\phi)$ the potential term, which is usually motivated by some theoretical model. This kind of models assume that the Dark energy term comes from a new physical field.

If we recall from the acceleration equation (2.13), we need a value of the equation of state $w_{DE} \equiv P_{DE}/\rho_{DE} < -1/3$, which, in the case of a scalar field translates in the requirement of a sufficiently flat potential, $\dot{\phi}^2 \gg V(\phi)$, or *slow roll condition*. Additionally we require a form of $V(\phi)$ such as to have a long enough matter domination era to ensure the proper amount of structure formation at late times.

At earlier times, during the radiation domination era, the scalar field must fulfil stringent conditions on its energy density, Ω_ϕ, in order to be compatible with the abundance of light elements at the epoch of nucleosynthesis.

Some models for dark energy and dark matter have been proposed using gauge groups, similar to QCD in particle physics, and have been studied to understand the nature of Dark Energy De la Macorra (2003); de la Macorra and Stephan-Otto (2001) and also Dark Matter de la Macorra (2010, 2004).

In Chapter 4, we analyse a model for the equation of state of dark energy inspired in scalar field dynamics such as quintessence.

3.2 Modified gravity: $f(R)$ gravity

Within the models belonging to *modified gravity* theories, the origin of dark energy is proposed to be some geometric modification of Einstein gravity. Given that the General Relativity has proven to be very successful describing phenomena of different nature, its possible extensions or modifications have several restrictions imposed.

This section focuses on a particular kind of modification, known as $f(R)$ gravity, and in chapter 5 we present and analyze a parametric model inspired in this kind of theories.

The general action for a $f(R)$ theory of gravity is given by

$$S = \frac{1}{2\kappa^2}\int d^4x\sqrt{-g}f(R) + S_m(g_{\mu\nu},\psi), \tag{3.3}$$

where S_m is the standard matter action and ψ represents collectively the matter fields which obey the known conservation equations.

There are two approaches to derive field equations from action (3.3), and in what follows we work in the *metric formalism* and following the ideas detailed in the review by Jaime et al. (2012). In this formalism, variation of action (3.3) with respect to the metric $g_{\mu\nu}$ results in the field equations:

$$f_R R_{\mu\nu} - \frac{1}{2}f g_{\mu\nu} - (\nabla_\mu\nabla_\nu - g_{\mu\nu}\Box)\, f_R = \kappa^2 T_{\mu\nu} \tag{3.4}$$

where f_R indicates $\partial_R f$, $\Box = g^{\mu\nu}\nabla_\mu\nabla_\nu$ is the covariant D'Alambertian and $T_{\mu\nu}$ is the energy-momentum tensor of matter. Equations (3.4) can be rewritten in terms of the Einstein tensor, $G_{\mu\nu} = R_{\mu\nu} - g_{\mu\nu}R/2$, as follows

$$\begin{aligned} &f_R G_{\mu\nu} - f_{RR}\nabla_\mu\nabla_\nu R - f_{RRR}(\nabla_\mu R)(\nabla_\nu R) \\ &\quad + g_{\mu\nu}\left[\frac{1}{2}(Rf_R - f) + f_{RR}\Box R + f_{RRR}(\nabla R)^2\right] = \kappa^2 T_{\mu\nu}, \end{aligned} \tag{3.5}$$

where the term $(\nabla R)^2$ indicates $g^{\mu\nu}(\nabla_\mu R)(\nabla_\nu R)$. Taking the trace of this equation and using $T \equiv T^\mu \mu$, we obtain:

$$\Box R = \frac{1}{3f_{RR}}\left[\kappa^2 T - 3f_{RRR}(\nabla R)^2 + 2f - Rf_R\right], \tag{3.6}$$

Using (3.6) into (3.5) we can find the expression for $G_{\mu\nu}$ and the total energy-momentum tensor:

$$\begin{aligned} G_{\mu\nu} =& \frac{1}{f_R}\left[f_{RR}\nabla_\mu\nabla_\nu R + f_{RRR}(\nabla_\mu R)(\nabla_\nu R)\right. \\ & \left. -\frac{g_{\mu\nu}}{6}(Rf_R + f + 2\kappa^2 T) + \kappa^2 T_{\mu\nu}\right] \end{aligned} \tag{3.7}$$

Equations (3.6) and (3.7) are the basic equations for $f(R)$ theories.

A second order differential equation for the Ricci scalar can be obtained taking the trace of (3.4) and from (3.5) we get the modified Friedman equations:

$$\ddot{R} = -3H\dot{R} - \frac{1}{3f_{RR}}\left[3f_{RRR}\dot{R}^2 + 2f - f_R R + \kappa T\right], \tag{3.8}$$

$$H^2 = -\frac{1}{f_{RR}}\left[f_{RR}H\dot{R} - \frac{1}{6}(Rf_R - f)\right] - \frac{\kappa T_t^t}{3f_R}, \tag{3.9}$$

$$\dot{H} = -H^2 - \frac{1}{f_R}\left[f_{RR}H\dot{R} + \frac{f}{6} + \frac{\kappa T_t^t}{3}\right], \tag{3.10}$$

where $H = \dot{a}/a$.

We notice that in the particular case of $f(R) = R$ the field equations reduce to those of General Relativity.

Several restrictions need to be imposed to the otherwise general $f(R)$ function, in order to make them stable and cosmologically viable models for Dark energy (see for instance Amendola et al. (2007)). For instance, just as in the case of scalar fields, we need to ensure that we have a sufficiently long matter domination era. On the other hand, gravity is severely constrained by local gravity tests, which also imposes several conditions on the $f(R)$ function:

(i) $f_R > 0$ for $R \geq R_0$.

(ii) $f_{RR} > 0$ for $R \geq R_0$.

(iii) $f(R) \to R - 2\Lambda$ for $R \gg R_0$.

(iv) $0 < \frac{Rf_{RR}}{f_r}(r = -2) < 1$ at $r = -\frac{Rf_R}{f} = -2$,

where R_0 is the Ricci scalar at present epoch.

The following are viable $f(R)$ models for dark energy:

a) Hu & Sawicki model [1] (Hu and Sawicki, 2007)

$$f(R) = R - R_{\rm HS}\frac{c_1\left(\frac{R}{R_{\rm HS}}\right)^n}{c_2\left(\frac{R}{R_{\rm HSHS}}\right)^n + 1}\,, \tag{3.11}$$

b) Starobinsky model (Starobinsky, 2007)

$$f(R) = R + \lambda R_S\left[\left(1+\frac{R^2}{R_S^2}\right)^{-q} - 1\right], \tag{3.12}$$

c) The exponential model (Linder, 2009)

$$f(R) = R + \beta R_*(1 - e^{-R/R_*}). \tag{3.13}$$

All the parameters involved in these functions, n, c_1, c_2, R_{HS}, R_S, and R_*, should be constrained according to observations. For instance, for the Hu & Sawicki model with $n = 4$, $c_1 \approx 1.25 \times 10^{-3}$, $c_2 \approx 6.56 \times 10^{-5}$ and $R_{HS} \approx 0.24H_0^2$.

These models can provide an accelerated evolution, with a $w \approx -1$. In the case of Hu & Sawicki (3.11) and Starobinsky models (3.12), such evolution goes asymptotically to the de Sitter point ($R_{(z\to-1)} > 0$). In the case of the Exponential model (3.13), the future is asymptotically $R_{(z\to-1)} = 0$ with a transient but apparently long enough accelerated epoch.

3.3 Parameterization of the Equation of State of Dark Energy

Now, in a phenomenological approach, there is a vast amount of proposals to parameterize the dark energy equation of state. Some are listed in the bibliography Chevallier and Polarski (2001); Linder (2003); Doran and Robbers (2006); Krauss et al. (2007); Linder (2006b); Rubin et al. (2009); Sollerman et al. (2009); Mortonson et al. (2010); Hannestad and Mortsell (2004); Jassal et al. (2005); Ma and Zhang (2011); Huterer and Turner (2001); Weller and Albrecht (2002); Huang et al. (2011); de la Macorra (2015); Barboza and Alcaniz (2008).

These are an attempt to describe the dynamics of dark energy without specifying a particular theory and to confront it with observations through the relation of the dark energy density and its equation of state parameter, $w(z)$:

$$\rho(z) = \rho_0 \exp\left(\int_0^z dz' \frac{3[1+w(z')]}{1+z'}\right), \tag{3.14}$$

[1] In the Hu-Sawicki model the parameters c_1 and c_2 are related with Ω_m^0 and f_R^0 respectively and according as is explained in (Hu and Sawicki, 2007)

In terms of the Hubble parameter, $H \equiv (\frac{1}{a})\frac{da}{dt}$, equation (2.11) can be rewritten as

$$H^2 = \left(\frac{\dot{a}}{a}\right)^2 \tag{3.15}$$

$$= H_0^2 \left[\Omega_m^{(0)}(1+z)^3 + \Omega_r^{(0)}(1+z)^4 + \Omega_{DE}^{(0)} f_{DE}(z)\right] \tag{3.16}$$

were $\Omega_i^{(0)} \equiv \frac{\rho_i^{(0)}}{\rho_{cr}^{(0)}}$, with $\rho_{cr}^{(0)} \equiv \frac{3H_0^2}{8\pi G}$, and $H_0 = 100 \cdot h \cdot km/sMpc^{-1}$ is the value of $H(z)$ today. Subscript (0) indicates quantities evaluated at z=0. The term $f_{DE}(z)$ encodes the dynamics of dark energy fluid parameterized by its EoS as function of redshift, $w_{DE}(z)$. This derives from equation (3.14) for the $\rho_{DE}(z)$ term alone:

$$f_{DE}(z) = exp\left(3\int_0^z dz' \frac{1+w_{DE}(z')}{1+z'}\right) \tag{3.17}$$

The most popular among them is the Chevallier-Polarski-Linder parametrization (or CPL) Chevallier and Polarski (2001); Linder (2003). This can be seen as a Taylor expansion of the equation of state around $a(t) = a_0$. It gives the equation of state parameter w for the dark energy as a linear function of the scale factor a, namely

$$w(a) = w_0 + w_a(1-a) \tag{3.18}$$

$$w(z) = w_0 + w_a \frac{z}{1+z}$$

expression that has been widely used in many cosmological observational analysis.

Some other models proposed in the literature are the Linear model (3.19) (Cooray and Huterer, 1999) and the Barboza-Alcaniz model (3.20) (Barboza and Alcaniz, 2008):

$$w(z) = w_0 - w_i z \tag{3.19}$$

$$w(z) = w_0 + w_i \frac{z(1+z)}{1+z^2} \tag{3.20}$$

Today's value of the dark energy EoS (represented by the parameter $w_0 \equiv w(z = 0)$ in equations (3.19), (3.19), (3.20) and (4.1) is restricted by observations to be close to -1 ($w = -1.019^{+0.075}_{-0.080}$ according to the 95% limits imposed by *Planck* data combined with other astrophysical measurements Ade et al. (2016a)). Nevertheless, the behaviour and properties at different cosmic epochs is much poorly constrained by current observations.

Figure 3.1 shows four different parameterizations for dark energy equation of state as function of redshift, namely equations (3.19)-(3.20) and (4.1). The latter is introduced in chapter 4 and the constraints imposed by observations upon its free parameters are discussed.

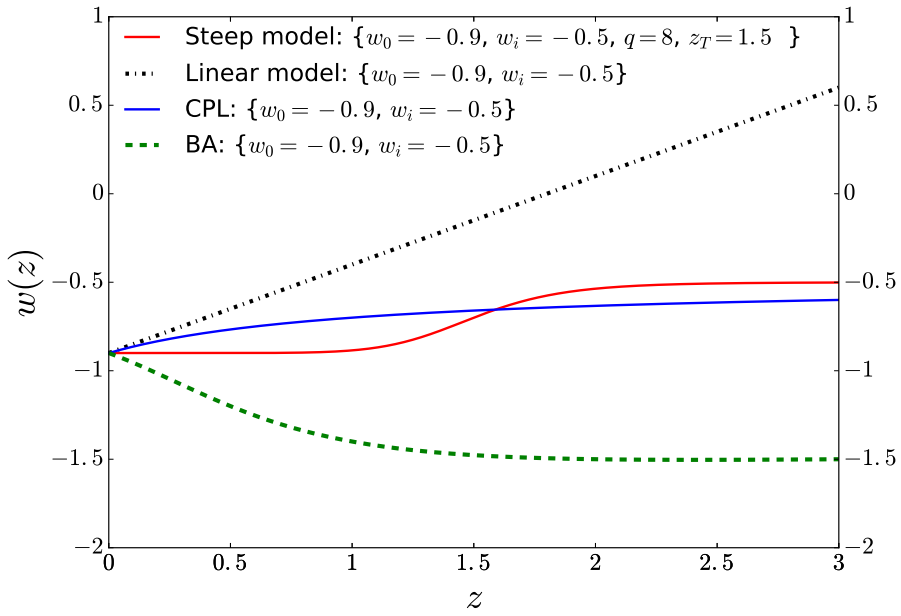

Figure 3.1: Evolution of the equation of state for different parametrizations. The blue solid curve corresponds to equation (3.19). The long dashed green curve represents the BA Barboza and Alcaniz (2008) parametrization introduced in equation (3.20). The dot-dashed black curve corresponds to the parametrization introduced in Cooray and Huterer (1999) shown in (3.19). And the red solid curve corresponds to equation (4.1), whose details are discussed in section 4.1

4 Steep Equation of State

The contents of this chapter are contained in the paper entitled "Probing a Steep EoS for Dark Energy with latest observations", (M. Jaber and A. de la Macorra), Astropart. Phys. 97, 130 (2018).

4.1 Steep equation of State for Dark Energy

As it was stated previously the behaviour and properties of DE state equation are fairly well constraint at redshift $z = 0$ but they are poorly understood by current observations as a function of time. Therefore the interest in studying w at a late time and see if a transition in the EoS takes place. Inspired by scalar field dynamics, the parametrization used here is

$$w(z) = w_0 + (w_i - w_0)\frac{(z/z_T)^q}{1 + (z/z_T)^q} \tag{4.1}$$

which reduces to the CPL equation of state (3.19) in the case where $q = z_T = 1$:

$$\begin{aligned} w(z)|_{z_T=q=1} &= w_0 + (w_i - w_0)\frac{z}{1+z} \\ &= w_0 + w_a(1-a) \end{aligned} \tag{4.2}$$

but it possesses a richer structure allowing for a steep transition to take place at a pivotal redshift $z = z_T$ with a steepness modulated by the exponent q. The value $w(z_T) = (w_0+w_i)/2$ gives the middle point of the transition between w_0 and the early time $w_i = w(z \gg 1)$. This transition is motivated by scalar field dynamics such as quintessence models.

One thing to be noted is that this EoS does not have a constant slope within the two regimes: $w(z = 0) \to w_0$, $w(z >> 0) \to w_i$, but it makes a transition between them at a redshift $z = z_T$, taking a value of $w(z_T) = \frac{w_0+w_i}{2}$. The parameter q modulates the steepness of the transition featured: the greater the value for q, the steeper the transition we will have, as figure 4.1 shows.

Recalling equation (3.15) we see how the dynamics for dark energy set by its equation of state drives the expansion of the Universe at late times:

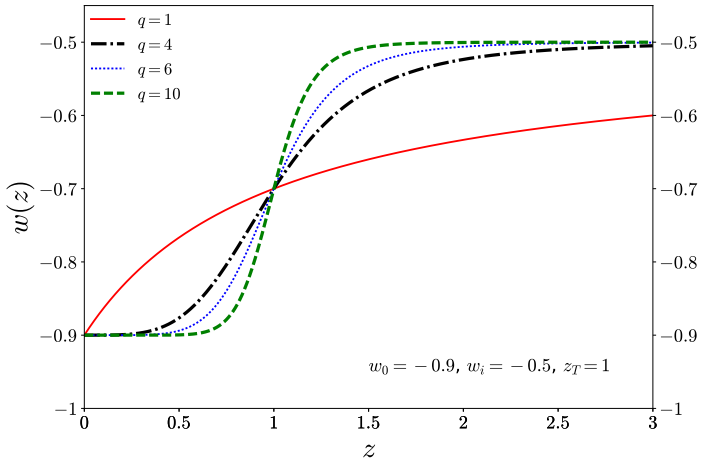

Figure 4.1: Evolution of the DE EoS in equation (4.1) with $q = 1$ (solid red), $q = 4$ (black dot-dashed), $q = 6$ (blue dotted), and $q = 10$ (green dashed). The value for the other parameters were fixed to $w_0 = -0.9$, $w_i = -0.5$ and $z_T = 1$. The solid red curve takes the special case $q = z_T = 1$, representing the CPL parametrization (3.19).

$$H(z) = H_0\sqrt{\Omega_r(1+z)^4 + \Omega_m(1+z)^3 + \Omega_{DE}F(z)}, \tag{4.3}$$

where the function $F(z)$ encodes the information of the Dark Energy fluid, as prescribed by its equation of state:

$$\begin{aligned} F(z) &\equiv \frac{\rho_{DE}(z)}{\rho_{DE}(0)} \\ F(z) &= \exp\left(-3\int_0^z dz' \frac{1+w(z')}{1+z'}\right). \end{aligned} \tag{4.4}$$

4.2 Background analysis

Observational data

Baryon Acoustic Oscillations

To test the dynamics of Dark Energy, measurements of the expansion history of the Universe at late times when it is driven by the DE component, are required. Ever since its first detection (Colless et al. (2003) and Eisenstein et al. (2005)) the Baryon Acoustic Oscillation (BAO) feature has been widely used as a powerful probe for cosmology becoming the standard rulers of choice just as Type Ia supernovae (SNIa) were at the early part of the 21st century during the beginning of the so called “distance revolution".

Data set	**Redshift**	$r_{BAO}(z)$
6dF	0.106 (Beutler et al., 2011)	0.336 ± 0.015
SDSS DR7	0.15 (Ross et al., 2015)	0.2239 ± 0.0084
SDSS(R) DR7	0.35 (Padmanabhan et al., 2012)	0.1137 ± 0.0021
SDSS-III DR12	0.38 (Alam et al., 2016)	0.100 ± 0.0011
	0.61	0.0691 ± 0.0007
SDSS-III DR11	2.34 (Delubac et al., 2015)	0.0320 ± 0.0013
	2.36 (Font-Ribera et al., 2014)	0.0329 ± 0.0009

Table 4.1: $r_{BAO}(z)$ measurements used. The ones corresponding to SDSS data were inverted from the published values of $D_V(Z)/s_d$ and those corresponding to Lyα-F data were obtained from the reported quantities $D_A(z)/s_d$ and $D_H(z)/s_d$.

The BAO feature, as was described in chapter 2, has become the best way to probe the late time dynamics of the Universe and in consequence that of DE. It is the cosmological tool used by several experiments like the SDSS-IV (Dawson et al., 2016) and the Dark Energy Survey (DES) (Abbott et al., 2005) and the main probe that will be used by future experiments like the Dark Energy Spectroscopic Instrument (DESI) (Levi et al., 2013) and Euclid (Laureijs et al., 2011). Nevertheless a complete analysis should rely on the data provided by recombination era, since the CMB provides the most accurate constraints on the cosmological parameters.

The observational points from the six-degree-field galaxy survey (6dFGS (Beutler et al., 2011)), Sloan Digital Sky Survey Data Release 7 (SDSS DR7 (Ross et al., 2015)) and the reconstructed value (SDSS(R) (Padmanabhan et al., 2012)), as well as the latest result from the complete BOSS sample SDSS DR12 ((Alam et al., 2016)), and the Lymann-α Forest (Lyα-F) measurements from the Baryon Oscillation Spectroscopic Data Release 11 (BOSS DR11 (Font-Ribera et al., 2014), (Delubac et al., 2015)) were chosen. Table 4.1 summarizes them all. Since the volume surveyed by BOSS and WiggleZ (Kazin et al., 2014) partially overlap (see (Beutler et al., 2016b) for more details) data from the latter is not used in this work.

Local value of H_0

The present value of Hubble constant has been determined observationally from direct measurement of the local dynamics, as in the latest work of A. Riess *et al* in Riess et al. (2016), but also from BAO measurements either from galaxy surveys or from the Lyman-α forest and it can be derived as well from CMB experiments such as Planck.

Regarding the work of A. Riess *et al* (AR16), their best estimate in units of $km \cdot s^{-1}Mpc^{-1}$ reports a value of

$$H_0 = 73.21 \pm 1.74, \tag{4.5}$$

the accuracy of which was achieved in great deal due to the utilization of maser system in NGC1258 both to calibrate and as an independent anchor for the cosmic distance ladder.

Cosmic Microwave Background

The Cosmic Microwave Background is the most precise cosmological data set. The angle subtended by the first peak is determined with exquisite precision (Ade et al. (2016a)):

$$\theta_* = (1.04077 \pm 0.00032) \times 10^{-2} \tag{4.6}$$

Following the report of the Planck collaboration (P15) Ade et al. (2016b) and Galli et al. (2014) we use *Planck TT+TE+EE+lowP* which denotes the combination of likelihood at $l \leq 30$ using TT, TE, and EE spectra with the low-l temperature+polarization likelihood.

However, it has been shown (Wang and Mukherjee (2007), Mukherjee et al. (2008), Ade et al. (2016b)) that the information of CMB power spectra can be compressed within few observables such as the angular scale of sound horizon at last scattering, $l_A \equiv \pi/\theta_*$, and the scaled distance to last scattering surface, $R \equiv \sqrt{\Omega_M H_0^2} d_A(z_*)$.

We keep the flat geometry and the baryon density fixed and thus we can add the CMB information to BAO and H_0 measurements by means of the observables $\{\theta_*, \omega_c \equiv \Omega_c h^2\}$. The corresponding covariance matrix is

$$\mathcal{C}_{CMB} = \begin{array}{c} \\ \omega_c \\ \theta_* \end{array} \begin{array}{c} \begin{array}{cc} \omega_c & \theta_* \end{array} \\ \begin{pmatrix} -23.5248 & -2.2078 \\ -2.207815 & 1.063561 \end{pmatrix} \end{array} \times 10^{-7} \tag{4.7}$$

The angle of horizon at last scattering is defined to be

$$\theta_* \equiv \frac{r_s(z_*)}{d_A(z_*)} \tag{4.8}$$

where $r_s(z_*)$ is the horizon size at the decoupling epoch ($z_* \approx 1090.06$ according to Planck Ade et al. (2016a)), defined by the integral in equation (2.35) evaluated from z_* to ∞, and $d_A(z_*)$ is the comoving distance to last scattering surface:

$$d_A(z_*) = \int_0^{z_*} \frac{dz'}{H(z')} \tag{4.9}$$

The reported value for the Hubble constant by P15 is $H_0 = 67.8 \pm 0.9$ Ade et al. (2016a), which assumes a ΛCDM universe and is known to be in tension with AR16 at the 3.4σ level.

Statistical analysis

Additionally to the free parameters in equation (4.1) we also investigate the constraints on the physical density of cold dark matter $\omega_c \equiv \Omega_c h^2$ and H_0 (or equivalently h), resulting in the set $\vec{\alpha} = \{w_0, w_i, z_T, q, \omega_c, h\}$.

We considered uniform priors on the parameters: $h \in$ [0.5, 1], $\omega_c \in$ [0.001, 0.99], $w_0 \in$[-1, 0], $w_i \in$[-1, 0], $q \in$ [1, 10] and $z_T \in$ [0, 3].

The goodness of the fit is analysed using a standard χ^2 approach, as several other works in the literature do (for example, Gong et al. (2015); Moresco et al. (2016a)). This is possible as the reported errors on the data are Gaussianly distributed (Alam et al., 2016), (Sanchez et al., 2016).

To determine the best-fitting values (BFV), we minimize the χ^2 goodness-of-fit estimator,

$$\chi^2 = (\vec{m} - \vec{d})^T \vec{C}^{-1} (\vec{m} - \vec{d}) \tag{4.10}$$

where $\vec{m}$ are theoretical values for each observable , $\vec{d}$ the data, and $\vec{C}$ the corresponding covariance matrix. In order to avoid the inclusion and marginalisation of nuisance parameters we do not make use of the latest supernovae sample (namely the Joint Light-curve Analysis Betoule et al. (2014)) and rely on the BAO datasets along with the latest H_0 determination and the compressed CMB likelihood.

The joint analysis of the different data sets is done by adding their respective χ^2 functions.

For the BAO measurements we use the χ^2 function defined as

$$\chi^2_{BAO} = \vec{y}^T_{BAO} \mathcal{C}^{-1}_{BAO} \vec{y}_{BAO}, \tag{4.11}$$

where $\vec{y}_{BAO} \equiv r^{Th}_{BAO}(\vec{\alpha}|z_i) - r^{Obs}_{BAO}(z_i)$ is the difference between theoretical prediction for $r_{BAO}(z)$ according to (2.51) and the values listed in table 4.1, and $\mathcal{C}^{-1}_{BAO}$ is the inverse of the covariance matrix containing the observational errors for the measurements.

Since the data points used in this work are not correlated we have a diagonal matrix whose elements are the square-root of the errors reported in table 4.1. The value of Ω_m and $\rho_{DE} \equiv \Omega_{DE} h^2$ were derived from the best fitting value for ω_c and H_0 for each model and $\omega_b \equiv \Omega_b h^2 = 0.02225$ from P15 Ade et al. (2016a).

With the matrix (4.7) we can build the χ^2_{CMB} function:

$$\chi^2_{CMB} = \vec{y}^T_{CMB} \ \mathcal{C}^{-1}_{CMB} \ \vec{y}_{CMB} \tag{4.12}$$

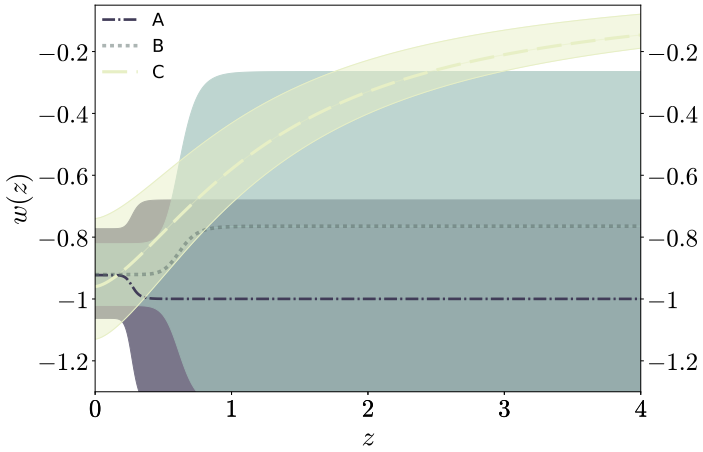

Figure 4.2: Evolution of Equation (4.1) according to the best fit values obtained with different data combinations.

where $\vec{y}_{CMB}$ is the corresponding data vector defined as

$\vec{y}_{CMB} = \left[\omega_c^{Th} - \omega_c^{Planck}, \quad \theta_*(\vec{\alpha})^{Th} - \theta_*^{Planck}\right]^T$, and $\mathcal{C}_{CMB}^{-1}$ is the inverse of matrix (4.7).

Following a Bayesian analysis, the best model is the one which minimizes the information criteria. The Akaike information criterion (AIC) is defined as

$$AIC = -2\ln\mathcal{L} + 2m, \tag{4.13}$$

where $\mathcal{L}$ is the maximum likelihood and m the number of parameters of the model. It has been argued in the literature that Bayesian Information Criterion is best suited than the AIC (see for instance Liddle (2004)), so we calculate the BIC too. This is defined to be:

$$BIC = -2\ln\mathcal{L} + 2m\ln N, \tag{4.14}$$

which also takes into account the number of data points used, N. The likelihood is connected to χ^2 function by $\ln\mathcal{L} = -\chi^2/2$.

Results at Background level

To compare results among our model and ΛCDM we present the reduced χ^2, making explicit the number of parameters, and we also report the corresponding values of the Akaike Information Criterion (AIC) and the Bayesian Information Criterion (BIC) Liddle (2004) in Tables 4.2 and 4.3.

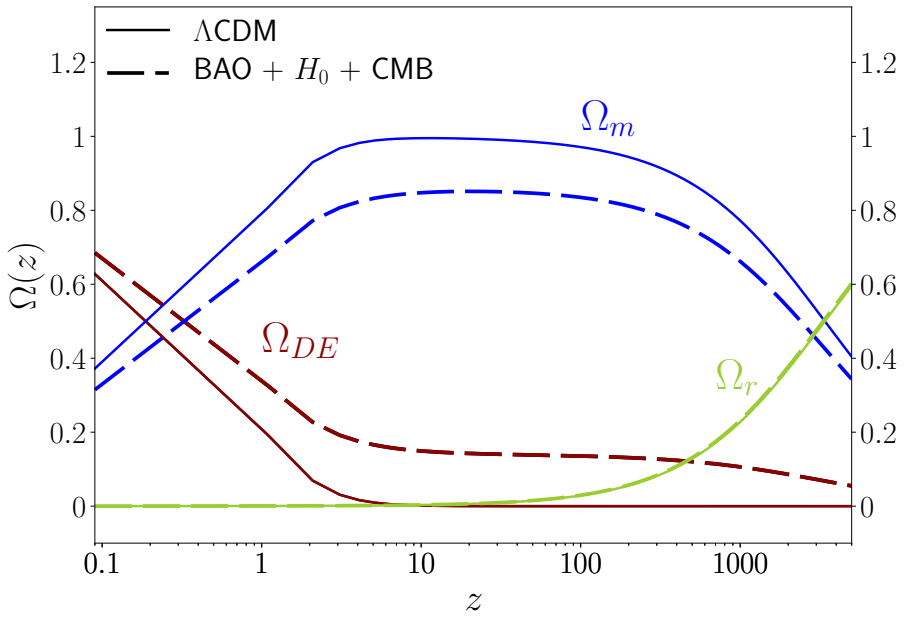

(a) Evolution of the fractional densities of Dark Energy, matter and radiation as function of redshift.

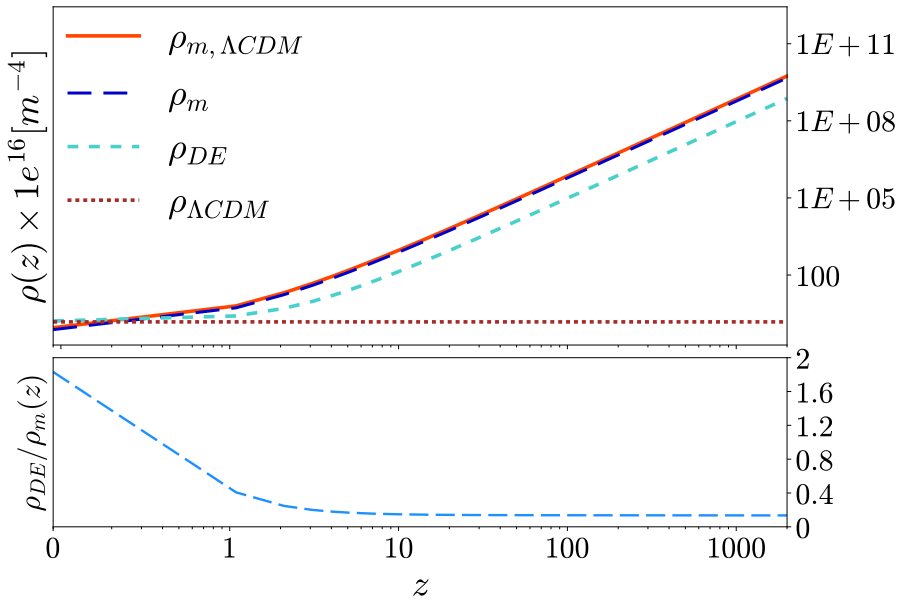

(b) Evolution of Dark Energy and matter densities as function of redshift. In the bottom panel the ratio of Dark Energy to matter density is shown.

Figure 4.3: Comparison of the evolution of volume density and fractional densities according to ΛCDM and Equation (4.1) with the BFVs from BAO+H_0+CMB datasets (Result "C" in Table 4.2).

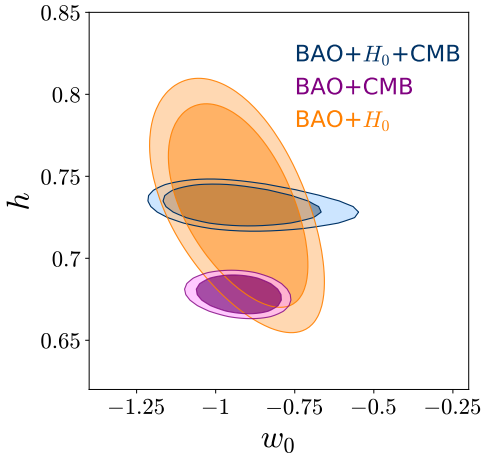

(a) Confidence contours at 1 and 2σ values in the $h - \Omega_m$ parameter space.

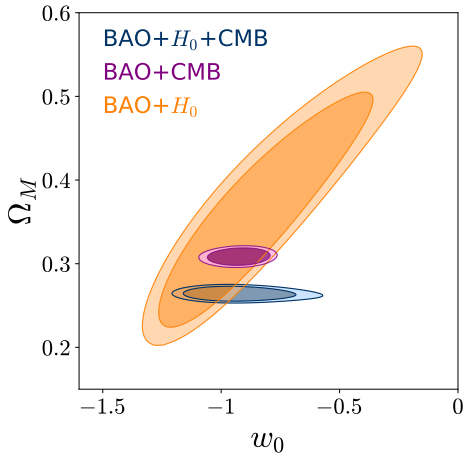

(b) Confidence contours at 1 and 2σ values in the $\Omega_m - w_0$ parameter space.

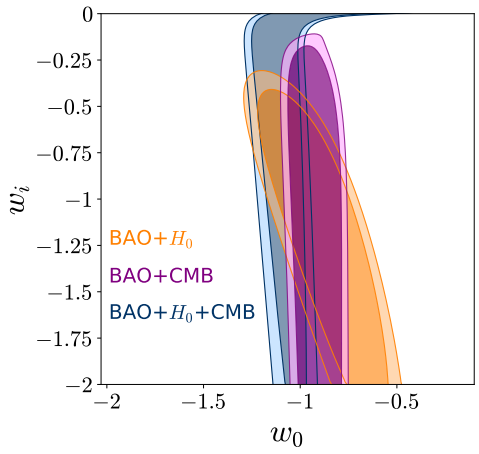

(c) Confidence contours at 1 and 2σ values in the $w_i - w_0$ parameter space.

Figure 4.4: Confidence contours at 1 and 2-σ level for the model (4.1) using the different combinations of data shown in Table 4.2.

BAO + H_0

Local measurements (column "A" in table 4.2) point to a dynamical DE presenting a late and abrupt transition ($z_T = 0.28$, $q = 9.97$) from an initial value $w_i = -0.99$ to a present value $w_0 = -0.92$.

The dynamics shows an evolution of DE similar to a cosmological constant Λ for $z \gg z_T$ however close to present time ($z < 0.28$) a sharp transition towards a larger value of w occurs. The transition is restricted to late-times $z_T \leq 1.08$ at 1σ level with a steep EoS ($q \geq 7.19$) and a value of w at present time in the region $-1.07 \leq w_0 \leq -0.78$. However, due to the lack of precision data at early times the value at high redshifts is less tightly constrained by data from BAO and H_0, as indicated in Figure 4.2 by the dot-dashed curve.

The value for H_0 holds in agreement with the reported measurement from AR16 used as prior for this calculation and the physical density of CDM was restricted to be $\omega_c \in (0.136, 0.1812)$. By combining these values we find a fractional matter density of $\Omega_m = 0.334^{+0.052}_{-0.044}$. The reduction in absolute χ^2 compared to a cosmological constant (outcome A_Λ, Table 4.3) is of 4.8%.

BAO + CMB

The dynamics for DE resulting from the use of BAO data and CMB reduced likelihood (column "B", Table 4.2) indicates the preference for a steep transition ($q = 9.8$) from the initial value $w_i = -0.77$ to the present value $w_0 = -0.92$ at a pivotal redshift $z_T = 0.63$. With 68% of confidence, $w_0 \in (-0.82, -1.02)$ and $w_i \leq -0.27$ at early times. The transition is constrained to be abrupt, $q \geq 6.9$ with a lower limit on the transition epoch $z_T \geq 0.10$. This corresponds to the dotted line in Figure 4.2. The value for $\omega_c \in (0.1164, 0.1226)$ lies within the range imposed by CMB priors and the value for H_0 is lower, in agreement with P15 (Ade et al. (2016a)). These yield a value for the fractional density of matter, $\Omega_m = 0.308 \pm 0.008$. In this case the reduction in the absolute χ^2 is 20.2% compared to a cosmological constant (outcome B_Λ, Table 4.3).

BAO + CMB + H_0

Case "C" in table 4.2 shows that a late time and smooth transition (z_T=1.31, $q = 1.5$) was preferred by data, with an initial value $w_i = 0$ to a present value $w_0 = -0.96$. This implies that DE behaves as matter at early times ($z \gg 1.31$) and the long-dashed line in Figure 4.2 displays this particular dynamics. We see that dynamics of DE allows to consistently fit the variables from CMB along with the local value of H_0, since the inclusion of H_0 in model C only increased χ^2 by 0.2% compared to model B. However,

from Table 4.3 we see that the addition of H_0 in ΛCDM model (B_Λ and C_Λ) severely penalizes the fit by increasing χ^2 by 19%, showing a tension in the value for H_0 from CMB and local measurements.

In this case, the DE density at early times is not negligible since it has $w_i = 0$. This results in a contribution at decoupling of order $\Omega_{DE} = 10\%$ (see for instance Figure 4.3a), adding an extra component that behaves like dust ($\propto a^{-3}$) at large redshifts. The ratio of DE density to ordinary matter ($\omega_c + \omega_b$) is nearly constant from $z \gtrapprox 5$ (as depicted in Figure 4.3b) and has a value $\rho_{DE}(z_*)/\rho_m(z_*) = 0.16$ which changes several cosmological parameters, for instance the equivalence epoch, $a_{eq} \equiv \rho_r(a_{eq})/\rho_m(a_{eq})$, is smaller modifying the distance to the last scattering surface and the sound horizon at recombination. This is an interesting toy model worthwhile of further studies, and it will also impact CMB power spectrum and Large Scale Structure formation. In this case the reduction in absolute χ^2 compared to a cosmological constant (outcome C_Λ, Table 4.3) is of 42.8%.

Having a non-negligible DE at earlier times, allows to put tighter constraints on the parameters: $\{w_i, q, z_T\}$. At the 1-σ level, the present value of $w(z)$ is constrained to be close to -1, $w_0 \in (-1.13, -0.74)$, while the high redshift value is tightly restricted to be a dust-like solution, $w_i \in (0.04, -0.02)$. The transition is constrained to be smooth, with an exponent $q \in (1, 2.8)$ and to occur in an epoch $z_T \in (0.87, 2.73)$.

A DE component which is non-negligible at early times as been studied in the literature and is known as Early Dark Energy (see for example Linder and Robbers (2008)).

From both, Table 4.2 and Figure 4.4 we can draw the following general results. The value for w_0 is tightly constrained by observations and the scenario $w_0 = -1$ is included within 1σ error for all the cases. Generally speaking, for the outcomes where DE density becomes negligible at earlier times, we obtained weak constraints for the high redshift value of the EoS, w_i, the transition time, z_T, and the exponent q.

We have shown that the absolute χ^2 is reduced for SEoS hinting on a dynamical DE. In comparison to a Cosmological Constant scenario, the reduction is of 4.8% for case "A", 20.2% for "B" and 42.8% for "C". However, the reduced numbers of data points and the number of free parameters of SEoS does at this stage not favour it compared to ΛCDM using a bayesian analysis, e.g. for AIC or BIC. Still, it is worth keeping in mind that understanding the dynamics of DE is a central question in cosmology and that observational experiments such as SDSS-IV (eBOSS), DES, DESI, LSST are currently or about to start measuring the evolution of DE. An improved determination of dynamics of DE will allow us to constrain theoretical models from either particle

Steep Equation of State for DE			
	"A"	"B"	"C"
Parameter	BAO + H_0	BAO+CMB	BAO+CMB+H_0
w_0	$-0.92^{+0.15}_{-0.14}$	-0.92 ± 0.10	$-0.96^{+0.22}_{-0.17}$
w_i	-0.99(≤-0.67)	-0.77 (≤ -0.27)	$0^{+0.04}_{-0.02}$
q	9.97(≥ 7.19)	9.8(≥ 6.9)	$1.5^{+1.3}_{-0.5}$
z_T	0.28(≤ 1.08)	0.63(≥ 0.10)	$1.31^{+1.42}_{-0.44}$
$\Omega_c h^2$	$0.1568^{+0.0244}_{-0.0208}$	0.1195±0.0031	0.1195±0.0034
$100 * h$	$73.22^{+4.2}_{-4.1}$	67.80±0.9	73.26 ± 1.0
Ω_m	$0.334^{+0.052}_{-0.044}$	0.308±0.008	0.264 ± 0.008
χ^2/(d.o.f.)	9.59/2	9.77/3	9.79/4
AIC	153.51	94.84	56.89
BIC	153.99	96.02	58.70

Table 4.2: Results for SEoS. The bottom panel contains the BFV and 1σ errors for the free parameters as result from the combined analysis of BAO data (table 4.1) along with the local value of H_0 and CMB priors (4.7). The value for Ω_m was derived as explained in the text. The bottom panel contains the χ^2 for the best fit and the number of degrees of freedom, as well as the AIC and BIC values for each fit.

physics or Modified Gravity. In such a case the free parameters of our SEoS could be derived and shade light in the understanding of DE properties.

Effect of the parameters in the Cosmological observables

A separate analysis using a Boltzmann solver was made. In this analysis we incorporated the equation of state (4.1) in the Code for Anisotropies in the Microwave Background (CAMB) (Lewis et al., 2000).

CAMB is a code written in Fortran which computes the CMB anisotropy and the matter power spectra by solving the perturbation equations for each one of the cosmological fluids up to linear order.

The different observations investigated are:

- The module of the luminous distance from Supernovae measurements: $\mu = 5 * \log_{10}(d_L/10pc)$, where d_L is the luminous distance introduced in equation (2.29).

- The BAO distance, as reported by several surveys $r_{BAO} = s(z_d)/D_V(z)$ (see equation (2.51)).

ΛCDM			
	"A_Λ"	"B_Λ""	"C_Λ"
Parameter	BAO + H_0	BAO+CMB	BAO+CMB+H_0
$\Omega_c h^2$	0.1476 ± 0.0052	$0.1201^{+0.0088}_{-0.0099}$	0.1203 ± 0.0017
$100 * h$	$73.56^{+2.0}_{-2.3}$	70.20 ± 0.5	70.99 ± 0.5
Ω_m	$0.3139^{+0.023}_{-0.026}$	0.2889 ± 0.004	0.2889 ± 0.004
χ^2/(d.o.f.)	10.05/6	11.74/7	13.98/8
AIC	147.82	88.80	52.23
BIC	147.98	89.20	52.83

Table 4.3: Results for a Cosmological Constant. BFV and 1σ errors for the free parameters as result from the combined analysis of BAO data (table 4.1) along with the local value of H_0 and CMB priors (4.7). The value for Ω_m was derived as explained in the text. The bottom panel contains the χ^2 for the best fit and the number of degrees of freedom, as well as the AIC and BIC values for each fit.

- The linear matter power spectrum at present time, $P(k) \equiv \langle|\delta_m(k, a_0)|^2\rangle$, which was introduced in (2.53), in terms of the correlation function.
- CMB temperature and polarization anisotropies spectrum as function of multipole, C_l^{TT}, C_l^{TE}, C_l^{EE}

The effect of the parameters of equation (4.1) in different observables is shown in Figures 4.6-4.9.

In figure 4.6 we notice weaker dependence on the value for w_0 in all the observables. The luminosity distance modulus increases as the value of w_0 approaches negative values. The BAO ratio increases as w_0 approaches 0, and the matter power spectrum gets severely distorted when $w_0 = 0$. As for the CMB anisotropies, we note that the peaks shift towards the left as $w_0 \to 0$. These evidence tell us that the cosmological observables strongly depend on the present value of the dark energy equation of state, $w(z = 0) = w_0$.

Figure 4.7 shows a not so strong dependence on the value for $w_a = w_i - w_0$ in the observables, but we can still see the distortions in the distances and power spectra. In this case, the luminosity distance modulus also increases as the value of w_a approaches negative values, and the BAO ratio looks very degenerated with w_a value in the redshift range $z \in [0, 0.3]$, but we note this ratio increases as w_a approaches 0 for $z \geq 0.3$. As for the matter power spectrum, we see again that it gets distorted towards smaller amplitude values when $w_a = 0$. As for the CMB anisotropies, we note the greater shift in the peaks for C_l^{TE} and C_l^{EE}. The position of the peaks shift towards smaller values of the multipole, l, as $w_a \to 0$.

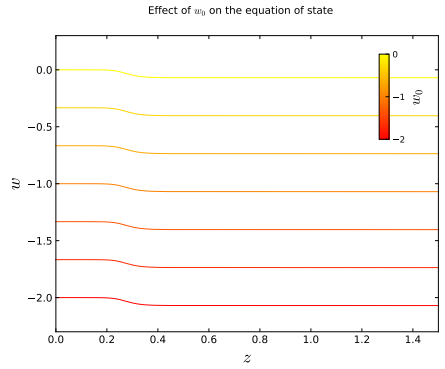

(a) Different values of w_0 in the shape of $w(z)$.

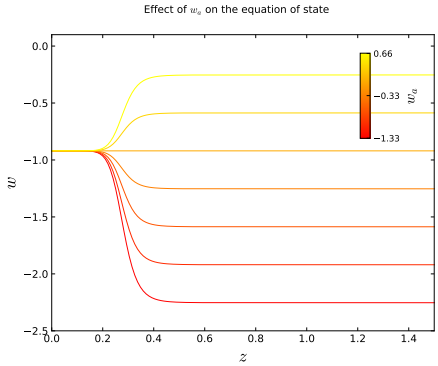

(b) Different values of $w_a \equiv w_i - w_0$ in the shape of $w(z)$.

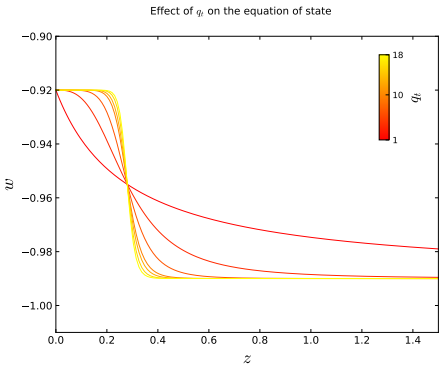

(c) Different values of q in the shape of $w(z)$.

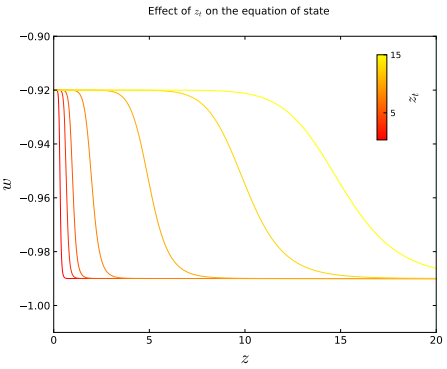

(d) Different values of z_T in the shape of $w(z)$.

Figure 4.5: Effect of different parameters in the equation of state (4.1). The values of free parameters are set to the BFV obtained from "BAO+H_0" constraints (table 4.2) and varied one at once in each panel.

The case for q and z_T is completely different, as we can see in Figures 4.8 and 4.9. In these cases we see that there is absolutely no dependence of the observables even for extreme variations of the values $q \in [1, 18]$, $z_T \in (0, 15]$. This tells us about the lack of constraints coming from observations on the value for these two parameters.

Tension

An interesting question arises from the fact that we have used the local value for H_0 as reported by Riess et al. (2016) and information of the CMB in the compressed likelihood as detailed in (4.12). It has been reported in the literature that there exists a 3.4% tension among the value reported by Riess et al. (2016) and the one extrapolated from CMB data and reported by Ade et al. (2016a).

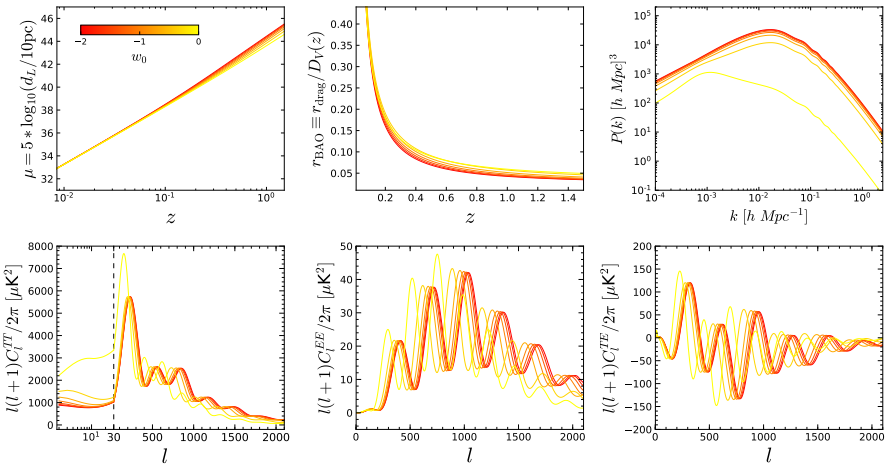

Figure 4.6: Effect of different values of w_0 in different observables.

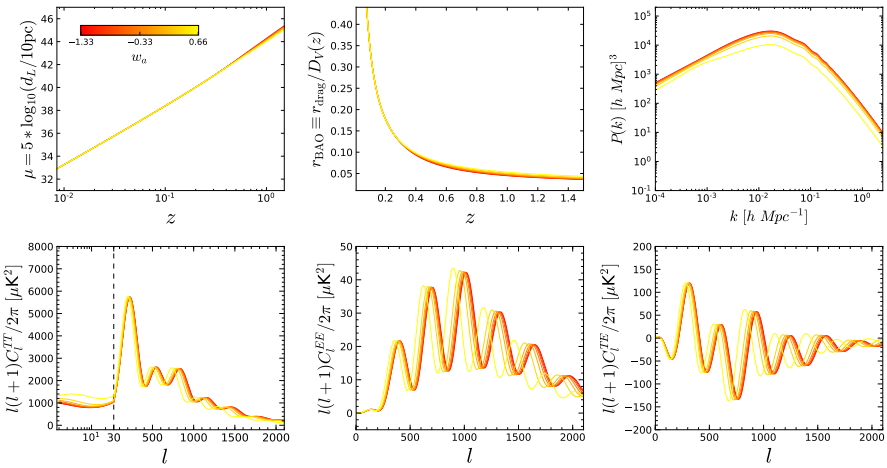

Figure 4.7: Effect of different values of $w_a \equiv w_i - w_0$ in different observables.

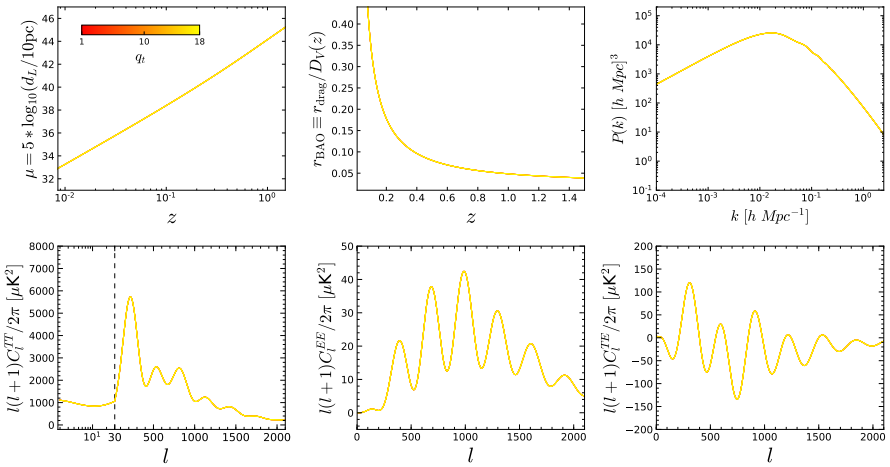

Figure 4.8: Effect of different values of q in different observables.

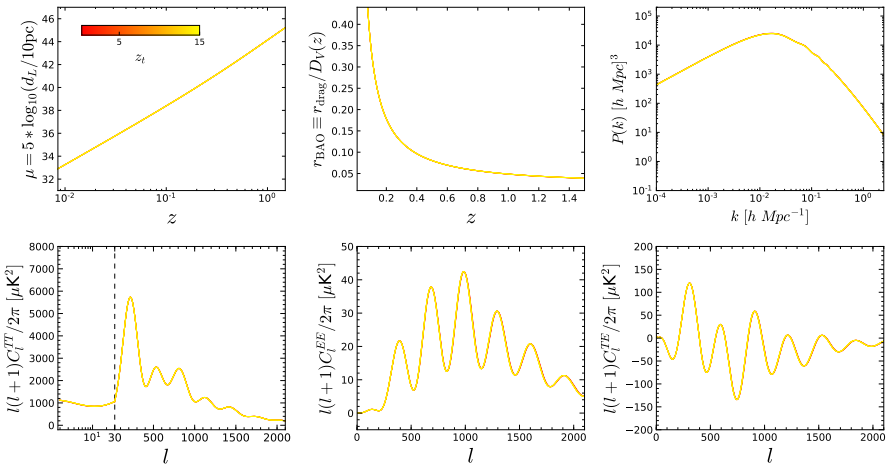

Figure 4.9: Effect of different values of z_T in different observables.

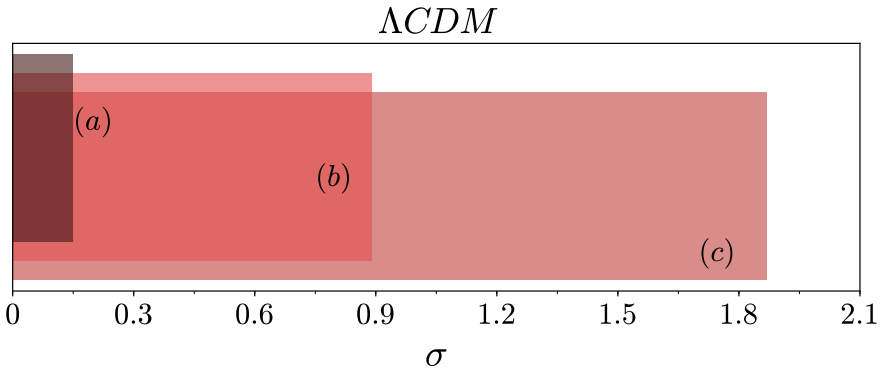

(a) Assuming a Cosmological Constant

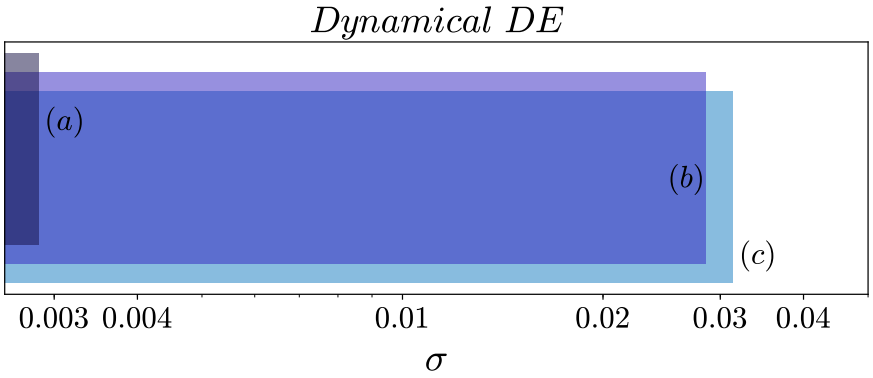

(b) Assuming parametrization (4.1)

Figure 4.10: Tension between data sets expressed in σ-distance between best fits. (a) Shows the distance among χ^2_{BAO} and $\chi^2_{BAO+H_0}$, (b) the distance between χ^2_{BAO} and $\chi^2_{BAO+CMB}$ and (c) between χ^2_{BAO} and $\chi^2_{BAO+H_0+CMB}$, normalized to their corresponding 1σ value.

To quantify the amount of tension present in our analysis when we combine different datasets, we computed the distance between the best fit values (the point in parameter space where the χ^2 is minimized, explicitly indicated in the bottom panel of Tables 4.2 and 4.3). In order to make a fair comparison we need to take into account the different number of parameters involved in each model. To accomplish this we reported the distance between best fit points in sigma units, that is, normalized to the 68% confidence value, which depends on the number of free parameters and hence it is different for ΛCDM and the model (4.1).

We chose the BFV corresponding to BAO, this is, the value of $\chi^2_{BAO,model}$ as the pivotal point to refer the tension from different datasets.

The results are shown in figures 4.10a and 4.10b. We notice that the addition of

new data sets virtually does not increase the best fit when a dynamical dark energy is assumed: the biggest change we get is $\Delta\chi^2 \sim 0.03\sigma$ whereas it changes up to $\Delta\chi^2 \sim 1.87\sigma$ for ΛCDM.

Remarks & Conclusion: Statistical analysis at background level

We presented a parametrization for the Dark Energy equation of state and found the constraints compatible with BAO measurements (contained in Table 4.1) combined with the latest local determination of Hubble constant (Riess et al. (2016)). Additionally we used the compressed CMB likelihood from Planck (Ade et al., 2016a), by means of the sound horizon at decoupling, θ_*, and $\omega_c h^2$. The constraints for free parameters, $\{w_0, w_i, q, z_t, \omega_c, H_0\}$, and their 68% errors resulting from the combined analysis of the datasets were obtained.

We find that a Dynamical form of DE drastically reduces the tension among local measurement of the Hubble constant and the one extrapolated from recombination era by Planck. Whereas for a ΛCDM model, tension between the local determination of H_0 (Riess et al. (2016)) and the value derived from Planck (Ade et al. (2016a)) remains, we find that it is possible to simultaneously conciliate the observations from BAO, H_0 and CMB by means of a dynamical Dark Energy (Figures 4.10)

The reduced numbers of data points and the number of free parameters in the SEoS model does not favour it compared to ΛCDM. However, understanding the dynamics of DE is a central question nowadays in cosmology and a great deal of effort has been focused to construct observational experiments (Dawson et al. (2016)-LSST Science Collaboration et al. (2009)) to determine the evolution of DE. With a more precise dynamics of DE, theoretical models derived from particle physics or modifications to the gravity sector may give a sound derivation of some of the free parameters used in our steep EoS and in this case a dynamical DE would be favoured over ΛCDM. From the qualitative analysis of the impact of the parameters in the observables produced by CAMB, we learn that this model will hardly be constraint with data by means of a standard Montecarlo exploration.

To summarize, the study of dynamics of Dark Energy is a matter of profound implications for our understanding of the Universe and its physical laws. Although the measurements from CMB are the most precise data sets in Cosmology, the best way to analyse the properties of DE comes from the low redshift regime, where the BAO feature is the most robust cosmic ruler. In this work we have contributed towards that direction, and we have presented the constraints for a dynamical DE model coming from the analysis of BAO distance measurements combined with the most recent H_0 determination and CMB information. Further theoretical and observational effort must be carried out to obtain a better understanding of DE.

4.3 Growth of linear matter perturbations with dynamic Dark Energy

Up to this point we have compared the background evolution of the model against distance measurements. In this section I will elaborate on the growth of perturbations during the matter-DE domination era when we assume this as the model for Dark Energy. The set of equations we will solve correspond to the non-relativistic limit of the perturbative formalism, derived in section 2.4. We recall equation (2.84) for a mixture of matter and dark energy:

$$\frac{d^2\delta_i}{dt^2} + 2\left(\frac{1}{a}\frac{da}{dt}\right)\frac{d\delta_i}{dt} - \left[4\pi G\bar{\rho}\Sigma_j\epsilon_j\delta_j - \frac{(c_s^2)_i k^2}{a^2}\delta_i\right] = 0, \tag{4.15}$$

where we have dropped the k subscript to refer to a Fourier component. We can further use $\frac{d}{dt} = aH(a)\frac{d}{da}$ and $H^2 = \frac{8\pi G}{3}\bar{\rho}$ and write it down in terms of scale factor, $a(t)$:

$$a^2\frac{d^2\delta_i(a)}{da^2} + a\left(3 + \frac{\dot{H}}{H^2}\right)\frac{d\delta_i(a)}{da} - \left[\frac{3}{2}\Sigma_j(\Omega_j\delta_j) - \frac{(c_s^2)_i k^2}{a^2H^2}\delta_i(a)\right] = 0, \tag{4.16}$$

$$i, j = \text{matter, dark energy.}$$

We can start by taking a smooth dark energy, $\delta_{DE} = 0$, in which case we have only one equation to describe the evolution of matter overdensities, for which we know $c_s^2 = 0$:

$$a^2\frac{d^2\delta_m(a)}{da^2} + \frac{3}{2}\left[1 - \Omega_{DE}(a)w_{DE}(a)\right]a\frac{d\delta_m(a)}{da} - \frac{3}{2}\Omega_m(a)\delta_m(a) = 0, \tag{4.17}$$

where we additionally used the continuity equation (2.14) and assumed the closure relation for a flat and late-time Universe: $\Omega_m + \Omega_{DE} = 1$.

In Equation (4.17), $w_{DE}(a)$ is the parametrization introduced in (4.1) written in terms of the scale factor. To study the effect of a DE model different to ΛCDM in the evolution of matter over-densities is the aim for this section.

In order to solve for $\delta_m(a)$ in equation (4.17) we set initial conditions in the matter dominated era, $a_{ini} = 10^{-3}$; since we know that during this epoch, the solution for the growth function is $D_+(a) = a$, we have $\delta_m(a_{ini}) = a_{ini} = 10^{-3}$ and $\delta'_m(a_{ini}) = 1$.

Regarding the solution for $w_{DE}(a)$ we choose to explore three different scenarios which will be referenced in the following discussion:

Case (I): to use the SEOS model and set the free parameters to the best fit corresponding to "BAO + H_0" dataset, this is, $\{w_0, w_i, q, z_T\} = \{-0.92, -0.99, 9.97, 0.28\}$ (see table 4.2, for reference)

Case (II): to take the corresponding CPL (3.19) limit by taking z_T = q = 1, but keeping $\{w_0, w_i\} = \{-0.92, -0.99\}$,

Case (III): to compare to a ΛCDM solution.

To see the effect of each parameter we will vary the values for $\{w_0, w_i, q, z_T\}$ separately while fixing the rest to the values above indicated.

The solution to (4.17) is shown in figures 4.11-4.12 for different values of the parameters in the dark energy equation of state. The solutions for the three cases explained above are shown. The bottom panel shows the relative difference from each model to ΛCDM, this is $\Delta\delta_m(a) \equiv ((\delta_{m,\Lambda}(z) - \delta_m(z))/\delta_{m,\Lambda}(z)) \times 100$, where $\delta_{m,\Lambda}(z)$ corresponds to the growth of matter contrast when we assume a Cosmological Constant solution. To see the difference arising only from the dynamics of Dark Energy in (4.1) versus a cosmological constant, we have set Ω_m and H_0 to the same fiducial values (consistent with Planck 2015 report Ade et al. (2016a)).

We notice that from $\Delta\delta_m(a)$ we find differences from ΛCDM:

- of around 1% when we consider model (I) as in figure 4.11a
- of approximately 1.5% when we consider the CPL limit of model (I) (figure 4.11a)
- of 5% when we take the value $w_i = -0.77$ and let the rest of the parameters unchanged as prescribed in model (I) (figure 4.11b)
- of 3.7% when we take the CPL limit with $w_i = -0.77$
- of nearly 9% when a CPL solution is taken with the values $\{w_0 = -0.6, w_i = -0.99\}$ (figure 4.12),
- of almost 5% when we take SEoS model as model (I) but taking $w_0 = -0.6$ (figure 4.12)

Thus showing that even when considered only at a background level, the presence of a dynamic DE modifies the evolution of matter perturbations. It is important to note that the discrepancy between LCDM and a dynamic form of Dark energy is bigger for the CPL scenario in the case $\{w_0, w_i, q, z_T\} = \{-0.92, -0.99, 9.97, 0.28\}$ (figure 4.11a). In the case where we take $w_i = -0.77$ instead, the discrepancy is bigger for the SEoS scenario (figure 4.11b). In the latter, the discrepancy to LCDM, quantified by $\Delta\delta_m(z)$, can be as big as 4.5%, whereas in the former case, it is only of 1%.

The other parameter varied was w_0 (figure 4.12). In that case we notice that, the bigger the value for w_0, the bigger the discrepancy $\Delta\delta_m(z)$. However, it occurs that the

CPL model shows bigger discrepancy to LCDM than SEoS. Besides, the models CPL ($w_0 = -0.8, w_i = -0.99$) and SEoS ($w_0 = -0.6, w_i = -0.99, q = 9.97, z_T = 0.28$) are within 1% from each other, showing that, at least at level of linear growth of matter overdensities, both models could not be discriminated. In other words, a steep transition ($q = 9.97$) at a later time ($z_T = 0.28$) between the pivotal values of $w_i = -0.99$ and $w_0 = 0.6$ cannot be distinguished from a smooth transition ($q = 1$) at a later time ($z_T = 1$) between the pivotal values $w_i = -0.99$ and $w_0 = -0.8$.

Clustering Dark Energy

The ansatz $\delta_{DE} = 0$ is correct only for ΛCDM case, but if we are taking an EoS for DE which is not constant in time, this is no longer valid. If DE perturbations are considered, we have the following system of coupled equations:

$$\begin{aligned} a^2\delta_m''(a) + a\frac{3}{2}\left[1 - w(a)\Omega_{DE}(a)\right]\delta_m'(a) & \\ -\frac{3}{2}\left[\Omega_m(a)\delta_m(a) + \Omega_{DE}(a)\delta_{DE}(a)\right] = 0 & \quad (4.18a) \\ a^2\delta_{DE}''(a) + a\frac{3}{2}\left[1 - w(a)\Omega_{DE}(a)\right]\delta_{DE}'(a) & \\ + \left(\frac{c_s^2k^2}{a^2H^2(a)} - \frac{3}{2}\Omega_{DE}(a)\right)\delta_{DE}(a) & \\ -\frac{3}{2}\Omega_m(a)\delta_m(a) = 0 & \quad (4.18b) \end{aligned}$$

where $\delta_{DE}(a)$ represents the dark energy density contrast, i.e., $\delta_{DE} \equiv \frac{\delta\rho_{DE}}{\bar{\rho}}$, where $\bar{\rho}$ is the total background density ($\bar{\rho} = \rho_m + \rho_{DE}$ in the late time Universe). Assuming adiabatic initial conditions, we have $\delta_{DE}(a_{ini}) = (1+w(a_{ini}))\delta_{m,ini}$, and $\delta_{DE}'(a_{ini}) = \frac{-k^2\tau(a_{ini})}{3a_{ini}^2H(a_{ini})}\delta_{DE}(a_{ini})$. In this case we start solving the system of equations (4.18) from a_{ini} to the present time, where a_{ini} is fixed by the time of entrance for the k-mode into the horizon: $aH(a) = k$.

If we model DE as a perfect fluid then we have $c_s^2 \equiv \frac{\delta P_{DE}}{\delta\rho_{DE}} = c_{ad}$. This is, we have:

$$\begin{aligned} c_{ad}^2 &\equiv \frac{\dot{P}}{\dot{\rho}} \quad (4.19) \\ &= w(t) - \frac{\dot{w(t)}}{3H(t)(1+w(t))} \\ &= w(a) - \frac{aw'(a)}{3(1+w(a))} \end{aligned}$$

The adiabatic speed of sound depends only on the EoS of dark energy fluid, hence this term does not add any new information to the model.

We can split the speed of sound into an adiabatic contribution and a non-adiabatic one:

$$c_s^2 \equiv= \frac{\delta p}{\delta \rho} = \frac{\dot{p}}{\dot{\rho}} + c_{non-ad}, \tag{4.20}$$

where the $c_{ad} \equiv \frac{\dot{p}}{\dot{\rho}}$ part is defined in equation (4.19). The non-adiabatic contribution, in principle, will carry the information of the microphysics of the fluid. Any entropic contribution to the relation $\delta P/\delta\rho$ will be encoded in this term. Since, at this point we are dealing with a phenomenological approach we model the non adiabatic contribution as an effective term with constant value ranging from 0 to 1, i.e., $c_s^2 = c_{ad} + c_{eff}$ where $c_{eff} \in [0, 1]$.

The adiabatic speed of sound, c_{ad} is plotted as function of scale factor in Figure 4.13, where we assumed the SEoS model with values $w_0 = -0.9$, $w_i = -0.6$, $z_T = 1$ and different values of the exponent, q. We notice that the value of the exponent imprints a bump in the c_{ad}, making it switch between negative and positive values.

To show the effect of the different parameters from equation (4.1) in the evolution of matter overdensities from the system (4.18), we choose to fix $c_{eff} = 1$ and to show the evolution of the k-mode $k = 0.01 Mpc^{-1}$.

As in the previous section, the values of the cosmological parameters is kept the same and we vary only those related to the dynamics of dark energy.

In figure 4.14 we show the evolution for $\delta_m(a)$ for the model (I), (II) and (III) as in the previous section. We keep the values for the parameters $\{w_0, q, z_T\} = \{-0.92, 9.97, 0.28\}$ and vary the value for w_i. The bottom panel of those figures shows the relative difference between the SEoS solution to the CPL limit, this is, it shows the difference between $q = 9.97$ and $z_T = 0.28$ to $q = 1 = z_T$.

In figure 4.14a we notice that the biggest difference between a steep transition and a smooth one, comes when we have $w_i = -0.77$ (or order 1.7%) and it decreases to $\sim 0.2\%$ for $w_i = -0.9$. There is no difference to CPL solution when we take $w_i = -0.92$ since we have $w_0 = -0.92 = w_i$ and the dependence on the time evolution of equation (4.1) disappears. The situation is different when we take the value $w_i = -0.94$ as in figure 4.14b. In that case the discrepancy between SEoS solution and CPL appears at the transition epoch, $z_T = 0.28$ and we get a difference of 2% between both solutions.

Evolution of matter over-density (4.18a) when the system (4.18) is solved can be seen in figure 4.15. For this scenario we notice that the system becomes extremely non-linear due to the term $\left(\frac{c_s^2 k^2}{a^2 H^2(a)} - \frac{3}{2}\Omega_{DE}(a)\right)\delta_{DE}(a)$ in equation (4.18b).

We modelled the speed of sound splitting it into an adiabatic contribution and an effective term, $c_s^2 = c_{ad}^2 + c_{eff}^2$, where c_{eff}^2 encapsulates the physics beyond the EoS of the dark fluid.

The characteristics of the term c_{ad}, *i. e.*, a sharper bump for a steeper transition in the EoS, as shown in figure 4.13, get imprinted in the evolution of δ_m via its coupling

with δ_{DE}.

We notice that the main effect of this non-adiabatic contribution is to suppress the growth of matter over-densities by several orders of magnitude. The shape and characteristic bump at the transition time is preserved (see figure 4.18).

4.4 Non-linear regime

As it was discussed in Section 2.4, the matter content of the Universe is modelled as a large collection of identical particles of mass m, interacting only through mutual gravitational attraction. For low densities and sub-horizon scales, such forces are adequately described by Newtonian gravity in a uniformly expanding background, with the Newtonian potential sourced by inhomogeneities in the density field.

As it was shown in the section 4.3, the presence of a dynamic form of dark energy can affect the growth of dark matter perturbations at linear order even if it is considered only at background level. If we further consider its perturbations we need to add a term to the speed of sound, $c_s^2 = \frac{dP_{DE}}{d\rho_{DE}} + c_{nad}$, where c_{nad} should be of order unity.

We reviewed the perturbative limit of this description. To study the regime where this limit breaks down and analyse the impact of non-linearities from the presence of dark energy in the large scale structure formation, we need to make an inspection using N-body simulations.

One way to do so is to use semi-analytic codes as COLA (COmoving Lagrangian Acceleration) (Tassev et al., 2013; Scoccimarro et al., 2012) which have a second order perturbative prescription to solve larger scales and a particle mesh code to deal with the smaller scales. This approach allows to speed up n-body calculations due to the incorporation of analytical solutions for the growth of perturbations the Lagrangian perturbation theory (LPT).

To this end I review some of the main equations in the LPT scheme and will present some preliminary results from the implementation of model (4.1) into the code COLA to analyse the effect of a different dynamics for Dark energy. The reason for using this scheme instead of Eulerian will be clear at the end of next subsection.

The contents of this section are subject of a work in preparation in collaboration with Dr. Octavio Valenzuela, Dra. Chandrachani Ningombam and Dr. Axel de la Macorra.

Lagrangian Perturbation Theory

We have reviewed Eulerian perturbation theory in section 2.4, in which we focus on describing the density and velocity fields of matter at the comoving coordinate system.

Now we review a different approach in which we focus on the trajectory of individual particles.

In this formalism we are describing the trajectory of a fluid element by its initial Lagrangian position, $\vec{q}$, its comoving Eulerian position, $\vec{x}(\vec{q},t)$, and the displacement field that maps them both, $\vec{\Psi}(\vec{q},t)$, according to:

$$\vec{x}(\vec{q},t) = \vec{q} + \vec{\Psi}(\vec{q},t). \tag{4.21}$$

Now the variable to follow is the displacement field and accordingly, the perturbation is performed now in terms of it

$$\vec{\Psi}(\vec{q},t) = \vec{\Psi}^{(1)}(\vec{q},t) + \vec{\Psi}^{(2)}(\vec{q},t) + ... + \vec{\Psi}^{(N)}(\vec{q},t). \tag{4.22}$$

From the mapping (4.21) and the conservation of mass, $\rho(\vec{x},t)d\vec{x} = \rho(\vec{q})d\vec{q}$, we obtain a relation between the matter density contrast δ and the displacement field:

$$1 + \delta(\vec{x},t) = J^{-1}(\vec{q},t) \tag{4.23}$$

$$\vec{J}(\vec{q},t) = \left|\frac{\partial\vec{x}}{\partial\vec{q}}\right| \tag{4.24}$$

where $J(\vec{},t)$ is the Jacobian of the transformation.

The equation of motion for matter particles in an expanding Universe with respect to conformal time, is:

$$\frac{d^2\vec{\Psi}}{d\tau^2} + \mathcal{H}(\tau)\frac{d\vec{\Psi}}{d\tau} + \nabla\Phi = 0, \tag{4.25}$$

taking the divergence we obtain:

$$\nabla_x \cdot \left(\frac{d^2\vec{\Psi}}{d\tau^2} + \mathcal{H}(\tau)\frac{d\vec{\Psi}}{d\tau} + \nabla\Phi = \right) - \frac{3}{2}\Omega_{m,0}\mathcal{H}\delta(\tau), \tag{4.26}$$

and using the chain rule we get:

$$\frac{\partial}{\partial x_i} = \left[\frac{d^3q}{d^3x}\right]_{ij}\frac{\partial}{\partial q_j} = \left[\delta_{ij} + \Psi_{i,j}\right]^{-1}\frac{\partial}{\partial q_j}, \tag{4.27}$$

in addition to the perturbative series (4.22) we get the linear solution:

$$\nabla_q \cdot \vec{\Psi}^{(1)} = -\nabla_q^2\Phi^{(1)}(\vec{q},\tau) = -\delta_1(\vec{x},\tau) = -D_1(\tau)\delta_1(\vec{q}) \tag{4.28}$$

$$D_1''(\tau) + \mathcal{H}(\tau)D_1'(\tau) = \frac{3}{2}\mathcal{H}^2(\tau)\Omega_m(\tau)D_1(\tau). \tag{4.29}$$

From there, the particle position in the linear Lagrangian perturbation theory is given by

$$\vec{x} = \vec{q} - \nabla_q^{-1}\delta_1(\vec{x},\tau). \tag{4.30}$$

This is known as Zel'dovich approximation and has been widely used in the literature to study the structure formation at large scales.

But in order to use the machinery of COLA we need to work out the next order, or second order Lagrangian perturbation theory (2LPT).

In this case we get

$$\nabla_q \cdot \Psi^{(2)} = -\nabla_q^2\Phi^{(2)}(\vec{q},\tau) = \frac{1}{2}D_2(\tau)\Sigma_{i\neq j}\left(\Psi^{(1)}_{i,i}\Psi^{(1)}_{j,j} - \Psi^{(1)\Psi^{(1)}_{j,i}}_{i,j}\right), \tag{4.31}$$

where $\Psi^{(1)}_{j,j} = \frac{\partial\Psi_i}{\partial q_j}$.

The position of the particle up to second order, is, then:

$$\begin{aligned}\vec{x} &= \vec{q} - \nabla_q^{-1}\delta_1(\vec{x},\tau) - \nabla_q^{-1}\delta_2(\vec{x},\tau) &(4.32)\\ &= \vec{q} - D_1\nabla_q\Phi^{(1)} - D_2\nabla_q\Phi^{(2)}, &(4.33)\end{aligned}$$

where $D_1(\tau)$ and $D_2(\tau)$ are the time-dependent growth functions. $D_1(\tau)$ follows equation (4.29), whereas $D_2(\tau)$ obeys the following equation:

$$D_2''(\tau) + \mathcal{H}(\tau)D_2'(\tau) - \frac{3}{2}\mathcal{H}^2(\tau)\Omega_m(\tau)D_2(\tau) = -\frac{3}{2}\mathcal{H}^2\left[D_1(\tau)\right]^2. \tag{4.34}$$

The reader can follow the extensive reviews on the matter like the one by Bouchet et al. (1995a) or Bernardeau et al. (2002). More recently, the inclusion of modified gravity models into the perturbative expansion in Lagrangian Perturbation Theory (LPT) has been made (Bose and Koyama, 2017) and (Aviles and Cervantes-Cota, 2017) and evermore, the inclusion of modified gravity theories in the COLA method has been done by Winther et al. (2017). Nevertheless, in what follows I restrain to standard LPT since the model (4.1) is considered only at background level.

In the COLA method we benefit from the fact that the temporal functions D_1 and D_2 can be factorized out, just as is shown in equation (4.32), and used to calculate an exact solution at large, quasi-linear scales.

In particular, we can split the equation of motion for DM particles like (Tassev et al., 2013)

$$T[\Psi_{res}] + T[D_1]\vec{\Psi}^{(1)} + T[D_2]\vec{\Psi}^{(2)} + \nabla\Phi = 0 \tag{4.35}$$

where $T[x] \equiv \frac{d^2x}{d\tau^2} + \mathcal{H}\frac{dx}{d\tau}$ and the contribution Ψ_{res} refers to the remaining displacement when we substract the 2LPT displacements from the full, non-linear displacement each particle should actually feel.

This residual displacement is the one that needs to be computed using the Particle-Mesh algorithm.

Particle mesh algorithms in a nutshell

Here I include a brief overview of the Particle-Mesh (PM) algorithm used by COLA to solve for the $T[\Psi_{res}]$ term. A very nice introduction to the subject is covered in Klypin (2000) and Klypin (2017).

The basic aim of a PM algorithm is to place the DM particles on a grid and to solve for the gravitational forces acting at each point of the grid, to calculate the corresponding displacement of the particles in an iterative way. In a very narrow description, this algorithm follows the next steps:

1. We place a mesh over our N_p DM particles and use a interpolation method like Cloud-in-Cell (CIC), which is a linear method, to calculate the mass density at each mesh point: $\rho(x)$.

2. The density is Fourier-transformed, $\rho(k)$ with help of the Fast Fourier Transform (FFT) routines[1]. With this we can solve the Poisson equation: $k^2\phi(k) = \frac{3}{2}\frac{\Omega_{m,0}}{a}\left[\rho(k) - 1\right]$

3. With the calculation of the gravitational potential $\phi(k)$ the force is computed in the real space by an inverse FFT of $F(\vec{k}) = \vec{k}\phi(\vec{k})$

4. Once the forces in each direction are calculated, the acceleration for each particle can be calculated using the CIC method to interpolate from the mesh points.

The acceleration computed in the last step is combined with the first and second order Lagrangian displacements to update the particle velocities and positions according to:

$$\mathbf{v}_{i+1/2} = \mathbf{v}_{i-1/2} - T[\mathbf{\Psi}_{res}]\Delta a_1, \tag{4.36}$$

$$\mathbf{r}_{i+1} = \mathbf{r}_i + \mathbf{v}_{i+1/2}\Delta a_2 + \Delta D_1\mathbf{\Psi}_1 + \Delta D_2\mathbf{\Psi}_2. \tag{4.37}$$

Here, $\Delta D = D_{i+1} - D_i$ represents the change in growth factors over the timestep, while Δa encodes the time interval.

[1] FFT discrete Fourier Transform are publicly available in hhtp://www.fftw.org/

The choice for Δa is not unique. For instance, the following recipe in terms of integrals of H(a) was proposed in Quinn et al. (1997):

$$\Delta a_1 = \frac{H_0}{a_i}\int_{a_{i-1/2}}^{a_{i+1/2}} \frac{da}{a^2 H(a)}, \tag{4.38}$$

$$\Delta a_2 = H_0 \int_{a_i}^{a_{i+1}} \frac{da}{a^3 H(a)}. \tag{4.39}$$

But Tassev et al. (2013) point out that a better choice for Δa for the COLA method, is:

$$\Delta a_1 = \frac{H_0}{nLPT}\frac{a_{i+1/2}^{nLPT} - a_{i-1/2}^{nLPT}}{a_i^{nLPT-1}} \tag{4.40}$$

$$\Delta a_2 = \frac{H_0}{a}\int_{a_i}^{a_{i+1}} \frac{a^{nLPT-3}}{H(a)} da. \tag{4.41}$$

with $nLPT = 2.5$.

Fast N-body simulations: Parameters of the model tested

For analyzing the non-linear evolution of overdensities with the COLA method we need to insert the evolution of our model into the solutions at first and second order for the growth functions $D_1(\tau)$ and $D_2(\tau)$.

To this end we use the BFVs for the parameters in SEoS model according to the constraints found from "BAO + H_0" datasets (see table 4.2). In a first stage we chose to focus on keeping the cosmological parameters fixed to the same values both in ΛCDM and SEoS models to be able to tell the difference coming only from the dynamical Dark energy.

We have set the values for the Cosmological parameters (fractional overdensities and H_0) to the values reported by Planck 2015 Ade et al. (2016a) labeled "TT + TE + EE + lowP + lens + ext".

In figure 4.19 we portrait the evolution of the Hubble rate as function of scale factor for both models: $SEoS$ and ΛCDM with cosmological parameters set as explained above. We notice a bump of 1.5% at the transition epoch, $a_T = 1/(1+z_T)$ with $z_T = 0.28$ with a steepness of $q = 9.97$.

To include this model into the code we need to solve for the Hubble function and introduce the solution as a table $\{a, H(a)\}$ for the code to interpolate between the values, from the initial time for the simulation until the value of each snapshot asked. It is common to set the initial conditions at $z_{ini} = 49$. In a similar fashion, the solutions for 2LPT growth functions, according to equations (4.29) and (4.34) must be provided for the code to interpolate and solve the analytical part of the models.

Model	Alias	w_0	w_i	q	z_T	$\Omega_{m,0}$	H_0	γ_1	b	γ_2
ΛCDM	I	-1	-1	1	1	0.3089	67.74	5/9	2	6/11
CPL	II	-0.92	-0.99	1	1	0.3089	67.74	0.5535	2.0751	0.5927
SEoS	III	-0.92	-0.99	9.97	0.28	0.3089	67.74	0.5527	2.0743	0.5912
SEoS	IV	-0.92	-0.99	9.97	0.28	0.3340	73.22	0.5533	2.0859	0.5936

Table 4.4: Parameters of the models included in the COLA simulations. Results from this section include model I and III as preliminary results from this work on progress.

The logarithmic growth function, $f(a) \equiv \frac{d\log D_m(a)}{d\log a}$, (2.81), we rewrite it here perturbatively, which means, we calculate the corresponding logarithmic growth for the solutions at first and second order:

$$f^{(1)}(a) = \frac{d\log D_m^{(1)}(a)}{d\log a} \tag{4.42}$$

$$f^{(2)}(a) = \frac{d\log D_m^{(2)}(a)}{d\log a} \tag{4.43}$$

where $D_m^{(1,2)}$ are the solutions at first and second order.

It is widely know in the literature that the following ansatz provide a precise fit for the logarithmic growth functions for standard LCDM models (Bouchet et al., 1995b):

$$f^{(1)}(a) \approx \Omega_m(a)^{\gamma_1}, \tag{4.44}$$

$$f^{(2)}(a) \approx b\Omega_m(a)^{\gamma_2}, \tag{4.45}$$

where $\gamma_1 = 5/9$, $b = 2$ and $\gamma_2 = 6/11$.

We used the same ansatz and fit for the parameters to match the evolution of $f^{(1,2)}$ according to the dynamics in the models considered (see for instance figures 4.22 and 4.23). The fits obtained are shown in Table 4.4, where we included ΛCDM for completeness.

The initial conditions for the models are included with a power spectrum at linear order at the initial redshift of the simulation. For our case, we are dealing with a model that behaves like a cosmological constant in the past ($w_i = -0.99$, model III in table 4.4), so we can propose the same LCDM power spectrum to set initial conditions at $z_i = 49$.

At this point we have run a simulation with the following characteristics:

From this analysis we expect to comparte:

a) The density fields from different models

Name	L_{box}	N_p	N_{mesh}	z_{ini}	n_{step}	z_{out}	N_{run}
L1024(low resolution)	1024	1024	2048	49	100	0,0.28,0.56,1,2	5
L512(high resolution)	512	1024	1024	49	200	0, 0.28, 0.56, 1, 2	5

Table 4.5: Parameters used in low and high-resolution N-body simulations

b) The matter power spectrum at different redshifts: $z = 0, 0.28, 0.56, 1, 2$

c) For the High-resolution simulations, the dark matter haloes two point correlation function where

   i) The dark matter haloes are found using the publicly available code Rockstar[2]

   ii) Whereas the two point correlation function is to be found using the CUTE code[3]

This analysis is ongoing work and will be submitted soon.

[2]https://bitbucket.org/gfcstanford/rockstar

[3]https://github.com/damonge/CUTE

4.5 Remarks & Conclusion

We presented a parametrization for the Dark Energy equation of state and found the constraints compatible with BAO measurements (contained in Table 4.1) combined with the latest local determination of Hubble constant (Riess et al. (2016)). Additionally we used the compressed CMB likelihood from Planck (Ade et al. (2016a)), by means of the sound horizon at decoupling, θ_*, and $\omega_c h^2$. The constraints for free parameters, $\{w_0, w_i, q, z_t, \omega_c, H_0\}$, and their 68% errors resulting from the combined analysis of the datasets were obtained.

We find that a Dynamical form of DE reduces the tension among local measurement of the Hubble constant and the one extrapolated from recombination era by Planck. Whereas for a ΛCDM model, tension between the local determination of H_0 (Riess et al. (2016)) and the value derived from Planck (Ade et al. (2016a)) remains (Table 4.3), we find that it is possible to simultaneously conciliate the observations from BAO, H_0 and CMB (Table 4.2) by means of a dynamical Dark Energy. The reduced numbers of data points and the number of free parameters in the SEoS does at this stage not favour it compared to ΛCDM. However, understanding the dynamics of DE is a central question nowadays in cosmology and a great deal of effort has been focused to construct observational experiments (Dawson et al. (2016)-LSST Science Collaboration et al. (2009)) to determine the evolution of DE. With a more precise dynamics of DE, theoretical models derived from particle physics or modifications to the gravity sector may give a sound derivation of some of the free parameters used in our steep EoS and in this case a dynamical DE would be favoured over ΛCDM.

Regarding the perturbative regime, we find that, when we take a smooth dark energy, the evolution of matter overdensities is sensitive to the parameters in equation (4.1). We showed how the value of the equation of state at large redshifts, w_i, enhances the discrepancy between a cosmological constant solution and SEoS model.

When the dark energy is allowed to cluster, we have an exponential growth of matter overdensities, sourced by the unstable growth of dark energy perturbations, δ_{DE} with a negative term c_{ad}. The characteristics of this term cand get imprinted in the evolution of δ_m via its coupling through δ_{DE}. To mange this exponential growth of density, we added an effective term, $c_{eff} = 1$, which can encode the microphysics of the fluid and the information that is not encapsulated in the equation of state alone. Even when we add this term, we found that the shape and characteristic bump at the transition time is preserved.

From the non-linear evolution, the results are still underway. We have presented the way to introduce this model into the COLA code, using the Lagrangian perturbation theory and the solutions there up to second order.

To summarize, the study of dynamics of Dark Energy is a matter of profound im-

plications for our understanding of the Universe and its physical laws. Although the measurements from CMB are the most precise data sets in Cosmology, the best way to analyze the properties of DE comes from the low redshift regime, where the BAO feature is the most robust cosmic ruler. In this work we have contributed towards that direction, and we have presented the constraints for a dynamical DE model coming from the analysis of BAO distance measurements combined with the most recent H_0 determination and CMB information. Further theoretical and observational effort must be carried out to obtain a better understanding of DE.

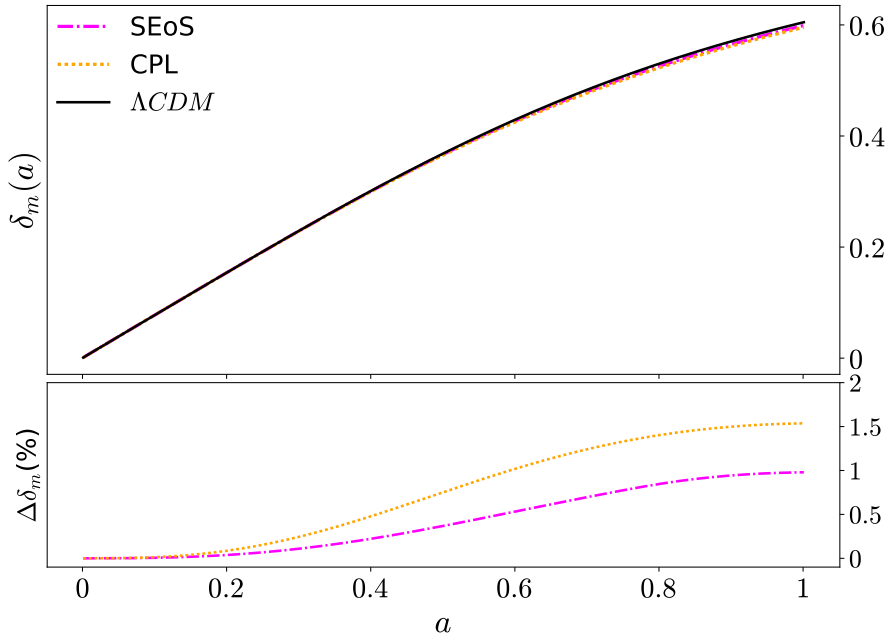

(a) $w_i = -0.99$

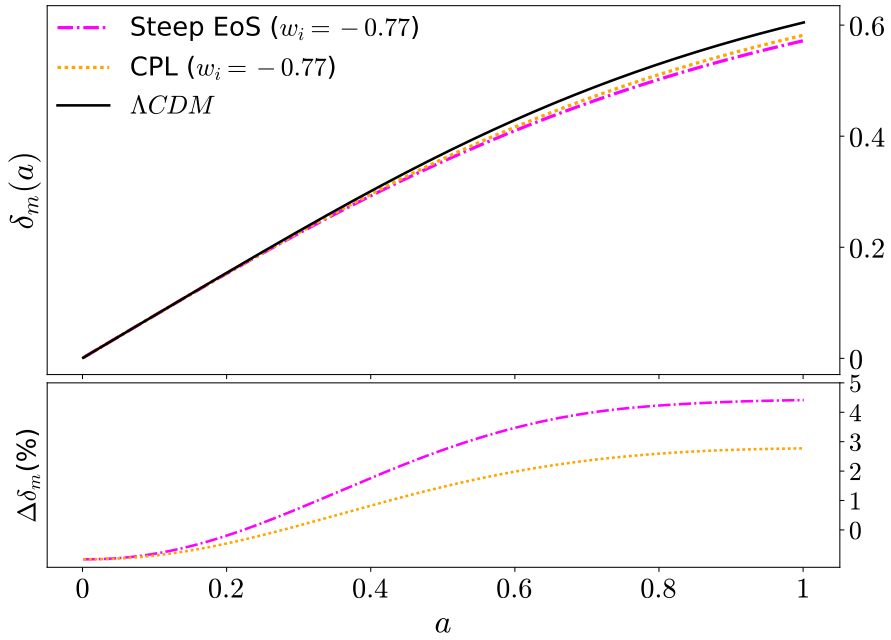

(b) $w_i = -0.77$

Figure 4.11: (Upper panel) Effect of w_i on the growth of matter overdensities assuming $\delta_{DE} = 0$ and SEoS (4.1) with parameters: $\{w_0, q, z_T\} = \{-0.92, 9.97, 0.28\}$ (magenta dot-dashed line). The CPL limit, *i. e.* $q = z_T = 1$ (orange dotted line) and ΛCDM (long-dashed blue line) are also shown. (Lower panel) Ratio of CPL and SEoS solutions to ΛCDM: $(\delta_m(a)/\delta_{m,LCDM}(a))\times 100$.

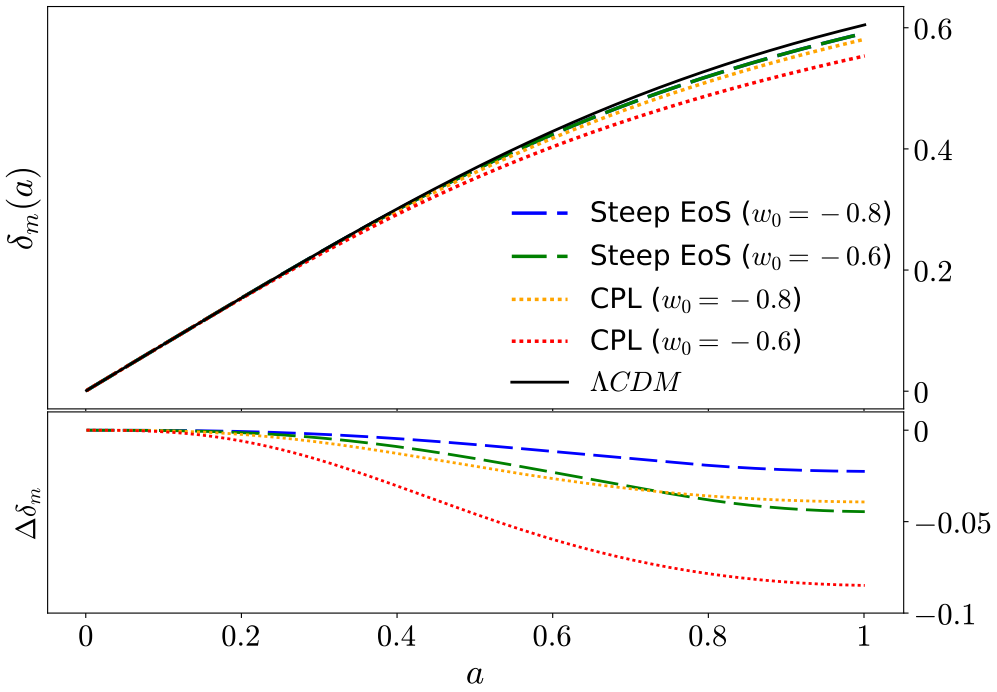

Figure 4.12: Effect of w_0 in the growth of matter overdensities assuming $\delta_{DE} = 0$ and SEoS (4.1) and with parameters: $\{w_i, q, z_T\} = \{-0.99, 9.97, 0.28\}$ with $w_0 = -0.8$ (long dashed green line) and $w_0 = -0.6$ (long dashed blue line). The dotted lines represent the corresponding CPL limit and the solid black curve, the LCDM solution

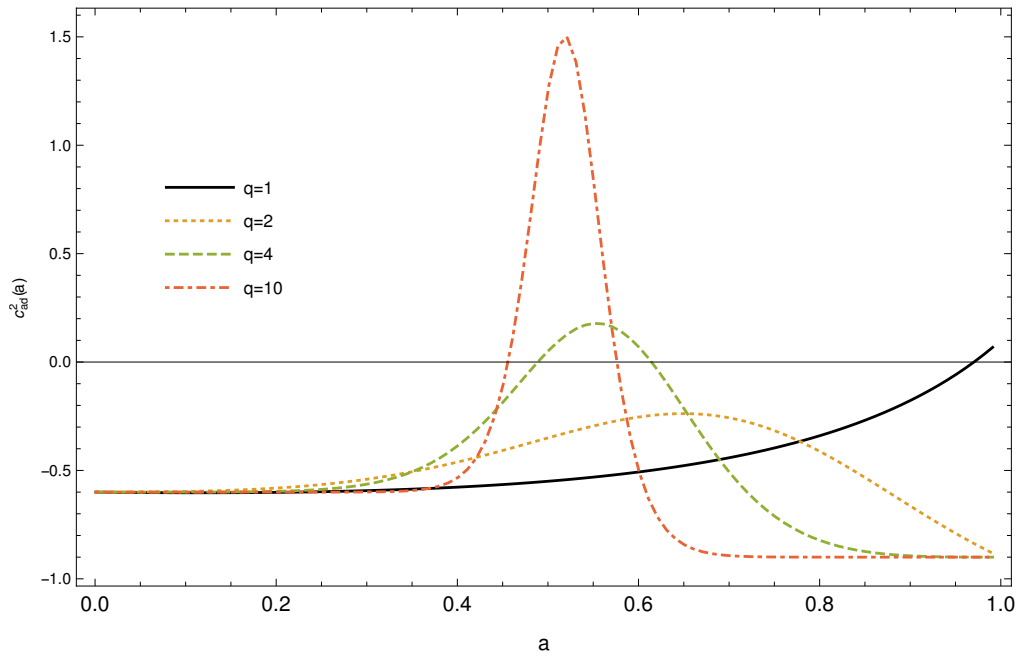

Figure 4.13: Adiabatic sound speed c_{ad} as function of scale factor assuming SEoS (4.1) with $w_0 = -0.9$, $w_i = -0.6$, $z_T = 1$ and different values of the exponent: $q = 1$(solid black curve), $q = 2$ (dotted orange), $q = 4$ (dashed green) and $q = 10$(dot-dashed red line).

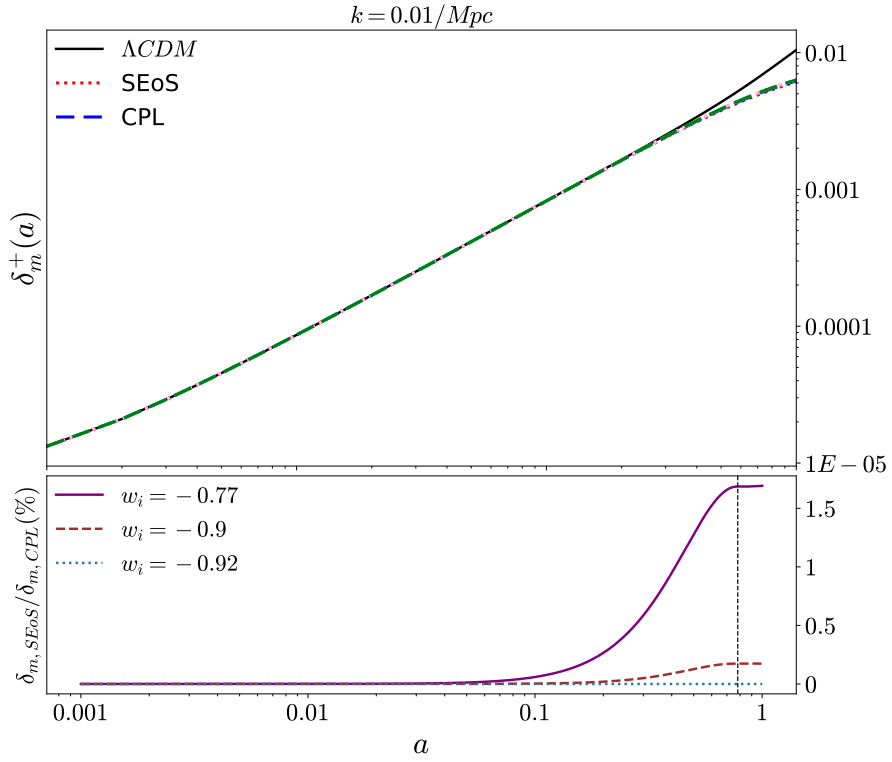

(a) $w_i = -0.77, -0.8, -0.92$

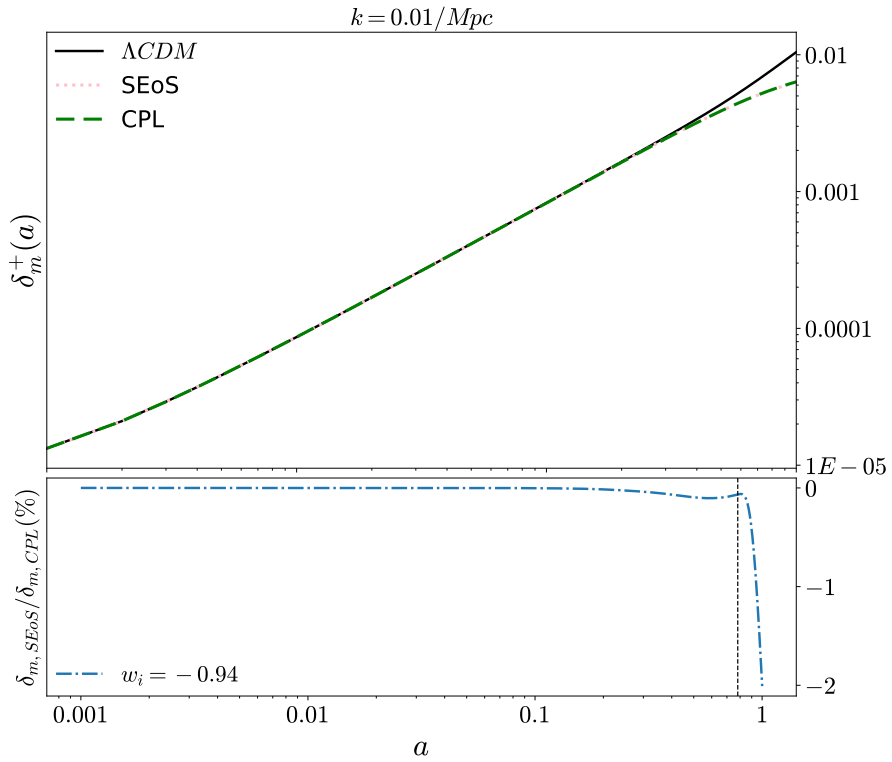

(b) $w_i = -0.94$

Figure 4.14: (Upper panel) Effect of w_i on the growth of matter overdensities in the presence of Clustering Dark Energy with an equation of state assuming $c_{eff} = 1$ and SEoS (4.1) with parameters: $\{w_0, q, z_T\} = \{-0.92, 9.97, 0.28\}$ (magenta dot-dashed line). The CPL limit (orange dotted line) and ΛCDM (long-dashed blue line) are also shown. (Lower panel) Ratio of CPL and SEoS solutions to ΛCDM: $(\delta_m(a)/\delta_{m,LCDM}(a))\times 100$.

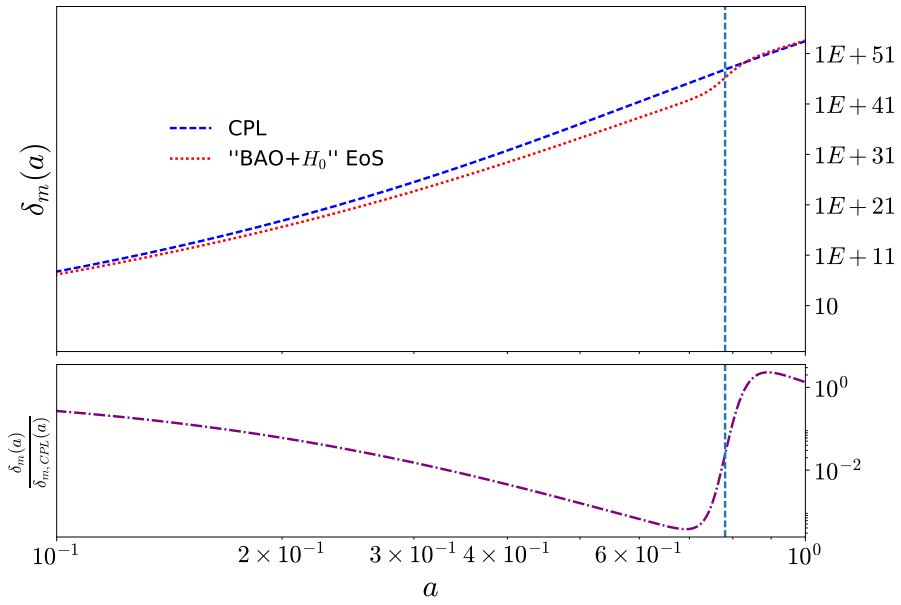

Figure 4.15: (Upper panel) Effect of w_i in the growth of matter overdensities from equations (4.18) when $\delta DE \neq 0$ and $c_{eff} = 1$. The best fit EoS referenced as "BAO + H_0" in table 4.2, and the corresponding CPL (3.19) limit are shown. (Lower panel) Ratio of "BAO + H_0" solution to CPL. The vertical dashed line represents the transition time, $a_T = 1/(1 + z_T)$ for z_T value of "BAO+H_0" from table 4.2.

.

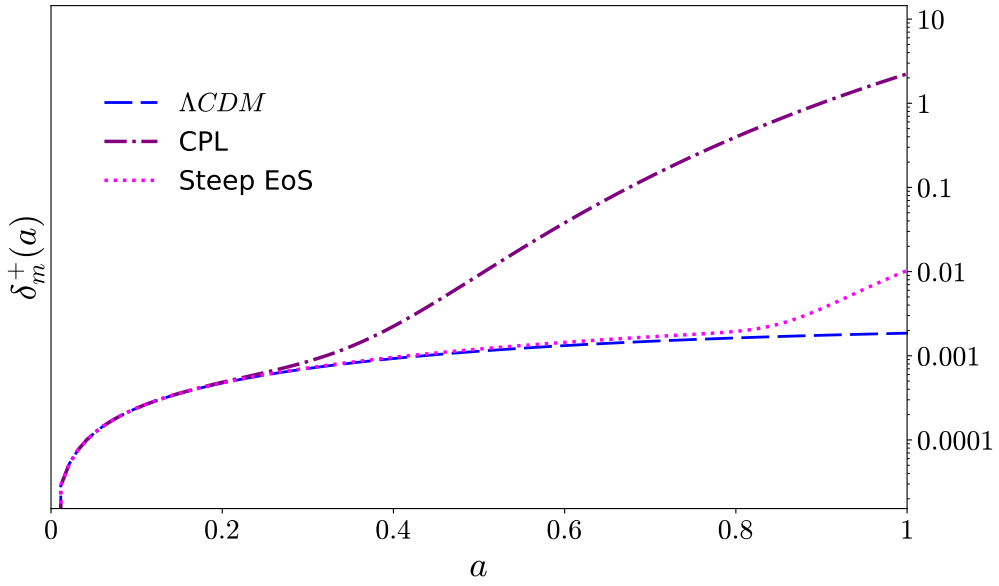

Figure 4.16: Solution for δ_m from the system of equations (4.18) using the model "BAO+H_0" from table 4.2 (magenta dot line), its CPL limit (purple dot-dashed line), and ΛCDM model (blue long-dashed line). In the two former cases the term $c_{eff} = 1$ added to the adiabatic speed of sound $c_s^2 = c_{ad}$ (4.19). We use a k-mode $k = 0.01 Mpc^{-1}$.

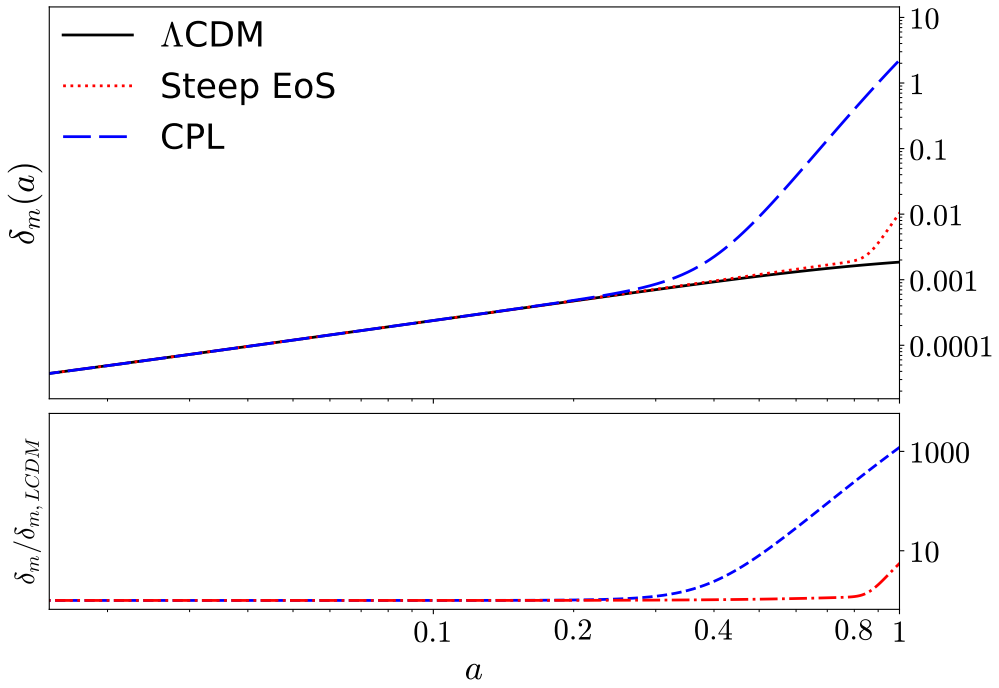

Figure 4.17: Same as in Figure 4.16 but in logarithmic scale. In the bottom panel we show the ratio between SEoS solution and ΛCDM, and the CPL limit (taking $q = z_T = 1$) to ΛCDM.

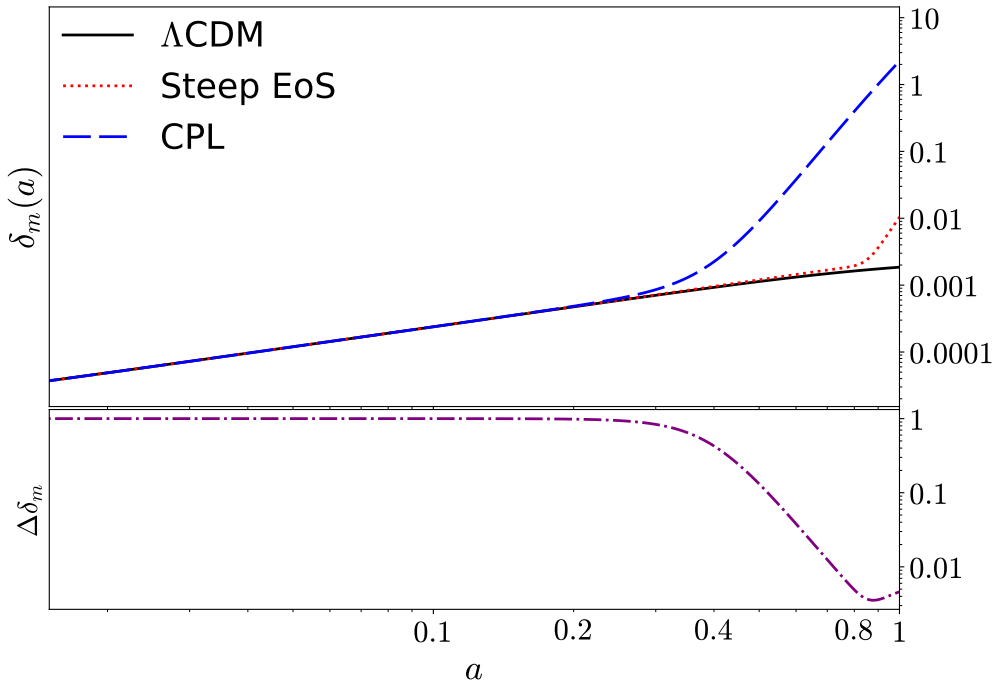

Figure 4.18: Same as in Figure 4.17 but in the bottom panel we show the ratio between SEoS solution and its CPL limit (taking $q = z_T = 1$) to ΛCDM to see the effect of an abrupt transition in the DE EoS.

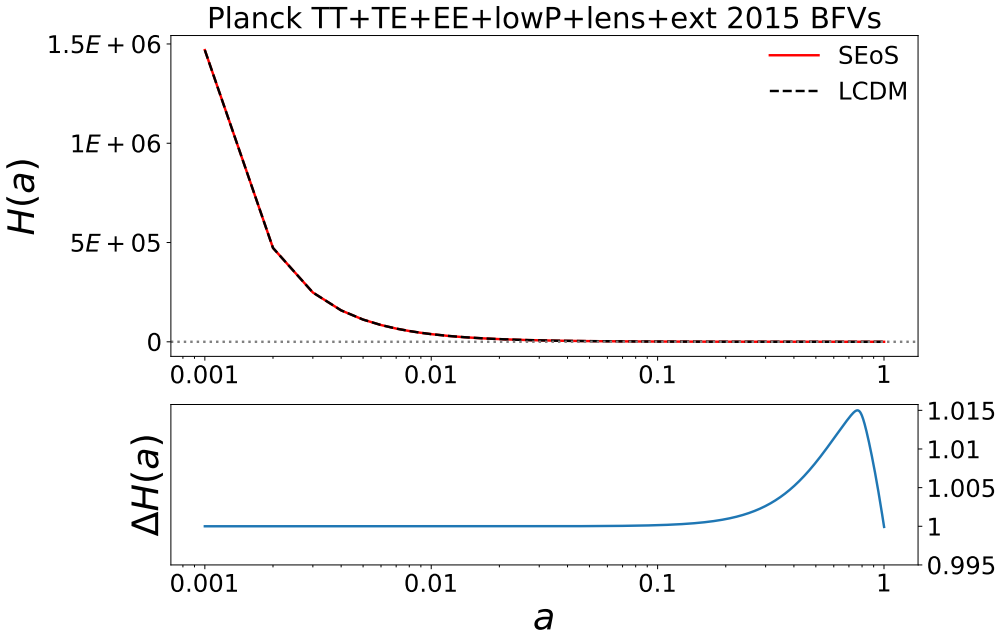

Figure 4.19: Evolution of the Hubble rate (4.3) as function of scale factor for Cosmological constant model (dashed black line) and for equation (4.1), dubbed as "SEoS" (for Steep Equation of State) with BFV from "$BAO + H_0$" results (solid red line) (table 4.2). The bottom panel shows the relative difference between both solutions. The cosmological parameters like fractional densities are kept to be the same value from the Planck report indicated in the title of the figure.

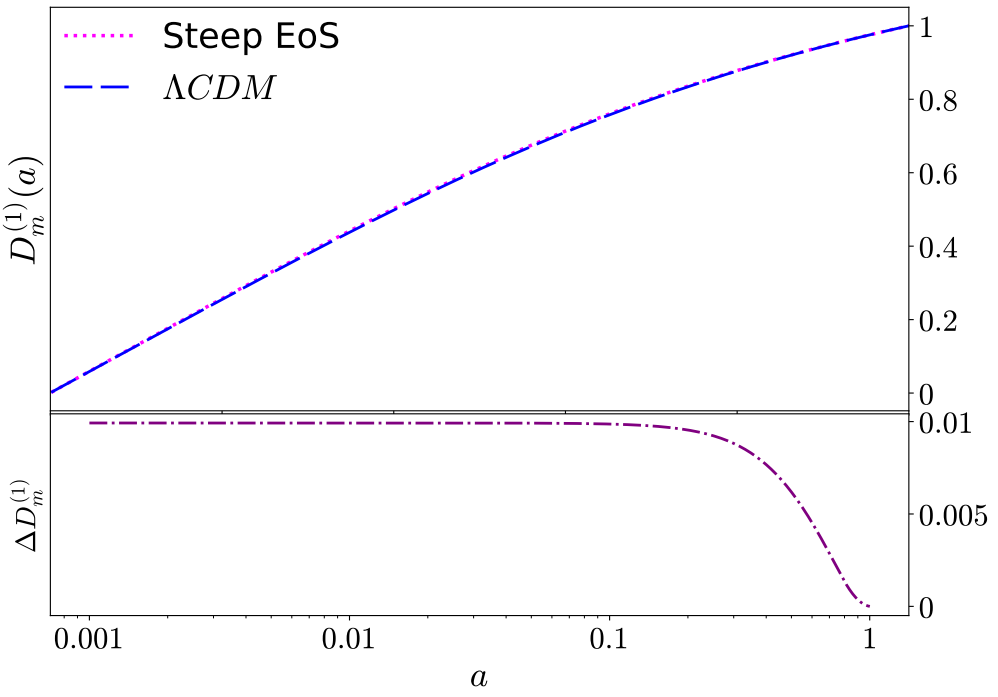

Figure 4.20: (Top panel) Solution to the growth function at first order as function of scale factor (4.29) including $SEoS$ model (4.1) in the background and a cosmological constant solution. (Bottom panel) Ratio between both solutions, this is $\Delta D_m^{(1)} = (D_{m,SEoS}^{(1)} - D_{m,LCDM}^{(1)})/D_{m,LCDM}^{(1)}$.

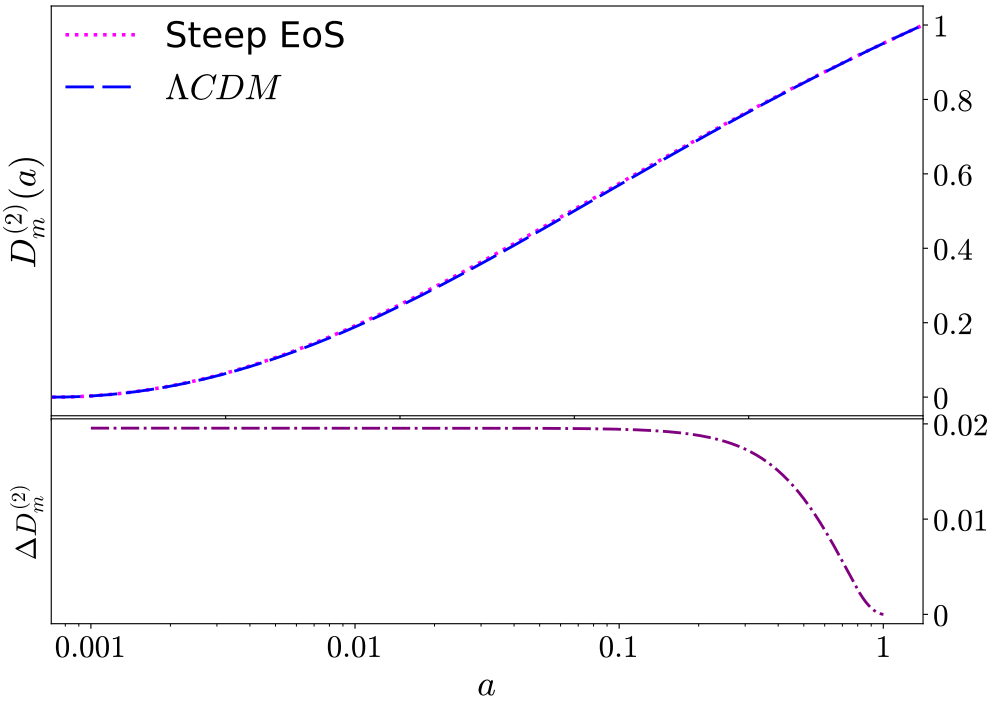

Figure 4.21: (Top panel) Solution to the growth function at second order as function of scale factor (4.34) including $SEoS$ model (4.1) in the background and a cosmological constant solution. (Bottom panel) Ratio between both solutions, this is $\Delta D_m^{(2)} = (D_{m,SEoS}^{(2)} - D_{m,LCDM}^{(2)})/D_{m,LCDM}^{(2)}$.

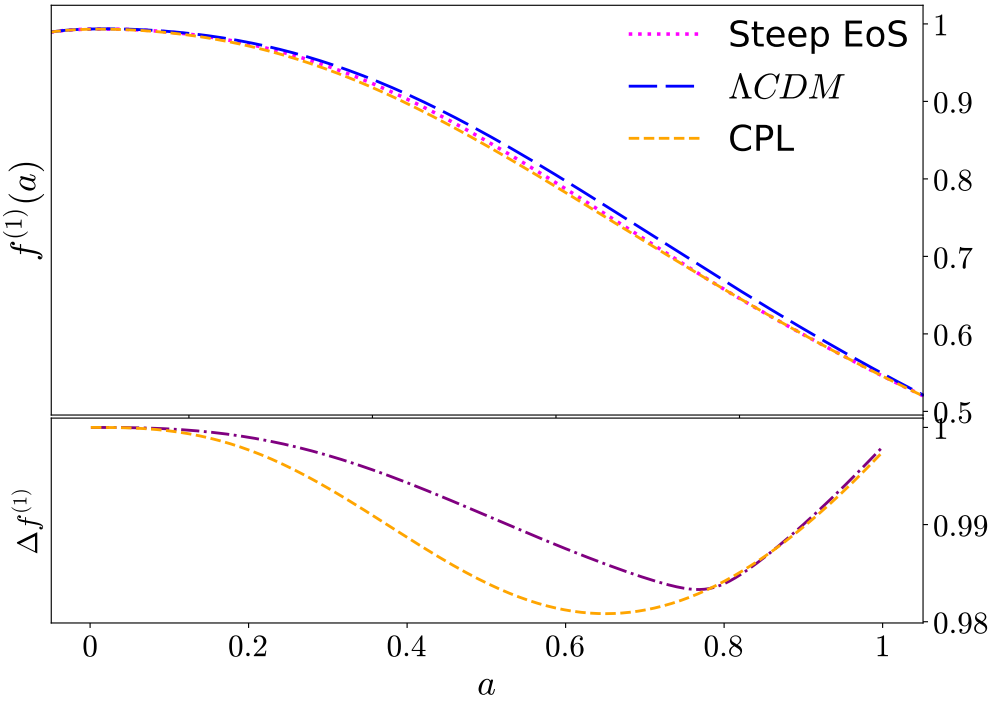

Figure 4.22: (Top panel) Solution to the logarithmic derivative of the growth function at first order, for $SEoS$ model (dotted line), its CPL limit (dashed line) and ΛCDM model (long-dashed line). (Bottom panel) The relative difference between $SEoS$ model and CPL model to the ΛCDM solution.

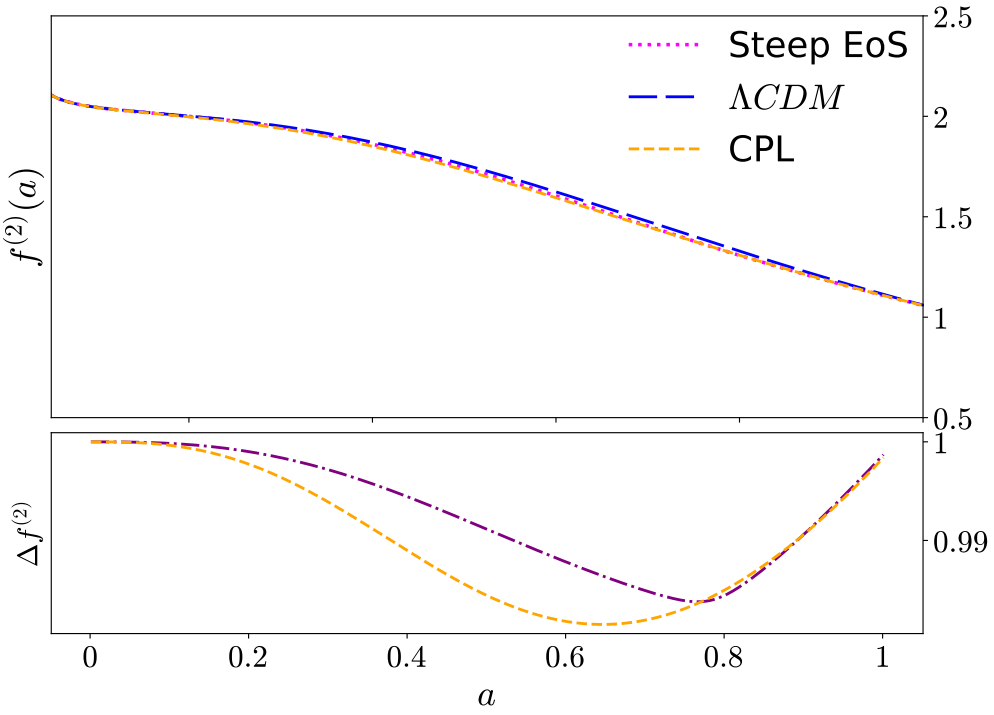

Figure 4.23: Same as in figure 4.22 but for the second order logarithmic growth function.

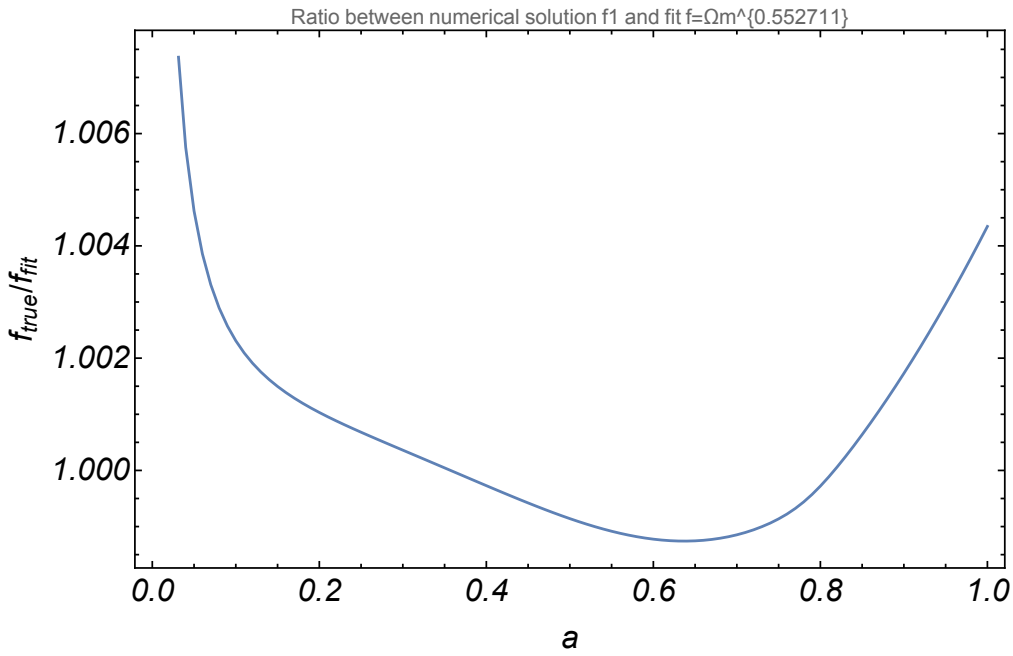

Figure 4.24: Comparison of the numerical fit for f_1 and the numerical solution in the case of $SEoS$ model with Planck cosmological parameters (Model III in Table 4.4.)

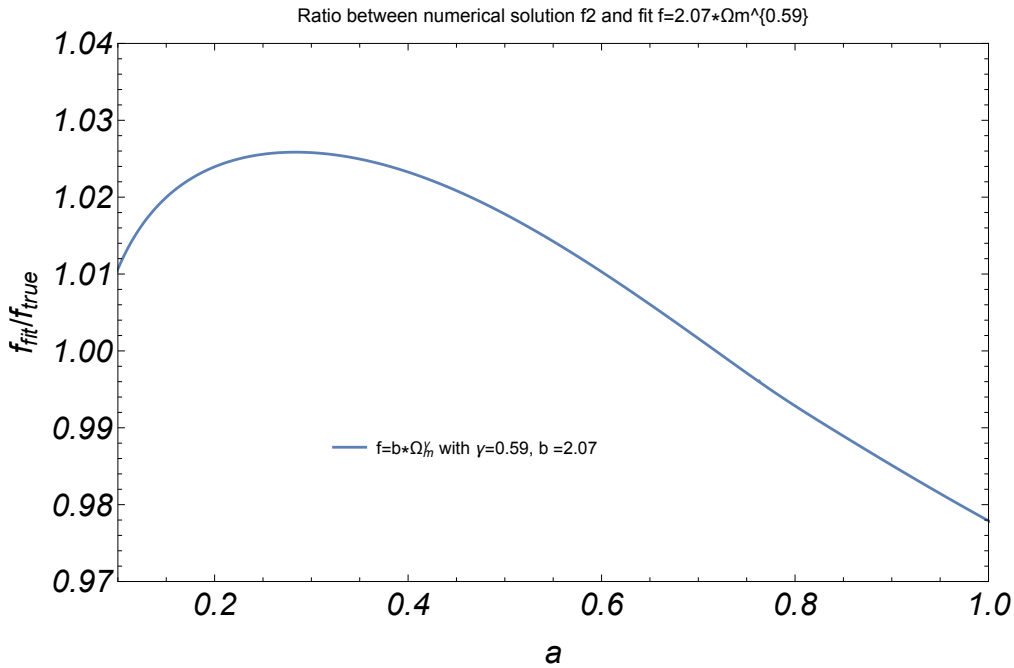

Figure 4.25: Same as in figure 4.24 but for the second order logarithmic growth function.

5

$f(\mathcal{R})$ for Surveys

In section 3.2 I have introduced the basic notions of $f(R)$ gravity models, including the properties that are imposed to make them viable dark energy candidates. In order to extract the cosmological dynamics of this kind of theories, in this chapter, we are using the Ricci scalar approach to $f(R)$ proposed in (Jaime et al., 2011) and later on used for cosmology in Jaime (2015); Berti et al. (2015).

5.1 $f(\mathcal{R})$ cosmology and geometric equation of state

We consider a homogeneous, isotropic universe described by the FLRW metric (2.5):

$$ds^2 = -dt^2 + a^2(t)\left[\frac{dr^2}{1-Kr^2} + r^2\left(d\theta^2 + \sin^2\theta d\phi^2\right)\right], \tag{5.1}$$

with $K = 0$.

Recalling equation (3.7):

$$\begin{aligned} G_{\mu\nu} = &\frac{1}{f_R}\left[f_{RR}\nabla_\mu\nabla_\nu R + f_{RRR}(\nabla_\mu R)(\nabla_\nu R)\right. \\ &\left. -\frac{g_{\mu\nu}}{6}(Rf_R + f + 2\kappa^2 T) + \kappa^2 T_{\mu\nu}\right] \end{aligned} \tag{5.2}$$

we note that the right-hand side of this equation defines the total energy momentum tensor (EMT), $T^{tot}_{\mu\nu}$, whereas the matter EMT, $T_{\mu\nu}$ corresponds to a fluid composed by baryons, dark matter and radiation, interacting only gravitationally.

We recall that for the baryons and DM component $p_m = 0$, whereas for radiation $p_{rad} = \rho_{rad}/3$. Under these assumptions, the corresponding equations for the Ricci scalar and the modifed Friedman equations are:

$$\ddot{R} = -3H\dot{R} - \frac{1}{3f_{RR}}\left[3f_{RRR}\dot{R}^2 + 2f - f_R R - \kappa\rho_m\right] \tag{5.3}$$

$$H^2 = \frac{\kappa}{3}(\rho + \rho_X) \tag{5.4}$$

$$\dot{H} = -H^2 - \frac{\kappa}{6}\left[\rho + \rho_X + 3(p_{rad} + p_X)\right] \tag{5.5}$$

where $\rho = -T^{\mu}_{\mu}$ is the total energy density of matter and ρ_X and p_X are the density and pressure of the *geometric dark energy* (GDE). In Jaime et al. (2014) the following definitions for ρ_X and p_X are given:

$$\rho_X = \frac{1}{\kappa^2 f_R}\left[\frac{1}{2}(f_R - f) - 3 f_{RR} H \dot{R} + \kappa^2 \rho (1 - f_R)\right] \tag{5.6}$$

$$p_X = -\frac{1}{3\kappa^2 f_R}\left[\frac{1}{2}(f_R + f) + 3 f_{RR} H \dot{R} - \kappa^2 (\rho - 3 p_{rad} f_R)\right] \tag{5.7}$$

which come from an EMT defined from (3.7) (which can be rewritten as $G_{\mu\nu} = \kappa T^{tot}_{\mu\nu}$) as follows:

$$T^X_{\mu\nu} \equiv T^{tot}_{\mu\nu} - T_{\mu\nu} \tag{5.8}$$

and so, the EoS for the geometric dark energy in $f(R)$ is given by:

$$w_X = \frac{3H^2 - 3\kappa P - R}{3(3H^2 - \kappa\rho)}, \tag{5.9}$$

where the Ricci scalar is given by $R = 6(\dot{H} + 2H)$, P and ρ are presure and density, respectively, of the matter and radiation content.

This EoS is obtained in (Jaime et al., 2012) where it is shown that this choice of the EoS has no degeneracies and in (Jaime et al., 2014) the conservation of $T^X_{\mu\nu}$ and $T^{tot}_{\mu\nu}$ is discussed.

As reviewed in 3.2, the cosmologically viable $f(R)$ models are the Starobinsky model (3.12), the Hu & Sawicki model (3.11), and the exponential model (3.13).

In order to test the cosmology derived from $f(R)$ theories we need to integrate the field equations from the past to the future, which are of fourth order on the metric and behave like attractors; therefore its implementation into Boltzmann codes for alternative models (Zumalacarregui et al., 2017) or surveys is complex and requires many assumptions.

5.2 Parameterizing the $f(R)$ cosmology

An interesting result was found by Zhao et al. (2017). Using all the currently available data, a non-parametric reconstruction for the equation of state of dark energy was performed and the resulting shape was quite distinctive, crossing the phantom divide line multiple times.

In this work, Zhao et al. (2017), performed a combination of the different observations in different bins (3 redshift bins or 9) and reconstruced the value for $w(z) = p_{DE}/\rho_{DE}$ for every bin, resulting in the different profiles depicted in figure 5.2. The ligth blue contour in Figure 5.1 corresponds to the fifth panel in the bottom of figure 5.2. The dark blue contours in 5.1 show a forecasting for DESI experiment.

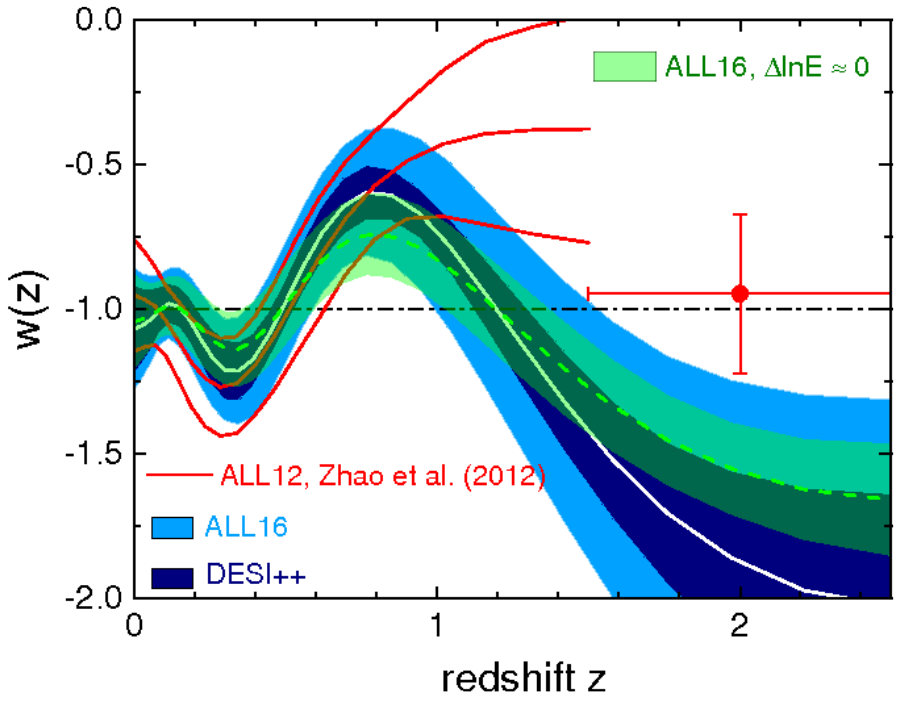

Figure 5.1: Reconstruction of the equation of state $w(z)$ of Dark energy as reported by Zhao et al. (2017).

It is important to stress out that the results shown in Zhao et al. (2017) lead to an Universe with a dynamical and no monotonic dark energy which have been obtained without assuming any theoretical model behind. If this result prevails when future surveys provide observations, a mechanism to account for this oscillatory behaviour will be required.

Moreover, the kind of oscillation portrayed in 5.1 cannot be produced with a single quintessence field (Shafieloo et al., 2012) and, although combinations of two or more fields could be invoked, there should be a physical motivation to support such combinations.

However, this profile can be produced by modified gravity, in particular, $f(R)$ gravity provides an oscillating evolution of $w_X(z)$ as a generic characteristic of the theory, as it was shown in (Jaime et al., 2014).

So, in (Jaime et al., 2018), we present the construction of a new parameterization for the EoS in order to reproduce a variety of $f(R)$ models between $[0.5\% - 0.8\%]$ of precision which can help to test these models in a straightforward way.

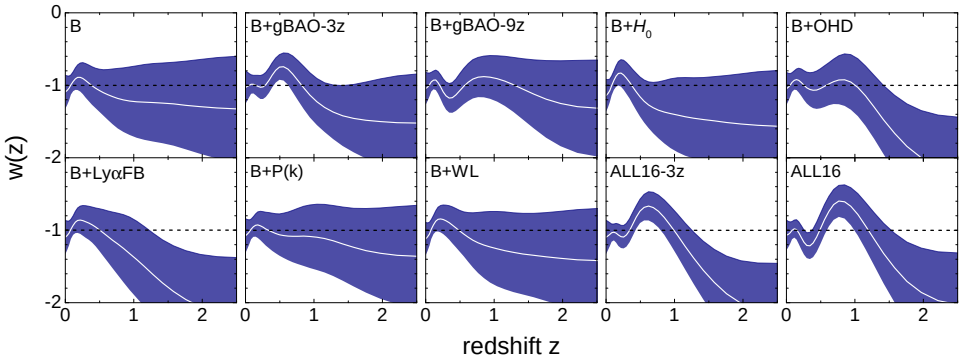

Figure 5.2: Process of reconstrucion of the equation of state for DE presented in (Zhao et al., 2017). This figure shows the dependence on the data sets used and the different number of bins to split the observational information (3 bins or 9 bins).

Solving $f(R)$ cosmology

Hereafter we focus on the three $f(R)$ models presented in 3.2 and recovered here for the sake of clarity. We recall that these have been chosen for being the cosmologically viable alternatives fulfilling the conditions stated in Section 3.2.

a) Hu & Sawicki model (Hu and Sawicki, 2007)

$$f(R) = R - R_{\rm HS}\frac{c_1\left(\frac{R}{R_{\rm HS}}\right)^n}{c_2\left(\frac{R}{R_{\rm HSHS}}\right)^n + 1}\,, \tag{5.10}$$

b) Starobinsky model (Starobinsky, 2007)

$$f(R) = R + \lambda R_S\left[\left(1+\frac{R^2}{R_S^2}\right)^{-q} - 1\right], \tag{5.11}$$

c) The exponential model (Linder, 2009)

$$f(R) = R + \beta R_*(1 - e^{-R/R_*}). \tag{5.12}$$

For these particular proposals the field equations were integrated numerically. The numerical integration is performed by using a fourth order Runge-Kutta integrator. Initial conditions are fixed in the past at some value of z where $\Omega_M(z)$ is very close to 1, the value of the EoS for the geometric dark energy is $\omega_X = -1$ at this value of redshift. The Hamiltonian constrains imposed by H^2 in (3.9) are used as an internal test in the

$f(R)$ model	$\Omega_M(z=0)$	Parameter values
Hu-Sawicki	0.20	$c_2 = 2.78 \times 10^{-5}$
	0.25	$c_2 = 7.98 \times 10^{-5}$
	0.30	$c_2 = 1.95 \times 10^{-4}$
Starobinsky 2007	0.20	$\lambda = 1.15$, $R_S = 1$
	0.25	$\lambda = 1.0$, $R_S = 1$
	0.30	$\lambda = 0.9$, $R_S = 1$
Exponential	0.20	$\beta = 0.5$, $R_* = 5$
	0.25	$\beta = 0.8$, $R_* = 5$
	0.30	$\beta = 0.6$, $R_* = 6$

Table 5.1: First column: $f(R)$ model, second column: Ω_m^0 and third column value of the parameters for each model. For the Hu-Sawicki model we have computed, for the three cases, the values for c_2 by taking $R_{HS} = 1$ and $f_R^0 = 0.01$ and the corresponding Ω_m^0 value, c_1 will be given by $c_1 = c_2 6(1 - \Omega_m^0)/\Omega_m^0$ (see (Hu and Sawicki, 2007) for a detailed explanation). For the Starobinsky model we have taken $n = 2$ for the three cases.

code (see Jaime et al. (2012) for a detailed revision about the implementation in cosmology). The values for the parameters of each $f(R)$ model are listed in table (5.1) as well as the value of $\Omega_M(z=0)$.

By integrating the field equations we will obtain the evolution for R and H and also $\dot{H}$, this is the information we need to compute the EoS w_X given by (5.9).

Fitting the numerical results: proposing a parameterization

In figure 5.3 we show some of the possible ways of fitting the numerical solution for Hu-Sawicki model. The result from numerical integration of the field equations is shown in a solid black curve. Dashed lines represent polynomial fittings of different orders and red dots the interpolation over the discrete values of redshift. In the bottom panel the residual of those fittings are shown.

According to the results shown in Table 5.1 and in Figure 5.3, we present the following proposal for a parametric EoS in $f(R)$:

$$w(z) = -1 + \frac{w_0}{1 + w_1 z^{w_2}} cos(w_3 + z) \tag{5.13}$$

where w_i are free parameters and z is the standard redshift given by $z = a_0/a - 1$. We notice that Equation (5.13) has a present value given by $w(z=0) = w_0 cos(w_3) - 1$, recovers $w_X = -1$ at large redshifts and allows oscillations in the range of interest for observations and future surveys.

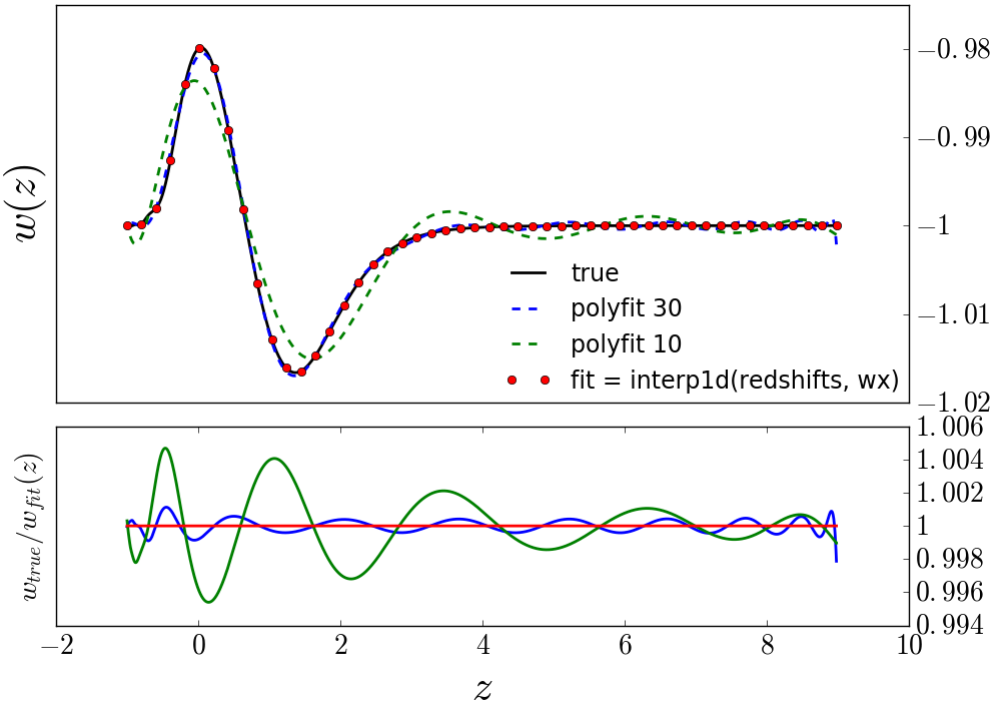

Figure 5.3: Numerical fits for the evolution of (5.9) for the particular case of the Hu & Sawicki (HS) model.

An alternative functional form for our ansatz is

$$w(z) = -1 + \frac{\bar{w}_0}{1 + w_1 z^{w_2}} cos(w_3 z^{0.66}) \tag{5.14}$$

which behaves adequately at $z \approx 3$. This is portrayed in figure 5.4. Nevertheless we opted to present equation (5.13) as our parameterisation in (Jaime et al., 2018) because of its simpler form and the fact that $w_X(z)$ is anyway going to -1 for $z \gtrapprox 3$. With that in mind, we will be alluding to equation (5.13) as the ansatz for modelling $f(R)$-like behaviour and contrasting with observations. Equation (5.13) will be dubbed *JJE parameterization* for brevity.

Testing the parameterization

In order to see how good fit (5.13) is, we used *Mathematica* software in order to fit the cosmological parameters, through the *Levenberg–Marquardt* algorithm although we checked several other algorithms for function minimization, and we got a fit precision of 10^{-10}.

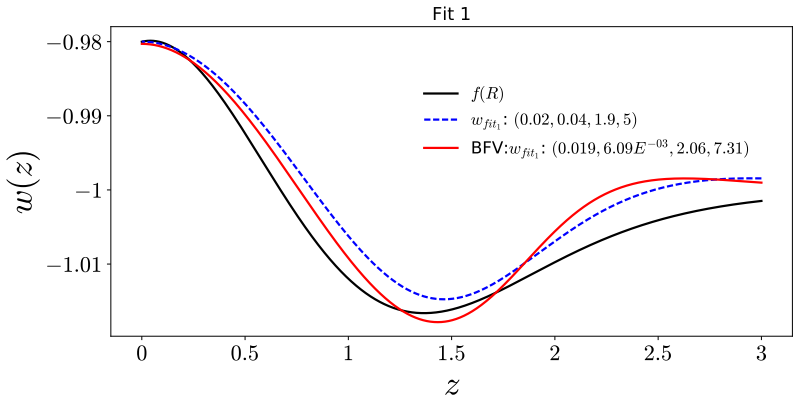

(a) Parameterization (5.13).

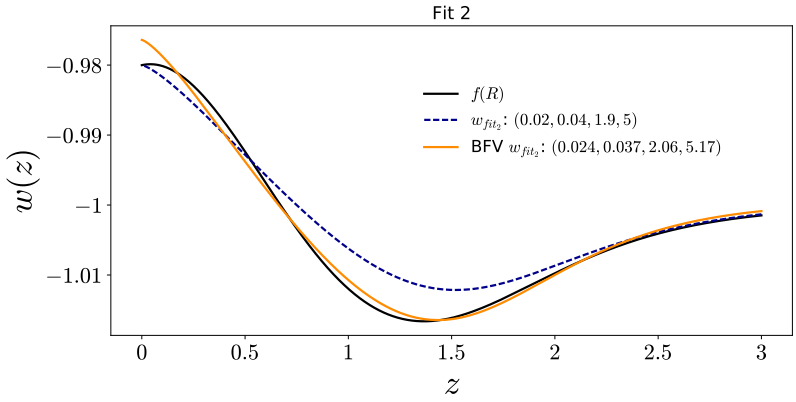

(b)

Figure 5.4: parameterization (5.14).

Figure 5.5: Evolution of the EoS according to equation (5.9) (solid black curve) and to ansatz (5.13) or (5.14) (dashed blue curve) for the values of its free parameters as indicated in the label. The red(orange) solid curve shows the functional form for the respective ansatz taking the parameters which optimize the fitting to the theoretical curve.

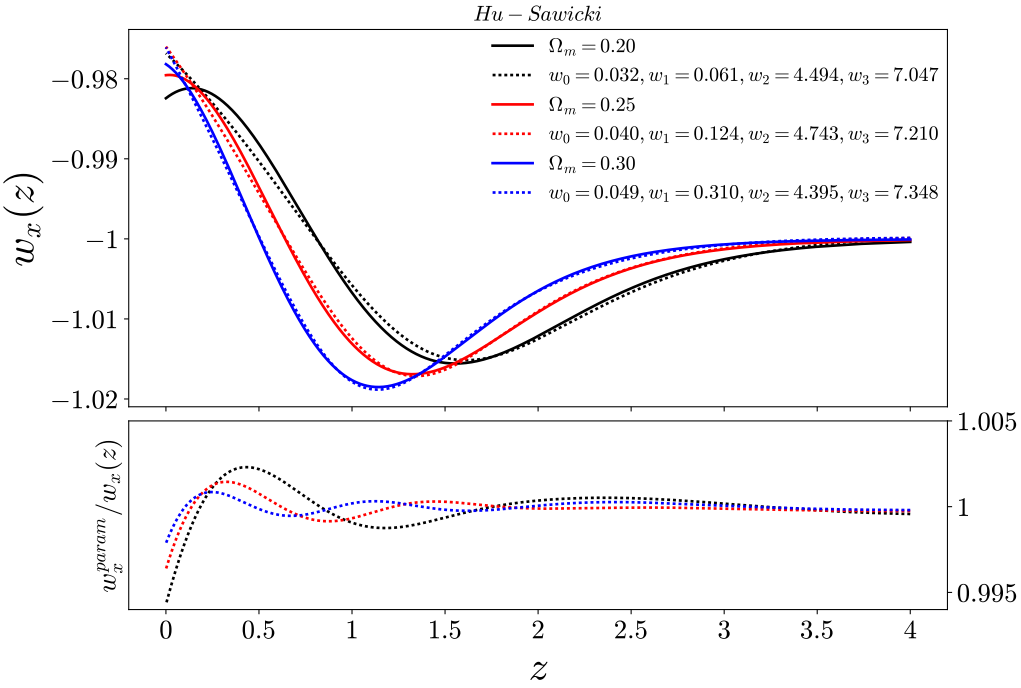

Figure 5.6: Upper frame: Geometric dark energy EoS for the Hu-Sawicki model (3.11) with different values of Ω_m^0. Solid lines represent the numerical integration of the field equations and their reconstruction (in dashed lines) comes from the best fit by using (5.13) (JJE parameterization). a) Black is for $\Omega_m^0 = 0.20$, b) Red is for $\Omega_m^0 = 0.25$ and c) Blue is for $\Omega_m^0 = 0.30$. Best fit parameters are shown in the plot for each case. Bottom frame: Evolution of the ratio parameterized $\omega_{X,param}$ and numerical EoS ω_X, where we see that values remain within 0.5%.

Figures 5.6-5.8 show the evolution for the models (3.11)-(3.13) and the best fit for each one of them by using our proposal (5.13).

We notice that the evolution can be recovered for (3.11) and (3.12) within 0.5% while for (3.13) fits are within 0.8% of precision.

These are more than reasonable values where current and future experiments can set a cut off over the cosmological parameters, e.g. for BOSS (BGS) and BOSS we have an enough statistical significance for our parameterisation at 1% below $z = 1$. Between $z = 1$ and $z = 2$, eBOSS and EUCLID would be within 1% accuracy for our fit (Aghamousa et al., 2016).

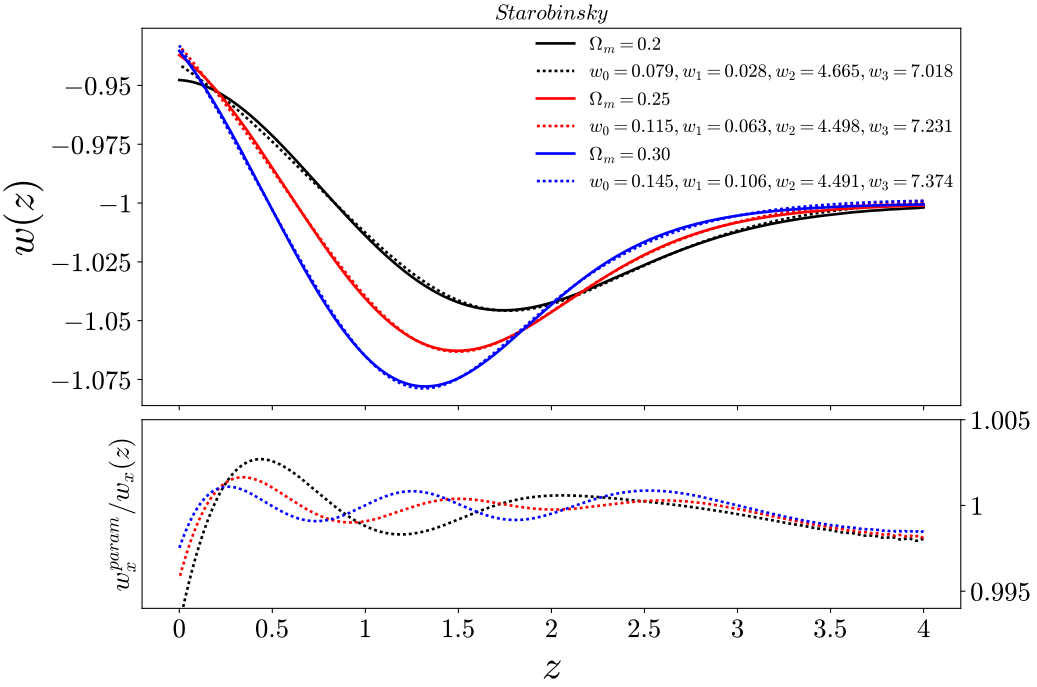

Figure 5.7: Upper frame: Geometric dark energy EoS for the Starobinsky model (3.12) with different values of Ω_m^0. Solid lines represent the numerical integration of the field equations and their reconstruction (in dashed lines) comes from the best fit by using (5.13) (JJE parameterization). a) Black is for $\Omega_m^0 = 0.20$, b) Red is for $\Omega_m^0 = 0.25$ and c) Blue is for $\Omega_m^0 = 0.30$. Best fit parameters are shown in the plot for each case. Bottom frame: Evolution of the ratio parameterized $\omega_{X,param}$ and numerical EoS ω_X, we see that values remains within 0.5%.

5.3 Statistical analysis

Data

Given that we are interested in modelling the late-time evolution of the universe we use observational data from BAO redshift surveys, SNeIA luminous distance from Union 2.1 (Suzuki et al., 2012) and the latest high-z measurements of $H(z)$ from Cosmic Chronometers (Moresco et al., 2016b).

We use measurements of the BAO peak from the galaxy redshift surveys six-degree-field galaxy survey (6dFGS (Beutler et al., 2011)), Sloan Digital Sky Survey Data Release 7 (SDSS DR7 (Ross et al., 2015)) and the reconstructed value (SDSS(R) (Padmanabhan et al., 2012)), as well as the latest result from the complete BOSS sample SDSS DR12 (Alam et al., 2016), and also from the Lyman-α Forest measurements from

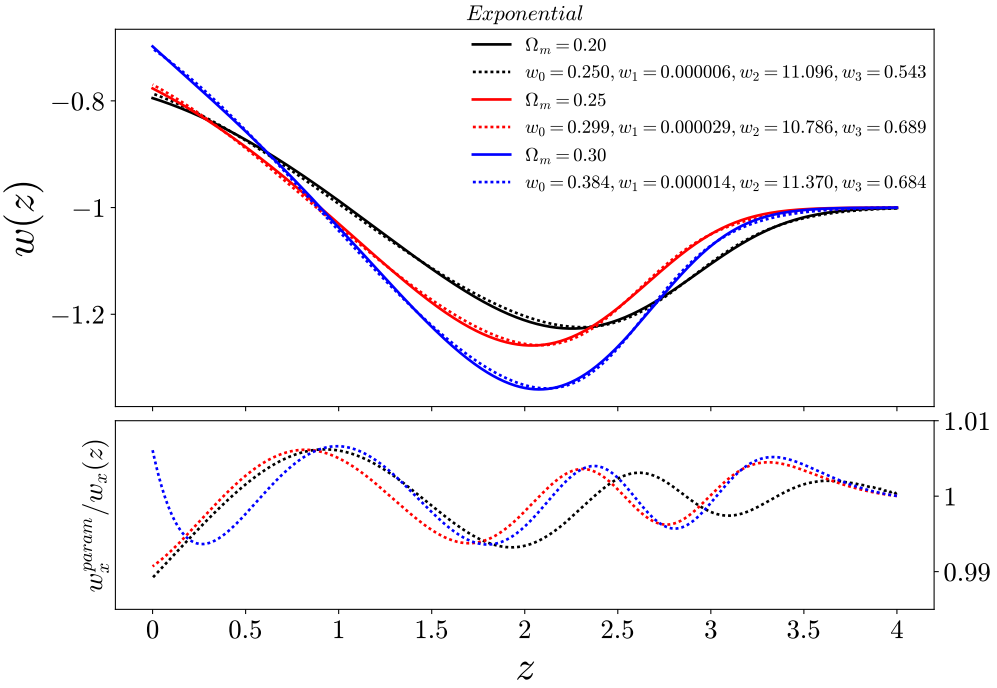

Figure 5.8: Upper frame: Geometric dark energy EoS for the Exponential model (3.13) with different values of Ω_m^0. Solid lines represent the numerical integration of the field equations and their reconstruction (in dashed lines) comes from the best fit by using (5.13) (JJE parameterization). a) Black is for $\Omega_m^0 = 0.20$, b) Red is for $\Omega_m^0 = 0.25$ and c) Blue is for $\Omega_m^0 = 0.30$. Best fit parameters are shown in the plot for each case. Bottom frame: Evolution of the ratio parameterized $\omega_{X,param}$ and numerical EoS ω_X, where we see that values remains within 0.8%.

the Baryon Oscillation Spectroscopic Data Release 11 (Since the volume surveyed by BOSS and WiggleZ (Kazin et al., 2014) partially overlap we do not use data from the latter in this work (see details in Beutler et al. (2016a)).

Even though the current supernovae compilation is given by the JLA sample (Betoule et al., 2014), we implemented the Union 2.1 sample since the apparent magnitude ratio is less than 0.2% in the redshift range of our interest (above $z = 1$) in comparison to the JLA sample.

In addition to the free parameters in (5.13) we vary the fractional amount of matter Ω_m and the value of H_0, by means of a standard χ^2 approach we find the constraints at 1 and 2-σ level.

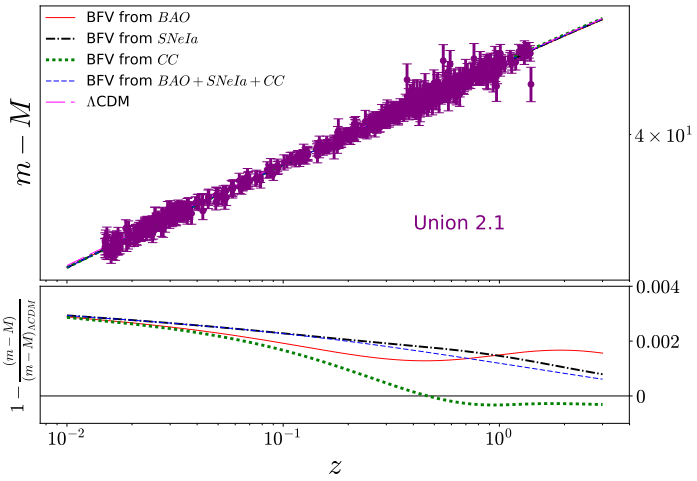

Figure 5.9: Fit of the Union 2.1 sample

Parameters	BAO	SNeIa (Union2.1)	CC
$w(z=0)$	-0.700	-1.052	-1.288
χ^2_{min}	9.550	542.770	15.930
$\chi^2_{\text{red}} = \chi^2_{\text{min}}/(\text{d.o.f})$	9.550	0.980	0.72
w_0	1.016	-0.179	0.288
w_1	9.244	0	10.0
w_2	1.271	1.277	3.142
w_3	3.606	9.788	3.292
H_0	71.505	70.230	72.51
Ω_m	0.352	0.271	0.261

Table 5.2: Results constrained from different data sets and the values of χ^2_{min} where d.o.f denotes the degree of freedom.

Confidence regions

Using a standard χ^2 approach we calculate the confidence contours in parameter space for the data just described and the EoS given by (5.13) incorporated through the Hubble expansion rate as explained in Section 3.3, in particular, using (5.13) in (3.15) through (3.17).

We are interested in the Ω_M-h parameter space and figures 5.10 and 5.11 show the difference when we assume ΛCDM and when we assume JJE parameterisation. From there we notice that the contours are tighter in the former case.

To compare our JJE model with ΛCDM we use the combination of the three differ-

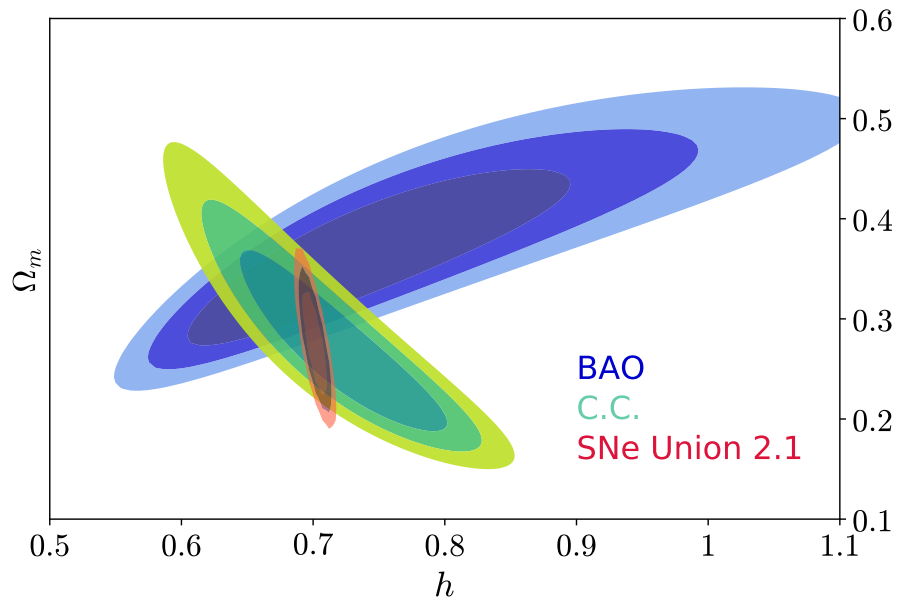

Figure 5.10: Constraints on the Ω_M-h space for the JJE parametrization (5.13).

ent data sets (SN+BAO+CC) and calculate the corresponding reduced-χ^2 estimator by taking into account the different number of degrees of freedom (d.o.f = ν) among the two models as $\chi^2_{\text{reduced}} = \chi^2_{min}/\nu$.

From the obtained values we find that JJE parameterisation and ΛCDM are consistent showing a difference of $\Delta\chi^2_{\text{reduced(JJE}-\Lambda\text{CDM)}} = 0.5\%$.

If we compare the reduced-χ^2 values to one for JJE model and ΛCDM we draw the following remarks.

JJE parameterisation with only using the BAO sample results in a χ^2_{reduced} larger that one, which correspond to a poor fit, whereas for the Union 2.1, CC and the combined data (BAO+Union 2.1+CC) there is an overfit ($\chi^2_{\text{reduced}} < 1$). For comparing both models, we ask which χ^2_{reduced} results closer to one. From that we find that our JJE parameterisation ($\nu = 6$) presents the best assessment ($\chi^2_{\text{reduced}} = 0.977$) in comparison to ΛCDM (with $\nu = 2$ and $\chi^2_{\text{reduced}} = 0.971$) and CPL (with $\nu = 4$ and $\chi^2_{\text{reduced}} = 0.973$) using the combined data. The same behaviour remains using each data set separately.

Tension

From figure 5.10 we note that the contours at 1-σ from the different data sets do overlap for the JJE parameterisation. If ΛCDM is assumed instead, we can see in figure 5.11, that a tension, expressed in units of percent by $\Delta\chi^2_{\text{reduced}} = (\chi^2_{\text{model}} - \chi^2_{\text{LCDM}})/\chi^2_{\text{model}}$,

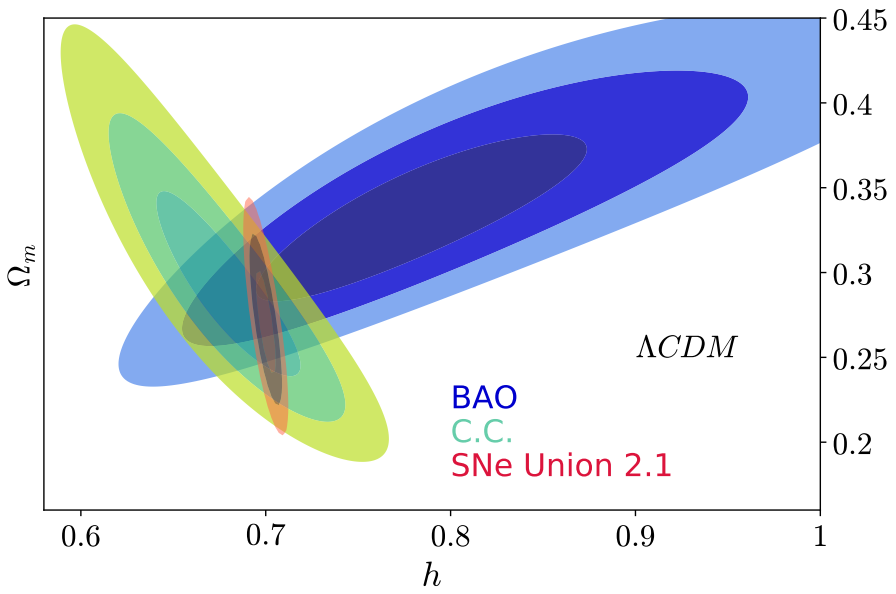

Figure 5.11: Constraints on the Ω_M-h space for ΛCDM model.

with $\Delta\chi^2{}_{\text{reduced (SN-BAO)}} = 0.961$ and $\Delta\chi^2{}_{\text{reduced (CC-BAO)}} = 0.348$ is present among the BAO and supernovae results.

5.4 Remarks & Conclusion

The scientific community is devoting a large amount of time and resources in the quest to understand the dynamics and nature of dark energy, working on current (SDSS-IV Dawson et al. (2016), DES Abbott et al. (2005)) and future (DESI Levi et al. (2013); Aghamousa et al. (2016), Euclid Laureijs et al. (2011), LSST **?**) experiments to study with very high precision the expansion history of the universe and thus be able to test interesting theoretical models. In the process of analyzing data coming, for instance, from galaxy redshift surveys, a cosmological model is used throughout the pipeline (**?**). Also, analysis of the CPL parameterisation using forecast for the eBOSS has been done in Ruggeri et al. (2017) to convert observed positions of the objects into coordinates.

Therefore, to implement in an easy and efficient way modified gravity theories in any kind of survey, we proposed the JJE parameterisation (5.13). Similarly, in future forecast analysis (**?**) a cosmological model will be needed to investigate the parameter constraints in modified gravity theories.

With the presented proposal we aim to put theoretical background to parameterizations of ω_X and also models for $f(R)$ gravity at the same level as other parameterisa-

tions into the pipeline and analysis of observational data and forecasts.

It is worth to mention that by introducing this parameterisation in surveys or using it for data analysis we are avoiding any other kind of assumption that are usually taken in $f(R)$. One of the most usual assumptions is the one related to the value of $f_R(z=0)$ [1] which is taken very close to 1 because of the Solar System constrains Hu and Sawicki (2007) or the structure formation Linder (2009). Nevertheless it is important to notice this constrictions are usually computed for the Hu-Sawicki model and such values do not necessarily apply to other models. By using the JJE parametrization we are making no assumption whatsoever over such values.

[1] Some other authors (like Hu and Sawicki (2007)) use a different notation, $f(R) = R + f(R)_{others}$ and constrictions to our f_R are given by $f_R = 1 + f_{others}$

6 Summary and outlook

The problem of cosmic acceleration is one of the biggest questions in our times. To unveil the nature of this acceleration several theoretical models have been proposed in the literature.

A great deal of both theoretical and observational effort is putting into this quest and one of the fundamental questions is to discriminate among an expansion driven by a Cosmological Constant or some other mechanism. The conjoined observational data available to the present time has brought a very distinctive shape for the reconstructed equation of state of dark energy which has revived the interest for dynamical dark energy models in the community. The several degrees of tension that have appeared when measurements become more precise can also be a hint for deviations of the standard paradigm of ΛCDM.

The presented thesis is an exploration of alternative models to a Cosmological constant in a parametric way: one model was inspired in dynamics of quintessence fields, whereas the second was inspired in the dynamics shown by $f(R)$ gravity models.

The work comprised in this thesis led to two publications (one more under submission)

- The first project tested the effect of a steep transition of state into the background quantities. We found that a high value for the steepness of the transition is preferred by data coming from Baryon Acoustic Oscillations and also the local determination of the Hubble constant. The perturbations of the model at linear order was included and we saw the effect of this transition imprinted in the evolution of matter overdensities. The non-linear evolution of the model is work ongoing but the theoretical basis for carrying on with that analysis were explained in this thesis.

- The second project introduced for the first time a parametrization inspired in $f(R)$ models which mimics the behavior of this kind of gravity with a precision of 0.8% for the three theories that are cosmologically viable. In a separate paper,

submitted to JCAP, we study the statistical tensions of the parameterization here proposed and compare it to other proposals in the literature.

A summary of the conclusions extracted in these publications and improvements we achieved, is presented below.

Steep Equation of state

Background behaviour and statistical analysis

In this part of the thesis we presented a parametrization for the Dark Energy equation of state with four free parameters which mimics the behavior of quintessence models and can allow for a steep transition between the two pivotal values. We presented the constraints for free parameters, $\{w_0, w_i, q, z_t, \omega_c, H_0\}$, and their 68% errors, compatible with BAO measurements combined with the latest local determination of Hubble constant (Riess et al. (2016)) and the compressed CMB likelihood from Planck (Ade et al., 2016a). The case of $BAO + H_0 + CMB$ gave the best constraints on the free parameters due to an early dust-like behaviour of the dark energy component. This model, although very interesting is ruled out by CMB constraints on the early dark energy models and the amount of matter that can be present at the time of recombination, and hence, is not cosmologically viable.

In this work we found that a Dynamical form of DE can reduce the tension among H_0 from local measurements and the one extrapolated using $LCDM$ as fiducial model by Planck. Whereas for a ΛCDM model, tension between the local determination of H_0 (Riess et al. (2016)) and the value derived from Planck (Ade et al. (2016a)) remains, we find that it is possible to simultaneously conciliate the observations from BAO, H_0 and CMB by means of a dynamical Dark Energy.

The reduced numbers of data points and the number of free parameters in the SEoS model does not favor it compared to ΛCDM. Nevertheless, with a more precise determination of dynamics of DE, theoretical models derived from particle physics or modifications to the gravity sector may give a sound derivation of some of the free parameters used in our steep EoS and in this case a dynamical DE would be favored over ΛCDM.

Linear and non-linear regime

In this part of the work we analyzed the growth of dark matter perturbations in two cases:

(i) Smooth dark energy ($\delta_{DE} = 0$)

(ii) Clustering dark energy ($\delta_{DE} \neq 0$)

In the first case, the solutions show a discrepancy from a ΛCDM scenario of few percent. The solutions for this case were also incorporated into the numerical code COLA (Tassev et al., 2013) to obtain the non-linear regime of this model.

From the case of clustering dark energy ($\delta_{DE} \neq 0$) we obtained that the characteristics of a steep transition in the equation of state of dark energy can get imprinted in the growth of structure through the adiabatic speed of sound term. To avoid solutions becoming non-linear exponentially fast, we introduced an effective term to compensate the excessive gravitational clustering caused by a negative c_{ad}^2 term. This analysis deserves further study.

$f(R)$ for surveys

In this part of the work, a parametrization inspired in $f(R)$ gravity models was introduced for the first time. This single equation manages to model three different theories of $f(R)$ with 4-free parameters. Given the amount of observational efforts put into the design of observations to constrain the nature of cosmic acceleration and the implicit use of a fiducial cosmology to interpret the data in such analysis we proposed the JJE parameterisation to implement in an easy and efficient way modified gravity theories in any kind of survey.

With JJE parameterisation we aim to put theoretical background to parameterizations of ω_X and also models for $f(R)$ gravity at the same footage as other parameterisations into the pipeline and analysis of observational data and forecasts.

In addition, we emphasize that by introducing this parameterisation in surveys or using it for data analysis we are avoiding any other kind of assumption that are usually taken in $f(R)$. For instance, one of the most usual assumptions is the one related to the value of $f_R(z = 0)$ which is taken very close to 1 because of the Solar System constrains Hu and Sawicki (2007) or the structure formation Linder (2009). Nevertheless it is important to notice this constrictions are usually computed for the Hu-Sawicki model and such values do not necessarily apply to other models.

By using the JJE parametrization we are making no assumption whatsoever over such values.

We also studied the reduction of the tension among different data sets and found that it is reduced for the case of JJE parametric EoS compared to other proposals in the literature.

Future work based on this thesis

On the basis of the work here presented several paths can be taken to further study these kind of model for cosmic acceleration.

A natural extension of this model is to look for the evolution of the cosmic web from simulations done under this schemes. We are looking already into the analysis of underdense regions in the evolved density fields constructed with the COLA method. This study aims to put to test the hypothesis that a dynamical form of dark energy can change the evolution of the inner structure in such underdense regions, called *voids*.

At the same footage we can perform this analysis if we depart from a modified gravity theory which can be implemented by means of the JJE parametric EoS.

Additionally, the inclusion of this second parametrization into Boltzmann codes such as CAMB can be performed. With this we expect to use the data coming from CMB temperature anisotropies and hence put better constraints in the free parameters from JJE EoS.

The most interesting questions arising from this side of the work are the possibility of reconstructing the $f(R)$ theory of gravity using constraints on our set of parameters $\{w_0, w_1, w_2, w_3\}$ coming from observations. In a different outcome we may find that the reconstructed profile using this set of parameters, cannot be explained by any of the $f(R)$ theories tested. In any case, the implications of any of these scenarios bare great importance for the current cosmological community and this work has been a contribution towards the quest of understanding the nature of cosmic acceleration.

Bibliography

T. Abbott et al. The dark energy survey. *arXiv:0510346*, 2005.

P. A. R. Ade et al. Planck 2015 results. XIII. Cosmological parameters. *Astron. Astrophys.*, 594:A13, 2016a. doi: 10.1051/0004-6361/201525830.

P. A. R. Ade et al. Planck 2015 results. XIV. Dark energy and modified gravity. *Astron. Astrophys.*, 594:A14, 2016b. doi: 10.1051/0004-6361/201525814.

Amir Aghamousa et al. The DESI Experiment Part I: Science,Targeting, and Survey Design. 2016.

Shadab Alam et al. The clustering of galaxies in the completed SDSS-III Baryon Oscillation Spectroscopic Survey: cosmological analysis of the DR12 galaxy sample. *Submitted to: Mon. Not. Roy. Astron. Soc.*, 2016.

L. Amendola and S. Tsujikawa. *Dark Energy: Theory and Observations*. Cambridge University Press, 2015. ISBN 9781107453982.

Luca Amendola, Radouane Gannouji, David Polarski, and Shinji Tsujikawa. Conditions for the cosmological viability of f(R) dark energy models. *Phys. Rev.*, D75: 083504, 2007. doi: 10.1103/PhysRevD.75.083504.

Lauren Anderson et al. The clustering of galaxies in the SDSS-III Baryon Oscillation Spectroscopic Survey: measuring D_A and H at z = 0.57 from the baryon acoustic peak in the Data Release 9 spectroscopic Galaxy sample. *Mon. Not. Roy. Astron. Soc.*, 439(1):83–101, 2014. doi: 10.1093/mnras/stt2206.

Alejandro Aviles and Jorge L. Cervantes-Cota. Lagrangian perturbation theory for modified gravity. *Phys. Rev.*, D96(12):123526, 2017. doi: 10.1103/PhysRevD.96.123526.

E. M. Barboza, Jr. and J. S. Alcaniz. A parametric model for dark energy. *Phys. Lett.*, B666:415–419, 2008. doi: 10.1016/j.physletb.2008.08.012.

James M. Bardeen. Gauge-invariant cosmological perturbations. *Phys. Rev. D*, 22: 1882–1905, Oct 1980a. doi: 10.1103/PhysRevD.22.1882.

James M. Bardeen. Gauge-invariant cosmological perturbations. *Phys. Rev. D*, 22: 1882–1905, Oct 1980b. doi: 10.1103/PhysRevD.22.1882.

Bruce A. Bassett and Renee Hlozek. Baryon Acoustic Oscillations. *arXiv:0910.5224*, 2009.

C. L. Bennett et al. Nine-Year Wilkinson Microwave Anisotropy Probe (WMAP) Observations: Final Maps and Results. *Astrophys. J. Suppl.*, 208:20, 2013. doi: 10.1088/0067-0049/208/2/20.

F. Bernardeau, S. Colombi, E. Gaztanaga, and R. Scoccimarro. Large scale structure of the universe and cosmological perturbation theory. *Phys. Rept.*, 367:1–248, 2002. doi: 10.1016/S0370-1573(02)00135-7.

Emanuele Berti et al. Testing General Relativity with Present and Future Astrophysical Observations. *Class. Quant. Grav.*, 32:243001, 2015. doi: 10.1088/0264-9381/32/24/243001.

M. Betoule et al. Improved cosmological constraints from a joint analysis of the SDSS-II and SNLS supernova samples. *Astron. Astrophys.*, 568:A22, 2014. doi: 10.1051/0004-6361/201423413.

F. Beutler, C. Blake, M. Colless, D. H. Jones, L. Staveley-Smith, L. Campbell, Q. Parker, W. Saunders, and F. Watson. The 6dF Galaxy Survey: baryon acoustic oscillations and the local Hubble constant. *MNRAS*, 416:3017–3032, October 2011. doi: 10.1111/j.1365-2966.2011.19250.x.

Florian Beutler, Chris Blake, Jun Koda, Felipe Marin, Hee-Jong Seo, Antonio J. Cuesta, and Donald P. Schneider. The BOSS–WiggleZ overlap region – I. Baryon acoustic oscillations. *Mon. Not. Roy. Astron. Soc.*, 455(3):3230–3248, 2016a. doi: 10.1093/mnras/stv1943.

Florian Beutler, Chris Blake, Jun Koda, Felipe A. Marín, Hee-Jong Seo, Antonio J. Cuesta, and Donald P. Schneider. The boss–wigglez overlap region – i. baryon acoustic oscillations. *Monthly Notices of the Royal Astronomical Society*, 455(3): 3230–3248, 2016b. doi: 10.1093/mnras/stv1943.

Michael R. Blanton et al. Sloan digital sky survey iv: Mapping the milky way, nearby galaxies, and the distant universe. *The Astronomical Journal*, 154(1):28, 2017.

George R. Blumenthal, S. M. Faber, Joel R. Primack, and Martin J. Rees. Formation of galaxies and large-scale structure with cold dark matter. *Nature*, 311, 1984. doi: 10.1038/311517a0.

Benjamin Bose and Kazuya Koyama. A Perturbative Approach to the Redshift Space Correlation Function: Beyond the Standard Model. *JCAP*, 1708(08):029, 2017. doi: 10.1088/1475-7516/2017/08/029.

F. R. Bouchet, S. Colombi, E. Hivon, and R. Juszkiewicz. Perturbative Lagrangian approach to gravitational instability. *Astron. Astrophys.*, 296:575, 1995a.

F. R. Bouchet, S. Colombi, E. Hivon, and R. Juszkiewicz. Perturbative Lagrangian approach to gravitational instability. *Astron. Astrophys.*, 296:575, 1995b.

R. R. Caldwell and Eric V. Linder. The Limits of quintessence. *Phys. Rev. Lett.*, 95: 141301, 2005. doi: 10.1103/PhysRevLett.95.141301.

Robert R. Caldwell and Marc Kamionkowski. The Physics of Cosmic Acceleration. *Ann. Rev. Nucl. Part. Sci.*, 59:397–429, 2009. doi: 10.1146/annurev-nucl-010709-151330.

Michel Chevallier and David Polarski. Accelerating universes with scaling dark matter. *Int. J. Mod. Phys.*, D10:213–224, 2001. doi: 10.1142/S0218271801000822.

Matthew Colless et al. The 2dF Galaxy Redshift Survey: Final data release. *arXiv:0306581*, 2003.

Asantha R. Cooray and Dragan Huterer. Gravitational lensing as a probe of quintessence. *The Astrophysical Journal Letters*, 513(2):L95, 1999.

Edmund J. Copeland, M. Sami, and Shinji Tsujikawa. Dynamics of dark energy. *Int. J. Mod. Phys.*, D15:1753–1936, 2006. doi: 10.1142/S021827180600942X.

Martin Crocce and Roman Scoccimarro. Renormalized cosmological perturbation theory. *Phys. Rev.*, D73:063519, 2006. doi: 10.1103/PhysRevD.73.063519.

M. Davis, G. Efstathiou, C. S. Frenk, and S. D. M. White. The evolution of large-scale structure in a universe dominated by cold dark matter. *Astrophysical Journal*, 292, 1985.

Kyle S. Dawson et al. The SDSS-IV extended Baryon Oscillation Spectroscopic Survey: Overview and Early Data. *Astron. J.*, 151:44, 2016. doi: 10.3847/0004-6256/151/2/44.

A. De la Macorra. Quintessence unification models from nonAbelian gauge dynamics. *JHEP*, 01:033, 2003. doi: 10.1088/1126-6708/2003/01/033.

A. de la Macorra. BDM dark matter: CDM with a core profile and a free streaming scale. *Astroparticle Physics*, 33:195–200, April 2010. doi: 10.1016/j.astropartphys.2010.01.009.

A. de la Macorra and G. Piccinelli. General scalar fields as quintessence. *Phys. Rev.*, D61:123503, 2000. doi: 10.1103/PhysRevD.61.123503.

A. de la Macorra and C. Stephan-Otto. Natural quintessence with gauge coupling unification. *Phys. Rev. Lett.*, 87:271301, 2001. doi: 10.1103/PhysRevLett.87.271301.

A. de la Macorra and C. Stephan-Otto. Quintessence restrictions on negative power and condensate potentials. *Phys. Rev.*, D65:083520, 2002. doi: 10.1103/PhysRevD.65.083520.

Axel de la Macorra. Dark group: dark energy and dark matter. *Phys. Lett.*, B585: 17–23, 2004. doi: 10.1016/j.physletb.2004.02.006.

Axel de la Macorra. Dark Energy Parametrization motivated by Scalar Field Dynamics. *arXiv:1511.04439*, 2015.

Timothée Delubac et al. Baryon acoustic oscillations in the Lyman α Forest of BOSS DR11 quasars. *Astron. Astrophys.*, 574:A59, 2015. doi: 10.1051/0004-6361/201423969.

R. H. Dicke, P. J. E. Peebles, P. G. Roll, and D. T. Wilkinson. Cosmic Black-Body Radiation. *APJ*, 142:414–419, July 1965. doi: 10.1086/148306.

Scott Dodelson. *Modern cosmology*. Academic Press, San Diego, CA, 2003.

Michael Doran and Georg Robbers. Early dark energy cosmologies. *JCAP*, 0606:026, 2006. doi: 10.1088/1475-7516/2006/06/026.

A. Einstein. Cosmological considerations in the general theory of relativity. *The Principle of Relativity (Dover, 1952), pp. 175-188*, 1917.

Daniel J. Eisenstein et al. Detection of the baryon acoustic peak in the large-scale correlation function of SDSS luminous red galaxies. *Astrophys. J.*, 633:560–574, 2005. doi: 10.1086/466512.

Andreu Font-Ribera et al. Quasar-Lyman α Forest Cross-Correlation from BOSS DR11 : Baryon Acoustic Oscillations. *JCAP*, 1405:027, 2014. doi: 10.1088/1475-7516/2014/05/027.

Silvia Galli, Karim Benabed, Fran çois Bouchet, Jean-Fran çois Cardoso, Franz Elsner, Eric Hivon, Anna Mangilli, Simon Prunet, and Benjamin Wandelt. Cmb polarization can constrain cosmology better than cmb temperature. *Phys. Rev. D*, 90:063504, Sep 2014. doi: 10.1103/PhysRevD.90.063504.

Yan Gong, Yin-Zhe Ma, Shuang-Nan Zhang, and Xuelei Chen. Consistency test on the cosmic evolution. *Phys. Rev.*, D92(6):063523, 2015. doi: 10.1103/PhysRevD.92.063523.

Steen Hannestad and Edvard Mortsell. Cosmological constraints on the dark energy equation of state and its evolution. *JCAP*, 0409:001, 2004. doi: 10.1088/1475-7516/2004/09/001.

Wayne Hu and Ignacy Sawicki. Models of f(R) Cosmic Acceleration that Evade Solar-System Tests. *Phys. Rev.*, D76:064004, 2007. doi: 10.1103/PhysRevD.76.064004.

Zhiqi Huang, J. Richard Bond, and Lev Kofman. Parameterizing and Measuring Dark Energy Trajectories from Late-Inflatons. *Astrophys. J.*, 726:64, 2011. doi: 10.1088/0004-637X/726/2/64.

Dragan Huterer and Hiranya V. Peiris. Dynamical behavior of generic quintessence potentials: Constraints on key dark energy observables. *Phys. Rev.*, D75:083503, 2007. doi: 10.1103/PhysRevD.75.083503.

Dragan Huterer and Michael S. Turner. Probing the dark energy: Methods and strategies. *Phys. Rev.*, D64:123527, 2001. doi: 10.1103/PhysRevD.64.123527.

Mariana Jaber and Axel de la Macorra. Probing a Steep EoS for Dark Energy with latest observations. *Astropart. Phys.*, 97:130–135, 2018. doi: 10.1016/j.astropartphys.2017.11.007.

Luisa G. Jaime. Diagnostic of $f(R)$ under the $Om(z)$ function. *Phys. Rev.*, D91(12):124070, 2015. doi: 10.1103/PhysRevD.91.124070.

Luisa G. Jaime, Leonardo Patino, and Marcelo Salgado. Robust approach to f(R) gravity. *Phys. Rev.*, D83:024039, 2011. doi: 10.1103/PhysRevD.83.024039.

Luisa G. Jaime, Leonardo Patino, and Marcelo Salgado. f(R) Cosmology revisited. 2012.

Luisa G. Jaime, Leonardo Patiño, and Marcelo Salgado. Note on the equation of state of geometric dark-energy in f(R) gravity. *Phys. Rev.*, D89(8):084010, 2014. doi: 10.1103/PhysRevD.89.084010.

Luisa G. Jaime, Mariana Jaber, and Celia Escamilla-Rivera. New parametrized equation of state for dark energy surveys. *Phys. Rev.*, D98(8):083530, 2018. doi: 10.1103/PhysRevD.98.083530.

H. K. Jassal, J. S. Bagla, and T. Padmanabhan. WMAP constraints on low redshift evolution of dark energy. *Mon. Not. Roy. Astron. Soc.*, 356:L11–L16, 2005.

Eyal A. Kazin et al. The WiggleZ Dark Energy Survey: improved distance measurements to z = 1 with reconstruction of the baryonic acoustic feature. *Mon. Not. Roy. Astron. Soc.*, 441(4):3524–3542, 2014. doi: 10.1093/mnras/stu778.

Anatoly Klypin. Numerical simulations in cosmology I: methods. 2000.

Anatoly Klypin. Methods for cosmological N-body simulations, 2017. [Online at skiesanduniverses.org/resources/KlypinNbody.pdf : accessed 19-July-2018].

Lawrence M Krauss, Katherine Jones-Smith, and Dragan Huterer. Dark energy, a cosmological constant, and type ia supernovae. *New Journal of Physics*, 9(5):141, 2007.

R. Laureijs, J. Amiaux, S. Arduini, J. . Augueres, J. Brinchmann, R. Cole, M. Cropper, C. Dabin, L. Duvet, A. Ealet, and et al. Euclid Definition Study Report. *ArXiv e-prints, arXiv:1110.3193*, October 2011.

Michael Levi et al. The DESI Experiment, a whitepaper for Snowmass 2013. *arXiv:1308.0847*, 2013.

Antony Lewis, Anthony Challinor, and Anthony Lasenby. Efficient computation of CMB anisotropies in closed FRW models. *Astrophys. J.*, 538:473–476, 2000. doi: 10.1086/309179.

Andrew R. Liddle. How many cosmological parameters? *Mon. Not. Roy. Astron. Soc.*, 351:L49–L53, 2004. doi: 10.1111/j.1365-2966.2004.08033.x.

Eric V. Linder. Exploring the expansion history of the universe. *Phys. Rev. Lett.*, 90: 091301, 2003. doi: 10.1103/PhysRevLett.90.091301.

Eric V. Linder. The paths of quintessence. *Phys. Rev.*, D73:063010, 2006a. doi: 10.1103/PhysRevD.73.063010.

Eric V. Linder. Dark Energy in the Dark Ages. *Astropart. Phys.*, 26:16–21, 2006b. doi: 10.1016/j.astropartphys.2006.04.004.

Eric V. Linder. The Dynamics of Quintessence, The Quintessence of Dynamics. *Gen. Rel. Grav.*, 40:329–356, 2008. doi: 10.1007/s10714-007-0550-z.

Eric V. Linder. Exponential Gravity. *Phys. Rev.*, D80:123528, 2009. doi: 10.1103/PhysRevD.80.123528.

Eric V. Linder and Georg Robbers. Shifting the Universe: Early Dark Energy and Standard Rulers. *JCAP*, 0806:004, 2008. doi: 10.1088/1475-7516/2008/06/004.

LSST Science Collaboration, P. A. Abell, J. Allison, S. F. Anderson, J. R. Andrew, J. R. P. Angel, L. Armus, D. Arnett, S. J. Asztalos, T. S. Axelrod, and et al. LSST Science Book, Version 2.0. *ArXiv e-prints, arXiv:0912.0201*, December 2009.

Chung-Pei Ma and Edmund Bertschinger. Cosmological perturbation theory in the synchronous and conformal Newtonian gauges. *Astrophys. J.*, 455:7–25, 1995. doi: 10.1086/176550.

Jing-Zhe Ma and Xin Zhang. Probing the dynamics of dark energy with novel parametrizations. *Phys. Lett.*, B699:233–238, 2011. doi: 10.1016/j.physletb.2011.04.013.

Karim A. Malik. 1st mexican school on cosmological perturbation theory: Lectures on cosmological perturbation theory.

Patrick McDonald and Arabindo Roy. Clustering of dark matter tracers: generalizing bias for the coming era of precision LSS. *JCAP*, 0908:020, 2009. doi: 10.1088/1475-7516/2009/08/020.

Michele Moresco, Raul Jimenez, Licia Verde, Andrea Cimatti, Lucia Pozzetti, Claudia Maraston, and Daniel Thomas. Constraining the time evolution of dark energy, curvature and neutrino properties with cosmic chronometers. *arXiv:1604.00183*, 2016a.

Michele Moresco, Lucia Pozzetti, Andrea Cimatti, Raul Jimenez, Claudia Maraston, Licia Verde, Daniel Thomas, Annalisa Citro, Rita Tojeiro, and David Wilkinson. A 6% measurement of the Hubble parameter at $z \sim 0.45$: direct evidence of the epoch of cosmic re-acceleration. *JCAP*, 1605(05):014, 2016b. doi: 10.1088/1475-7516/2016/05/014.

M. J. Mortonson, W. Hu, and D. Huterer. Testable dark energy predictions from current data. *PRD*, 81(6):063007, March 2010. doi: 10.1103/PhysRevD.81.063007.

V.F. Mukhanov, H.A. Feldman, and R. H. Brandenberger. Theory of cosmological perturbations. *Physics Reports*, 215(5):203 – 333, 1992. ISSN 0370-1573. doi: 10.1016/0370-1573(92)90044-Z.

Pia Mukherjee, Martin Kunz, David Parkinson, and Yun Wang. Planck priors for dark energy surveys. *Phys. Rev. D*, 78:083529, Oct 2008. doi: 10.1103/PhysRevD.78.083529.

Nikhil Padmanabhan, Xiaoying Xu, Daniel J. Eisenstein, Richard Scalzo, Antonio J. Cuesta, Kushal T. Mehta, and Eyal Kazin. A 2 per cent distance to z = 0.35 by reconstructing baryon acoustic oscillations – i. methods and application to the sloan digital sky survey. *Monthly Notices of the Royal Astronomical Society*, 427(3):2132–2145, 2012. ISSN 1365-2966. doi: 10.1111/j.1365-2966.2012.21888.x.

P. J. E. Peebles. *The large-scale structure of the universe*. 1980.

P.J.E. Peebles. *The large-scale structure of the universe*. 1980.

A. A. Penzias and R. W. Wilson. A Measurement of Excess Antenna Temperature at 4080 Mc/s. *APJ*, 142:419–421, July 1965. doi: 10.1086/148307.

S. Perlmutter et al. Meaurements of Omega and Lambda from 42 high redshift supernovae. *Astrophys. J.*, 517:565–586, 1999. doi: 10.1086/307221.

Thomas R. Quinn, Neal Katz, Joachim Stadel, and George Lake. Time stepping N body simulations. *Submitted to: Astrophys. J.*, 1997.

Bharat Ratra and P. J. E. Peebles. Cosmological Consequences of a Rolling Homogeneous Scalar Field. *Phys. Rev.*, D37:3406, 1988. doi: 10.1103/PhysRevD.37.3406.

Adam G. Riess et al. Observational evidence from supernovae for an accelerating universe and a cosmological constant. *Astron. J.*, 116:1009–1038, 1998. doi: 10.1086/300499.

Adam G. Riess et al. A 2.4% Determination of the Local Value of the Hubble Constant. *Astrophys. J.*, 826(1):56, 2016. doi: 10.3847/0004-637X/826/1/56.

Ashley J. Ross, Lado Samushia, Cullan Howlett, Will J. Percival, Angela Burden, and Marc Manera. The clustering of the SDSS DR7 main Galaxy sample – I. A 4 per cent distance measure at $z = 0.15$. *Mon. Not. Roy. Astron. Soc.*, 449(1):835–847, 2015. doi: 10.1093/mnras/stv154.

D. Rubin et al. Looking Beyond Lambda with the Union Supernova Compilation. *Astrophys. J.*, 695:391–403, 2009. doi: 10.1088/0004-637X/695/1/391.

Rossana Ruggeri, Will J. Percival, Eva-Maria Mueller, Hector Gil-Marin, Fangzhou Zhu, Nikhil Padmanabhan, and Gong-Bo Zhao. The extended Baryon Oscillation Spectroscopic Survey (eBOSS): testing a new approach to measure the evolution of the structure growth. 2017.

Varun Sahni. The Cosmological constant problem and quintessence. *Class. Quant. Grav.*, 19:3435–3448, 2002. doi: 10.1088/0264-9381/19/13/304.

Ariel G. Sanchez et al. The clustering of galaxies in the completed SDSS-III Baryon Oscillation Spectroscopic Survey: combining correlated Gaussian posterior distributions. *Submitted to: Mon. Not. Roy. Astron. Soc.*, 2016.

Roman Scoccimarro, Lam Hui, Marc Manera, and Kwan Chuen Chan. Large-scale Bias and Efficient Generation of Initial Conditions for Non-Local Primordial Non-Gaussianity. *Phys. Rev.*, D85:083002, 2012. doi: 10.1103/PhysRevD.85.083002.

Hee-Jong Seo and Daniel J. Eisenstein. Probing dark energy with baryonic acoustic oscillations from future large galaxy redshift surveys. *Astrophys. J.*, 598:720–740, 2003. doi: 10.1086/379122.

Arman Shafieloo, Varun Sahni, and Alexei A. Starobinsky. A new null diagnostic customized for reconstructing the properties of dark energy from BAO data. *Phys. Rev.*, D86:103527, 2012. doi: 10.1103/PhysRevD.86.103527.

J. Sollerman, E. Mörtsell, T. M. Davis, M. Blomqvist, B. Bassett, A. C. Becker, D. Cinabro, A. V. Filippenko, R. J. Foley, J. Frieman, P. Garnavich, H. Lampeitl, J. Marriner, R. Miquel, R. C. Nichol, M. W. Richmond, M. Sako, D. P. Schneider, M. Smith, J. T. Vanderplas, and J. C. Wheeler. First-Year Sloan Digital Sky Survey-II (SDSS-II) Supernova Results: Constraints on Nonstandard Cosmological Models. *APJ*, 703:1374–1385, October 2009. doi: 10.1088/0004-637X/703/2/1374.

Alexei A. Starobinsky. Disappearing cosmological constant in f(R) gravity. *JETP Lett.*, 86:157–163, 2007. doi: 10.1134/S0021364007150027.

Paul J. Steinhardt, Limin Wang, and Ivaylo Zlatev. Cosmological tracking solutions. *Phys. Rev. D*, 59:123504, May 1999. doi: 10.1103/PhysRevD.59.123504.

N. Suzuki et al. The Hubble Space Telescope Cluster Supernova Survey: V. Improving the Dark Energy Constraints Above z>1 and Building an Early-Type-Hosted Supernova Sample. *Astrophys. J.*, 746:85, 2012. doi: 10.1088/0004-637X/746/1/85.

Svetlin Tassev, Matias Zaldarriaga, and Daniel Eisenstein. Solving Large Scale Structure in Ten Easy Steps with COLA. *JCAP*, 1306:036, 2013. doi: 10.1088/1475-7516/2013/06/036.

Max Tegmark et al. Cosmological parameters from SDSS and WMAP. *Phys. Rev.*, D69:103501, 2004. doi: 10.1103/PhysRevD.69.103501.

Li-Min Wang and Paul J. Steinhardt. Cluster abundance constraints on quintessence models. *Astrophys. J.*, 508:483–490, 1998. doi: 10.1086/306436.

Yun Wang and Pia Mukherjee. Observational constraints on dark energy and cosmic curvature. *Phys. Rev. D*, 76:103533, Nov 2007. doi: 10.1103/PhysRevD.76.103533.

Steven Weinberg. The cosmological constant problem. *Rev. Mod. Phys.*, 61:1–23, Jan 1989. doi: 10.1103/RevModPhys.61.1.

Jochen Weller and Andreas Albrecht. Future supernovae observations as a probe of dark energy. *Phys. Rev.*, D65:103512, 2002. doi: 10.1103/PhysRevD.65.103512.

Christof Wetterich. The Cosmon model for an asymptotically vanishing time dependent cosmological 'constant'. *Astron. Astrophys.*, 301:321–328, 1995.

Hans A. Winther, Kazuya Koyama, Marc Manera, Bill S. Wright, and Gong-Bo Zhao. COLA with scale-dependent growth: applications to screened modified gravity models. *JCAP*, 1708(08):006, 2017. doi: 10.1088/1475-7516/2017/08/006.

Richard P. Woodard. Avoiding dark energy with 1/r modifications of gravity. *Lect. Notes Phys.*, 720:403–433, 2007. doi: 10.1007/978-3-540-71013-4_14.

Gong-Bo Zhao et al. Dynamical dark energy in light of the latest observations. *Nat. Astron.*, 1(9):627–632, 2017. doi: 10.1038/s41550-017-0216-z.

Miguel Zumalacarregui, Emilio Bellini, Ignacy Sawicki, Julien Lesgourgues, and Pedro G. Ferreira. hi class: Horndeski in the cosmic linear anisotropy solving system. *JCAP*, 1708(08):019, 2017. doi: 10.1088/1475-7516/2017/08/019.